THE UNIVERSITY OF
WARWICK

Library Declaration and Deposit Agreement

1. STUDENT DETAILS

Please complete the following:

Full name: ....SHREY PATHAK.....

University ID number: .....07590591.....

2. THESIS DEPOSIT

2.1 I understand that under my registration at the University, I am required to deposit my thesis with the University in BOTH hard copy and in digital format. The digital version should normally be saved as a single pdf file.

2.2 The hard copy will be housed in the University Library. The digital version will be deposited in the University's Institutional Repository (WRAP). Unless otherwise indicated (see 2.3 below) this will be made openly accessible on the Internet and will be supplied to the British Library to be made available online via its Electronic Theses Online Service (EThOS) service.
[At present, theses submitted for a Master's degree by Research (MA, MSc, LLM, MS or MMedSci) are not being deposited in WRAP and not being made available via EthOS. This may change in future.]

2.3 In exceptional circumstances, the Chair of the Board of Graduate Studies may grant permission for an embargo to be placed on public access to the hard copy thesis for a limited period. It is also possible to apply separately for an embargo on the digital version. (Further information is available in the *Guide to Examinations for Higher Degrees by Research*.)

2.4 *If you are depositing a thesis for a Master's degree by Research, please complete section (a) below. For all other research degrees, please complete both sections (a) and (b) below:*

(a) Hard Copy

I hereby deposit a hard copy of my thesis in the University Library to be made publicly available to readers (please delete as appropriate) ~~EITHER~~ immediately OR after an embargo period of .....0..... months/~~years~~ as agreed by the Chair of the Board of Graduate Studies.

I agree that my thesis may be photocopied. YES / ~~NO~~ (*Please delete as appropriate*)

(b) Digital Copy

I hereby deposit a digital copy of my thesis to be held in WRAP and made available via EThOS.

Please choose one of the following options:

✓EITHER My thesis can be made publicly available online. YES / ~~NO~~ (*Please delete as appropriate*)

OR My thesis can be made publicly available only after.....[date] (Please give date)
YES / NO (*Please delete as appropriate*)

OR My full thesis cannot be made publicly available online but I am submitting a separately identified additional, abridged version that can be made available online.
YES / NO (*Please delete as appropriate*)

OR My thesis cannot be made publicly available online. YES / NO (*Please delete as appropriate*)

3. GRANTING OF NON-EXCLUSIVE RIGHTS

Whether I deposit my Work personally or through an assistant or other agent, I agree to the following:

Rights granted to the University of Warwick and the British Library and the user of the thesis through this agreement are non-exclusive. I retain all rights in the thesis in its present version or future versions. I agree that the institutional repository administrators and the British Library or their agents may, without changing content, digitise and migrate the thesis to any medium or format for the purpose of future preservation and accessibility.

4. DECLARATIONS

(a) I DECLARE THAT:

- I am the author and owner of the copyright in the thesis and/or I have the authority of the authors and owners of the copyright in the thesis to make this agreement. Reproduction of any part of this thesis for teaching or in academic or other forms of publication is subject to the normal limitations on the use of copyrighted materials and to the proper and full acknowledgement of its source.
- The digital version of the thesis I am supplying is the same version as the final, hard-bound copy submitted in completion of my degree, once any minor corrections have been completed.
- I have exercised reasonable care to ensure that the thesis is original, and does not to the best of my knowledge break any UK law or other Intellectual Property Right, or contain any confidential material.
- I understand that, through the medium of the Internet, files will be available to automated agents, and may be searched and copied by, for example, text mining and plagiarism detection software.

(b) IF I HAVE AGREED (in Section 2 above) TO MAKE MY THESIS PUBLICLY AVAILABLE DIGITALLY, I ALSO DECLARE THAT:

- I grant the University of Warwick and the British Library a licence to make available on the Internet the thesis in digitised format through the Institutional Repository and through the British Library via the EThOS service.
- If my thesis does include any substantial subsidiary material owned by third-party copyright holders, I have sought and obtained permission to include it in any version of my thesis available in digital format and that this permission encompasses the rights that I have granted to the University of Warwick and to the British Library.

5. LEGAL INFRINGEMENTS

I understand that neither the University of Warwick nor the British Library have any obligation to take legal action on behalf of myself, or other rights holders, in the event of infringement of intellectual property rights, breach of contract or of any other right, in the thesis.

Please sign this agreement and return it to the Graduate School Office when you submit your thesis.

Student's signature:  Date: 29/5/13

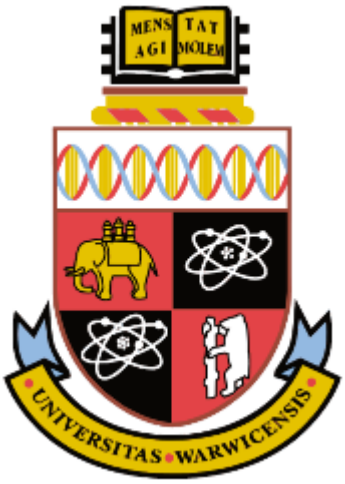

Piezoelectric Microsensors for Semiochemical Communication

by
Shrey Pathak
Microsensors and Bioelectronics Research Group
School of Engineering
University of Warwick

A thesis submitted to the University of Warwick
for the degree of Doctor of Philosophy
February, 2012

To great gene's

Table on Contents

List of Figures

List of Tables

Abstract

Chemical communication plays vital role in the mediating the behaviour of an organism living in the "odour space". The mechanisms by which odours are generated and detected by the organism has evolved over thousands of years and thus the potential advantages of translating this system into a fully functional communication system has opened new avenues in the area of multi-disciplinary research. This formed the basis of the Biosynthetic Infochemical Communications project – iCHEM whose central aim was to develop a new class of communication technology based on the biosynthesis pathways of the moth, *S. littoralis*. This novel infochemical communication system would consist of a "chemoemitter" unit which would generate a precise mix of infochemicals which after travelling through the odour space would be detected by a complementary tuned detector – the "chemoreceiver" unit comprising of a ligand specific detection element and an associated biophysical model functioning similar to the antennal lobe neuron of the moth. This combined novel system will have the capability of communicating by the help of chemicals only, in the vapour or liquid phase. For the work presented in this thesis, the novel concept of infochemical communication has been examined in the vapour and liquid phase by employing piezoelectric microsensors. This has been achieved and demonstrated throughout the thesis by employing chemo-specific acoustic wave microsensors. For vapour phase assessment, quartz crystal microbalance, were coated with different organic polymer coatings and incorporated in a prototype infochemical communication system detecting encoded volatiles. For liquid phase assessment, shear horizontal surface acoustic wave (SH-SAW) microsensors were specifically designed and immobilised within Sf9 insect cells. This GPCR based whole cell biosensing system was then employed to detect ligand specific activations thus acting as a precursor to the development of a fully functionalised OR based signalling system, thus contributing to the growing field of communication and labelling technology.

Acknowledgements

Firstly, I would like to thank my academic supervisors Dr. Marina Cole and Professor Julian W. Gardner for providing me with the opportunity to work in this field. Their constant guidance and support during the course of this Ph.D was invaluable and irreplaceable. I would also like to thank Dr. James Covington for his support and encouragement during crucial phases of this research. My special thanks goes to Dr. Zoltán Raćz for it was his skills as a classic Socratic scholar that has helped me develop a critical approach. I would like to thank Professor John Challiss from the Department Cell Physiology and Pharmacology, University of Leicester for allowing me to setup experiments in his laboratory. I would also like to thank his group members for making me feel welcomed with special thanks to Dr. Mellisa Jordan for conducting numerous experiments with me and sharing the (many)^2 frustrations and elations. At this juncture I would also like to thank all the members of the iCHEM project consortium. It was a pleasure being a part of a dynamic and an intellectually enlightened group of researchers.

Next, I would like to thank Mr. Frank Courtney and Mr. Ian Griffiths for their unparalleled assistance in all mechanical and technical matters. I am also grateful for the friendship and support of my fellow group members including Dr. Gurmukh Sehra, Dr. Fauzan Che-Harun, Dr. Philip King, Dr. Marina Talib, Dr. James Taylor, Dr. Simon Leigh, Ms. Cecilia Occhiuzzi, Ms. Nathalie Ouaret, Mr.Max Joseph, Mr. Chris Purssell and Mr. Sanju Thomas. During the course of this journey I was fortunate to make many friends and my special thanks go to Dr.Abou Jeng, Dr.Zhaoyang Yue and Swaraj and Antima Basu. This research wouldn't have been possible without the financial support of the iCHEM project consortium and I would like to thank the funding body. I would like to thank my parents, my brother and his family for their immeasurable support and patience during this process. It is thus not surprising that a thesis is not written in first-person as without the support, effort and contributions of all the above (named and un-named) it would be practically impossible to reach this point.

Declaration

The work described in this thesis was conducted by the author, except where stated otherwise, in the School of Engineering, University of Warwick and at the Department of Physiology and Pharmacology, University of Leicester, United Kingdom. The thesis has not been submitted for a higher degree at another university. The following are a list of chapter with contribution from partners and collaborators.

Chapter 3: Experiments performed by Mr. Shrey Pathak and Data Analysed by Dr. Zoltan Racz (University of Warwick)

Chapter 4: Theoretical Model developed in association with Professor Julian Gardner (University of Warwick), Dr Melissa Jordan (University of Leicester) and Professor John Challiss (University of Leicester)

Chapter 5: SH-SAW sensors frequency calculation performed in collaboration with Professor Julian Gardner, Dr Marina Cole, Dr. Zoltan Racz (University of Warwick), Dr. Danijela Markovic (University of Leicester) and Professor John Challiss (University of Leicester)

Chapter 7: Experiments performed at the University of Leicester, Department of Cell Physiology and Pharmacology, University of Leicester in collaboration with Dr. Melissa Jordan.

Parts of this work have been presented at international conferences and published in the scientific literature listed below:

- S. B. Olsson, Z. Rácz, W. P. Bula, N. Dimov, G. Carot-Sans, M. D. Jordan, S. Karout, L. S. Kuebler, D. Markovic, L. Muñoz, **S. Pathak**, R. A. J. Challiss, M. Cole, J. W. Gardner, J. G. E. Gardeniers, A. Guerrero, B. S. Hansson and T. C. Pearce, "*iChem: An insect-inspired biomimetic infochemical communication system*," 12th European Symposium for Insect Taste and Olfaction (ESITO), September 19-25, 2011, St. Petersburg, Russia.

- **S. Pathak**, M. D. Jordon, Z. Rácz, J. Challiss, J. W. Gardner, M. Cole, "*Ligand elicited secondary cellular responses using Surface Acoustic Wave Biosensors*", FET11, The European Future Technology Conference and Exhibition, 4th – 6th May, 2011, Budapest, Hungry.

- Z. Rácz, M. Cole, J. W. Gardner, **S. Pathak**, M. D. Jordon, J. Challiss, " *Cell-based Surface Acoustic Wave Resonant Microsensor for Biomolecular Agent Detection,",* The 16th International Conference on Solid State Sensors, Actuators and Microsystems, June 5-9, 2011, Beijing, China.

- M. Cole, J. W. Gardner, **S. Pathak**, Z. Rácz, J. Challiss, D. Markovic, "*Cell based biosensors for Biomedical Application*", Proceedings of the 7th IASTED International Conference, Biomedical Engineering, February 17th- 19th, 2010, Innusbruck, Austria.

- M. Cole, J. W. Gardner, Z. Rácz, **S. Pathak**, T. C. Pearce, J. Challiss, D. Markovic, B. S. Hansson, S. Olsson, L. Kubler, A. Guerroro, L. Munoz, G. Carot, J. G. E. Gardieners, N. Dimov, W. Bula, "*Biomimetic insect infochemical communication system*", The 8th Annual IEEE Conference on Sensors, October 25th – 28th, 2009, Christchurch, New Zealand.

- M. Cole, J. W. Gardner, **S. Pathak**, T. C. Pearce, Z. Rácz, "*Towards a biosynthetic infochemical communication system",* Eurosensors XXII conference, September 6th – 9th, 2009, Laussane, Switzerland.

Chapter 1
Introduction

The purpose of this first chapter is to contextualise the foundations on which the work presented in this thesis has been carried out. This chapter introduces the reader to the field of chemical communication, describing how an odour molecule or an odour plume plays an informative role in the survival of the species. The chapter introduces the reader to the scope of the research carried out in this thesis. Thereafter, aims and objectives of the current research have then been presented with the chapter concluding by providing a structural flow to the thesis.

1.1 Chemical Communication

Homo sapiens primarily depend on the stimuli of vision and acoustics for communication. This is in stark contrast to the organisms that live in the "odour space". Such organisms (both vertebrates and invertebrates) employ "odours" as their primary stimuli for communication and correspondingly mediate their behaviour through the sense of smell. In this so called "odour world", the chemical stimulus plays a vital role in helping the species in a range of activities spanning from location of potential sources of food to gaining shelter from potential predators [2]. For example, *Mythimna separate* (caterpillar) perceives day and night by recognising the blend of volatiles emitted by the host plant on which it lives, a female moth attracts its counterpart, the male, over a long distance by emitting sexual pheromones, a type of communication molecule, while some zooplanktic species form defensive structures upon sensing odours which indicate the presence of their predators [3] [4]. When one considers the plethora of environmental stimuli, it is the specificity (orientation and combination) of an encoded odour, or an infochemical as it carries information about food or predator, that is often the deciding factor which mediates the behaviour of the organism [3].

The infochemicals are detected by surface receptors, present on the antenna of an insect triggering a chain of biochemical reactions which translates the initial chemical signal into a neural signal. This signal is carried by the central and peripheral nerves and projected onto the brain thus generating a perception of the information detected [5][6]. This generated perception of the detected infochemical is what determines the behaviour of the insect. Similar to the process of odour detection, the generation of odour is also achieved by an organism through a set of complex processes, which involves several enzymatic reactions. This delicate process of odour emission and detection has evolved and refined over time by nature.

Assuming that the basis of chemical communication remains the same for insects presiding in a common space, the potential advantages of translating this mechanism of odour generation and detection into a novel infochemical communication system with varied applications has opened new avenues of multi-disciplinary research. This vision formed the basis of the Biosynthetic Infochemicals Communication's Project (iCHEM) a European Union STREP project which was established in 2007 [7]. The research work performed in this thesis is a part of the iCHEM project and has contributed towards its objectives.

1.2 Scope of Current Work - The Biosynthetic Infochemical Communication (iCHEM) project

The central aim of the iCHEM project was to "investigate, designed and implement" a novel communication system based on the pheromone [8], a type of chemical signal, biosynthesis pathway for detection of infochemical, encoded chemical signals, in the insect nervous system . The insect model which formed the basis of the research project was the moth *Spodoptera littoralis* [9]. This particular species was chosen in the current study because of two distinct factors:

- It has two distinct and well defined pheromone components.
- The biological detection and pheromone generation pathways are well characterised.

Each process of the biosynthetic pathway i.e. pheromone generation and detection was then deployed as a discrete system in the project finally contributing to the realisation of a novel infochemical communication system that would form to a new branch of information technology that employs chemical to transmit and receive information, **Figure 1.1** [7] [10] [11]. The communication technology would include a "chemoemitter" unit which would be capable of generating a precise mix (encoded information) of infochemicals and a corresponding

"chemoreceiver" unit which would be specifically tuned to detect and decode the emitted information. The pheromones of the moth *S. littoralis* comprises of hydrocarbon chain of alcohol (R-OH), aldehydes (R-COH), acetate ester (R-OO) and organyl chemical groups and can be produced in four clearly defined steps mediated by enzymatic reactions (where " R- " being a chain of carbon) [12] [13]. The steps include fatty acid synthesis, desaturation, hydrocarbon chain shortening, and reduction/functional group modification [13]. Each step outlined above could then be implemented as a microreactor module with the final synthesized chemical released by a temperature controlled micro-evaporator unit [7] [14].

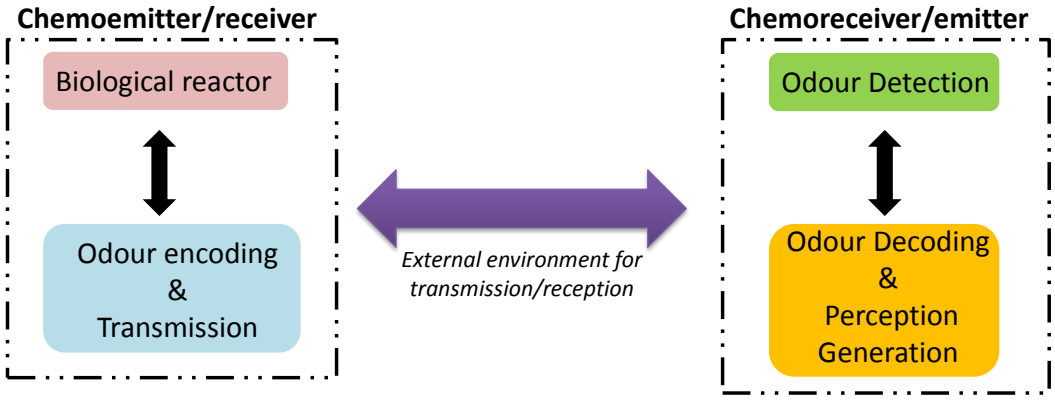

Figure 1.1: An infochemical communications system

The emitted infochemicals can be detected by a "chemoreceiver" unit that demonstrates a high degree of specificity and sensitivity to the infochemicals [7] - [11]. The detected chemical would be decoded by

employing a biophysical neuromorphic model that would mimic the ratiometric processing in the antenna lobe of the moth. Thus, in essence the chemoreceiver unit could be deconstructed into 2 different sub-systems each comprising of different sub-units. The first sub-system could comprise of a blend specific olfactory receptor based sensing system – employed to detect the pheromones. The second sub-system could be said to comprise of a biophysics neuronal model responsible for decoding the detected pheromone blend, as shown in **Figure 1.2** [7].

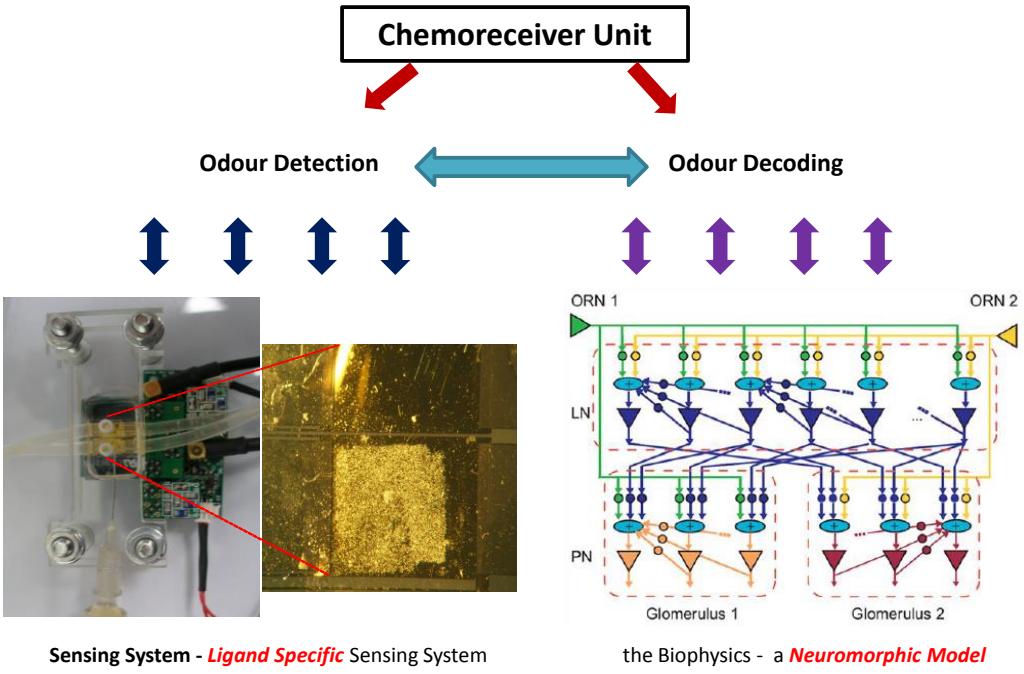

Figure 1.2 : The different subsystems comprising the chemoreceiver [14].

The research performed in this thesis has been aimed at enhancing the development of the chemoreceiver unit by designing, fabricating and characterising a ligand-specific acoustic wave sensing system. Such a system, as will be shown in later chapters of the thesis, has been designed by employing acoustic wave microsensors and the sensing properties have been examined in two different operational phases - vapour and liquid phase. For vapour phase assessment, a polymer coated quartz crystal microbalance (QCM) microsensors array was incorporated as part of a novel infochemical communication system detecting volatiles.

For liquid phase assessment, an insect cell-line – SF9 was immobilised on surface acoustic wave (SAW) microsensors. This setup was then integrated with an automated microfluidic setup and characterised with different concentration of neurotransmitters.

1.3 Objectives of the Current Research

This section outlines the key objectives of the current research.

Demonstrate the use of polymer coated Quartz Crystal Microbalance (QCM) – a class of acoustic wave microsensors, sensor array in the vapour phase for the detection of volatile organic chemicals emitted in a ratio's.

Examine the theoretical foundation of Surface Acoustic Wave (SAW) microsensors operating in the liquid phase.

Develop a theoretical model co-relating the acoustic wave penetration depths of the SAW sensor to the different regions within the immobilised Sf9 cells – thus providing the option of examining different regions within a whole cell.

Design shear horizontal wave based SAW (SH-SAW) microsensors – in a resonator configuration for liquid phase applications with central frequencies co-related to the acoustic wave penetration depth on 36° Y-cut X propagating lithium tantalate piezoelectric substrate.

Design Rayleigh surface acoustic wave (R-SAW) microsensors in a resonator configuration on a ST-cut quartz crystal – for vapour phase measurements.

Outline fabrication process steps for both the SH-SAW and the R-SAW sensors. Characterise the SH-SAW devices using a Network Analyser and integrate the SH-SAW devices with an oscillator circuit board.

Design and fabricate a biocompatible, polymer based, microfluidics unit to house the bio-selective coating and integrate it with the SH-SAW microsensor, an automated system consisting of valves, pumps and a temperature controlled incubator.

Develop a protocol for the deposition and characterisation of the Sf9 insect whole-cells in the SH-SAW microsensor surface, thus

demonstrating a novel fully functionalized G-protein coupled receptor (GPCR) cell based sensor.

Acoustically characterise the adherence profile Sf9 insect cells on the SH-SAW microsensor surface.

Examine the concept of ligand specific activation of Sf9 cell membranes proteins using octopamine hydrochloride – an invertebrate neurotransmitter.

1.4 Conclusion and Thesis Outline

This chapter introduced the reader to the field of chemical communication setting the context of the research presented in this thesis. This chapter also outlined the objectives of the work carried out in the subsequent chapters.

The next chapter, Chapter 2, examines key principles of odour detection and how a chemical signal is translated into an electrical signal that can be interpreted by the brain. This chapter provides an overview of the historical and current state of-the art detection techniques employed in the area of olfaction science e.g. electrochemical, optical, resonant microsensors and covering their basic operational principle and recent developments.

Chapters 3 examines how the simplest type of piezoelectric microsensor i.e. thickness shear mode (TSM) microsensor – the Quartz

Crystal Microbalance can be employed as a part of a prototype infochemical communication system to sense different fruit volatiles (chosen instead of odours for the current research). The microsensors were coated with a polymer coating and integrated with an automated chemoreceiver system demonstrating sensitivity to the ratiometric mixture of volatile compounds.

Chapter 4 introduces the reader to the operational principle of SAW microsensors and provides a detailed discussion of the different detection mechanisms involved. This chapter also introduces the reader to the various available design layout and configurations.

Chapter 5 outlines the design principle and the methodology of the SH-SAW and R-SAW sensors. Details of the various fabrication steps involved i.e. mask preparation, lithography etc. has been provided in the Appendix.

Chapter 6 introduces the reader to the various instrumentation techniques employed to characterise the wave characteristics of the fabricated SAW microsensors. This chapter also describes in details the design and fabrication principle of the different microfluidic components and demonstrates how they were integrated with the microsensor and other data acquisition components to form a fully automated test rig functional in liquid.

In Chapter 7, the SH-SAW microsensors were immobilized with Sf9 insect cells and their cell adherence was acoustically monitored. This chapter also demonstrates the concept of ligand-receptor interaction measuring acoustically the interactions between the endogenously expressed receptors on the Sf9 cell surface to a specific neurotransmitter - octopamine hydrochloride, at different concentrations. The chapter also extends the theoretical model developed in chapter 4 to explain the different results obtained.

Finally, Chapter 8 reviews the main aims and objective of the current research, contextualising its key findings and providing the future direction.

CHAPTER 2
Literature Review

2.1 Introduction

Insects are highly flexible, sensitive and free-moving organisms [15]. This understanding originated from the works of three ethologists – Karl von Frisch, Konrad Lorenz and Nikolaas Tinbergen, who were awarded the Nobel Prize in Physiology or Medicine in 1973 “for their discoveries concerning "organization and elicitation of individual and social behaviour patterns"” [16]. Of the three, Karl von Frisch was highlighted for his research on the ““language” of bees” which explained the mechanism adopted by bees to communicate information to each other or to the colony with the most famous being the round dance performed if they found honey close to their hive [16] [17].

The first known study employing invertebrate organisms such as insects, arthropods and arachnids as detectors were conducted by the United States Army in the year 1963 which lead to the development of detectors which could reliably detect intrusion [15]. One of the main reasons for employing insects as detection elements was the high degree of specificity on offer. In addition to this, it was found that insects would usually orient themselves towards the source of the plume or chemical and would also ,in some cases, interrogate specific locations [18]. This fact coupled with the low setup and running cost (e.g. cost of training an insect to recognise an odour molecule - moths and wasps could be trained to detect complex odours in the environment in minutes) was found to be attractive [15] [18].

The olfactory system of insects processes two major types of stimuli i.e. general odorants that signal food, predator and pheromones that are species specific and responsible to transport social and sexual information [19]. Although, there are two classes of stimuli's, from here on the term "infochemical" will be used to represent both as both classes do carry encoded information. Additionally it should be specified that as the work presented in this thesis is only aimed at detecting the odour/pheromone molecules and thus the analysis of the perception generated is beyond the purview of the current thesis.

This chapter begins by providing an overview to olfaction science and how insects detect odour molecules from a plume. That chapter goes on to examine how this knowledge inspired the development of olfactory biosensors in particular whole-cell and tissue-level biosensing techniques. Thereafter, the different classes of olfactory biosensing devices have been introduced along with their detection mechanisms.

2.1 Mechanism of Odour Transduction

Titus Lecretius Carus, the Roman philosopher and poet first described, in 50BC in his only known work *"On the Nature of Things : De Rerum Natura."* , a concept that there exists a plethora of odours in the environment [19][20]. This abstract knowledge was formally recognised and titled "Receptor Theory" by Amoore in the twentieth century [21]. It postulates that perception to a specific odour occurs only when the structure of the odour molecule and the binding sites match [21]. This theory was confirmed by Buck and Axel upon the discovery of the multigene family encoding receptor proteins [6] [19].

Although mammals detect odour through the odorant receptors located in the nasal epithelium, insects detect them through the antenna and the maxillary palp, as shown in **Figure 2.1**. Upon detecting an odour molecule, different downstream reactions are triggered that cause the generation of a neural signal which travels through the central nervous

system (CNS) of the insect finally projecting a perception of the encoded information onto the brain. This perception triggers the relevant behavioural pattern such as location of food, mates, avoiding predators etc. [3]. The antennas are populated with fine hair-like sensilla that are embedded with specialized olfactory receptor neurons (ORN) with each ORN tuned to identify only a specific an odour molecule, **Figure 2.1** [22] [15] [23].

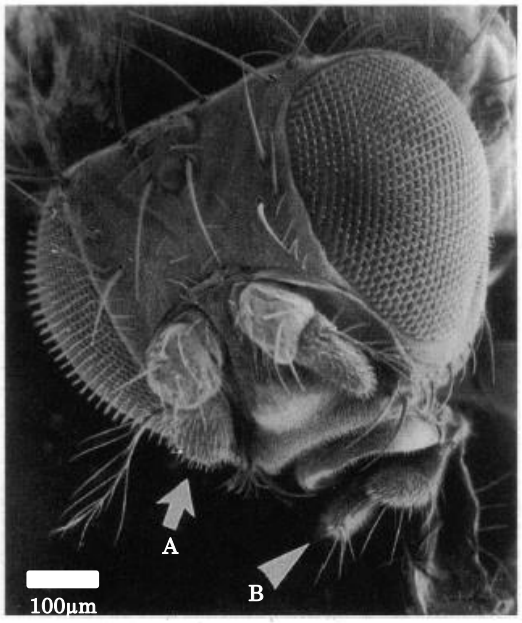

Figure 2.1: Scanning Electron Microscopy(SEM) image of Drosophila head showing the olfactory sensilla (A) and the maxillary pulp (B) [24] [25] [26].

But, Vassar et al. (1994) and Sullivan et al. (1995) found that in mammals, all the ORN's (expressing the same gene) converged to the same glomeruli present in the olfactory bulb [27] [28]. This meant that

activation of an ORN due to a specific odour referred to an activation of single glomeruli with the actual olfactory receptor (OR), which performed the sensing of the odour molecules, being present in the cell membrane – a viscoelastic matrix consisting of GPCR and other transmembrane proteins, in a particular orientation, **Figure 2.2**.

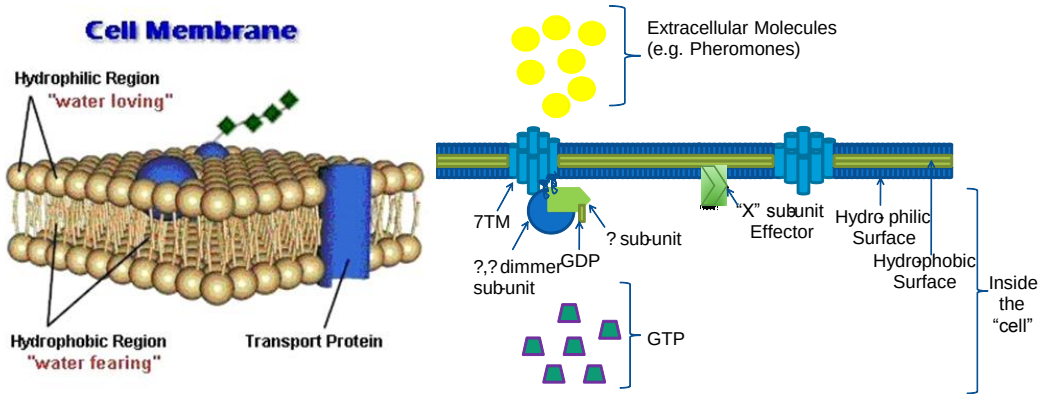

Figure 2.2: The fluid mosaic model of cell membrane along with a simplified view of the odour detection using membrane proteins (A), Insect olfaction through the seven transmembrane receptors (7TM) showing different levels from antennae to membrane [24] [25] [29].

The mechanism of the downstream reaction was characterised by Hu et al. in 1994 who found that upon detection of an odour molecule or a pheromone OR were activated which caused the intracellular cyclic adenosine monophosphate (cAMP) a derivative of adenosine monophosphate, levels in the cell to increase [30]. This elevated cAMP level was responsible in activating different ion-channels causing an increase to the Ca^{2+} ions concentration of the cell [30]. Such activity in-

turn caused the membrane potential of the olfactory sensory neuron (OSN) to be altered generating an electrical impulse which was subsequently processed by the olfactory bulb ultimately leading to the decoding of the significance of the odour plume. It was this ability to detect the volatile ligand/odour via the olfactory receptors at a biologically relevant concentration that played a crucial role in the expansion and development of olfactory biosensors and in the development of odour sensing equipment's [31] [32].

Thus, in order to study such a complex process of signal generation (odour detection and its transformation into an electrical signal), in a laboratory based setting, various olfactory biosensor have been traditionally employed. According to the modern definition, a biosensor is an analytical device that comprises of a biological or a biologically derived sensing layer integrated with a secondary transducer element. There are many different types of biological coatings available to the user, but, of them, whole-cell or tissue level measurements have extensively been employed in olfactory research [25]. The reason being that, although they are highly complex biological recognition elements, whole cells are a great source of intact sub-cellular machinery and provide a ready base for the identification of physiologically relevant events occurring when odour/infochemical recognition takes place at the membrane. Whole cells are also cost

efficient and stable during the production process and can be controlled from batch-to-batch i.e. cell colony age, cycle, etc. [33]. The following section provides a brief overview of the different olfactory biosensing techniques examining its principles and applications.

2.2 Olfactory Biosensing

Research in the areas of olfaction initially started about 100 years ago but a better understanding of the olfaction system and mechanism was only acquired in 1991 when Buck and Alex discovered the multi-gene family in rat, as mentioned earlier [6]. Since their discovery numerous assay techniques have been developed primarily to better understand the mechanism of olfaction or ligand-binding i.e. attachment of an oriented odour molecule (ligand) to a GPCR triggering the specific OR [34]. The research community soon realised that the detection of odorant/ligands by surface receptors at nano-molar (biologically relevant) concentration could also have applications in different areas of science e.g. assessment of food, wine, air quality, cosmetics and fermentation products, which lead to the creation and expansion of the field of olfactory biosensors. Such a biosensor setup consisted of a primary transducer element which could be an olfactory receptor, tissue or animal, coupled to a secondary transducer (electrochemical, optical, and resonant) that would generate the readout signal [25]. Although,

traditionally employed tissue or whole animal biosensing methods e.g. the use of canaries in mines and dogs to sniff-out narcotics, were in use for decades, this perception was soon altered when the ability to harvest biological whole cells transfected with OR's was acquired [35] [36]. This discovery revolutionised the area of olfactory biosensors as smaller devices with the ability to sense concentrations similar to naturally occurring biological processes ($<10^{-2}$ ppb ranges) could then be realised [25][37].

Historically, detection of odour concentrations from drugs, explosives, and different pathologies was carried out by electronic noses (e-nose) in order to remove any physical interference's (human or animal). These techniques offered sensitivity, reliability but lacked selectivity, one of the key requirements in olfactory biosensing. Selectivity of in most electronic nose application could be achieved by off-chip processing of data using neural network and other advances data mining techniques. With the new discovery of harvesting cell's with specific OR's, on chip-selectivity and sensitivity could soon now be realised as odorant molecules were specifically associated with an olfactory receptor and even subtle differences in the structure of the odorant molecule could modify the odour quality or the information being transmitted (in terms of odour sensing in insects). Therefore in order to increase the selectivity the chemically sensitive element of the

e-nose could now be replaced with a bio-e-nose consisting of naturally occurring OR transfected in a cell thus immobilised onto the sensing surface with sensitivities from low ppb range to range's lower than 10^{-6} ppb (in case of animals) [32] - [38] achieved.

Over the past decades various transducer technologies have been employed for the recognition of odorants and more generally have been broadly classified in three distinct categories i.e. electrochemical, optical and resonant **Table 1.** Of these the most employed methods include surface plasmon resonant, quartz crystal microbalance, direct electrochemical measurement and FET (field effect transistors). These methods have been proven to have the ability to detect odorant binding events in a stable manner, which is a prerequisite for high throughput screening and are thus preferred techniques employed in the field of direct olfactory sensing.

The following section review's the different transducer classes, examining their basic principles and reviewing their applications.

2.2.1 Electrochemical Transducers

Electrochemical techniques are one of the three commonly employed techniques in the field of olfaction. They offer the capability of detecting changes in charge accumulation (potential), current

(amperometric) or the conductive (conductometric) properties of the biological film [25].

Transducer Class	Technique	Measurand
Optical	Surface plasmon resonance(SPR), Florescence(including FRET luminescence) Bioluminescence	Light
Acoustic	Piezoelectric Resonators Bulk Acoustic Wave (BAW) Surface Acoustic Wave (SAW) Cantilever base microsensors	Mass
Electrochemical	Impedance/Conductometric Amperometric Potentiometric (voltage clamps, patch clamps, microelectrode array, FET based arrays)	Electrical/Chemical

Table 1: Different transducer classes, measurement techniques along with the respective measurand [25].

An electrochemical biosensor consists of a reference electrode, an auxiliary electrode and a sensing electrode. The sensing electrode serves as the transduction element while the auxiliary electrode provides current to the sensing electrode by establishing a connection to the electrolytic solution [39]. The commercially most employed techniques in this area is the FET based electrochemical sensors [25].

Example of electrochemical techniques employed in the area of olfaction science are electrochemical impedance spectroscopy (EIS),

which measures changes in the electrical resistance at the transducer surface, electroolfactogram (EOG), electroantennagram (EAG), voltage and patch clamping. Other techniques include the use of field effect transistors (FET) and light assessable potentiometric sensor (LAPS) [40].

Electrochemical field effect transistors (FET), are the most employed commonly employed microsensors and consist a metal oxide transistor which has a source, gate and a drain [41]. That gate metal is functionalized with a protein, peptide, nucleic acid which upon adsorption of the ligand or the target molecule causing the gate potential to be altered [41] [42], as shown in **Figure 2.3**.

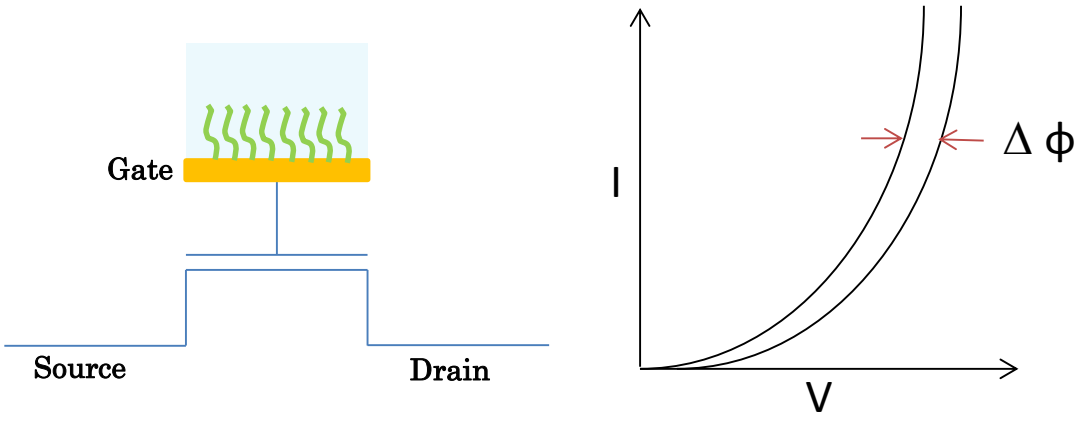

Figure 2.3: A biologically sensitive FET microsensor with an immobilised gate electrode [43].

Although, being sensitive to charge accumulation at the gate electrode, one of the many drawbacks of these types of microsensors is that due to miniaturization of transistor sizes, the oxide thickness decrease causing the gate leakage to drastically increase by orders of magnitude. Another cause of concern is the fact that such family of microsensors are fabricated using standard integrated circuit (IC) complementary metal oxide semiconductor (CMOS) technology [44]. For CMOS, aluminium (Al) is the metal of choice for the top-layer of the biosensor. Al on the other hand is not the preferred material in biosensing applications as it corrodes easily thus post-processing of the gate electrode is required [44]. Another hindrance to the commercial success of such electrochemical based biosensors is the need of an off-chip reference electrode [41] [45].

Other types of electrochemical techniques also include, potentiometric and impedimetric methods which include electrochemical impedance spectroscopy (EIS) [41]. In the former technique, a three electrode system is employed i.e. a reference, a counter and a working electrode. Electrical impedance is then measured between an electrodes with respect to the solution at a spectrum of frequencies [41]. This particular technology has also acquired recent interests in the development of nanotube based sensors based in the nano-meter scale [46].

Yoon et al. have demonstrated a setup in which the human olfactory receptor protein (hOR2AG1) were integrated with a conducting polymer nano- tubes into a FET platform while come authors have reported measuring sensitivities as low as 10's of femto-molar [47] [48]. Different types of electrochemical sensor have been successfully fabricated with different microorganisms acting as the biosensitive coating e.g. *E.coli*, yeast to name a few [49][50][51]. A whole-cell potentiometric biosensor for screening of toxins was proposed by May et al. attaching endothelial cells to a K^+ selective membrane, on which ion transport is almost completely inhibited by a confluent cell monolayer with sensors demonstrating that permeability of the cell monolayer increasing the ionic transfer producing a potential response [52].

Although the electrochemical transducers offer portability, cost-effectiveness and simplicity of operation, they have their own limitations – as outlined above, which include effects of interferents which are electrochemically active. Other limitations include long-term stability and reliability of the electrodes transducer electrodes [53].

2.2.2 Optical Transducers

In optical biosensors a significant change in the transducer response to incoming light is recorded that is caused by a significant changes in the conformation change of the biological layer or due to

ligand-receptor interaction as shown in **Figure 2.5**. Some of the techniques employed in standard optical assays include the measurement of florescence, bio- and chemo- luminescence, adsorbance. Förster Resonant Energy Transfer (FRET) is one of the florescence method which utilises changes (conformation or due to interaction) in the florescent dyed molecule to produce a florescence (increased or decrease) [54] [55].

Another recent popular label-free optical technique employed is the surface plasmon resonance (SPR) which relies on changes in the refractive index of the light incident on the sensor surface[56].

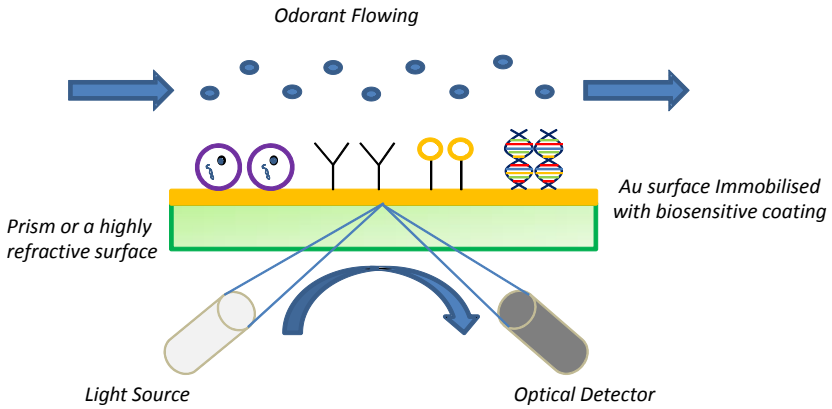

Figure 2.5: Optical technique employed in olfactory biosensing

Surface plasmons can be described as oscillations of the free electron density in a metal. These plasmons are excited when polarized light is diffracted on an interface between a dielectric and the deposited

metal, usually gold, at the angle of total reflection. One way to readout the sensor signal is to measure the intensity of the reflected light for different angles. At the angle where the plasmon's are excited, energy is adsorbed and the intensity of the reflected light has a minimum. This angle depends on the amount of mass adsorbed at the surface, as shown in **Figure 2.6** [41].

This technique has also been employed to characterize bio-molecular interactions in real time without any labelling and more specifically it has been reported in literature that this technique is extensively employed to characterise and study GPCR's [57][58][59]. This technique has also been employed to measure odorant detection by whole cells expressing odorant receptors (HEK-293 cells expressing OR I7) [60][61]. Although, optical transduction techniques are attractive in the field of olfaction due to their ability to reach low detection limits of ligand, the main drawback being their setup cost. Such techniques require a suitable light source which some might require an additional step e.g. sample preparatory stage or a pre-treatment of the surface.

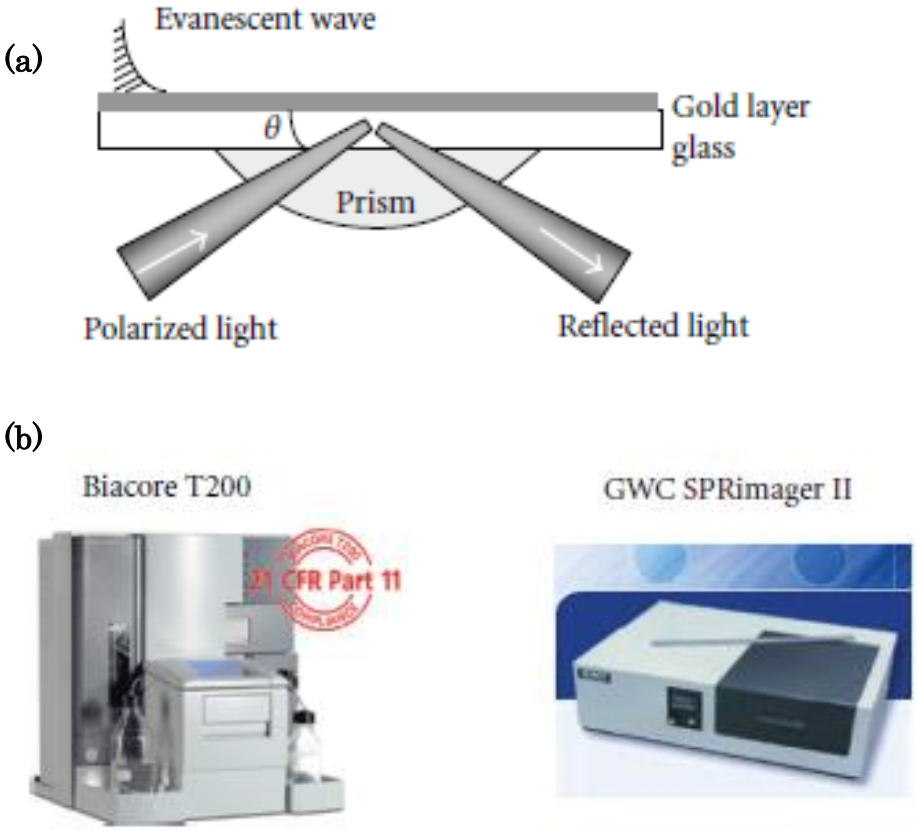

Figure 2.6: Surface plasmon resonance technique which employing light excited plasmons to sense the changes in the immobilized biological layer (a), commercially available SPR detection system - Biacore SPR T200 and GWC SPRImagerII (b) [62].

Additionally, surface chemistry is largely limited to noble metals and calibrations needs to be performed for different buffer solutions (as refractive index is in questions). Such requirements tend to compromise the cost-effectiveness and the portability of a biosensor setup.

2.2.3 Acoustic or Resonant Transducers

Acoustic transducers have been actively employed in the field of telecommunications for over 60 years [63] [64]. This family of transducers are based on the principle of piezoelectricity a property exhibited by a centrosymmetric crystal substrates [65]. According to the principle an electric polarisation is induced in the crystal structure when a strain is induced. The converse principle i.e. development of strain by applying an alternating field is a concept employed extensively in actuation [65].

Piezoelectricity is exhibited by a number of naturally occurring crystal e.g. quartz, although other materials which are employed for sensing applications include lithium niobate, lithium tantalate. Acoustic wave microsensors exploit this principle for the generation of an acoustic wave on the surface or in the bulk of the piezoelectric substrate. Both the types of waves, i.e. surface and bulk waves can be generated in a piezoelectric material by the help of a pair of pair of electrodes lithographically patterned on the surface of the substrate material, **Figure 2.7.**

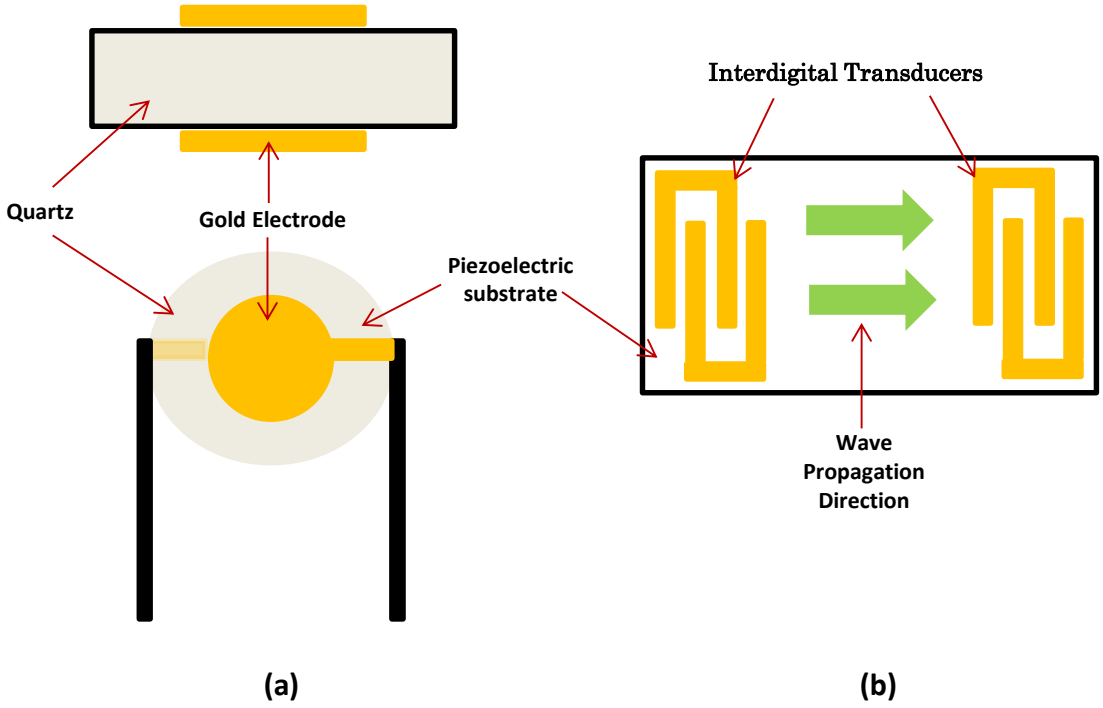

Figure 2.7: Acoustic wave microsensors (a) a Bulk Acoustic Wave (BAW) microsensor and (b) a Surface Acoustic Wave (SAW) Microsensor.

The magnitude and direction of the generated acoustic wave is a function of the piezoelectric substrate and its associated cut and depending on the sensing application a suitable substrate cut is chosen which then determines the type of acoustic wave generated by the patterned electrodes [66] [67] [68].

2.2.3.1 The Piezoelectric Effect

The term "piezoelectricity" was first introduced by Henkel almost a year after the concept was first demonstrated by the Curie brothers in

1880 [69] [70]. The curie brothers, while performing experiments on different crystals, observed that when a tensile or a compressive stress was applied to the opposite faces of a piezoelectric substrate a separation of gravity of positive and negative charges and vice-versa was produced [71][72]. As piezoelectric crystals lack a centre of inversion symmetry, application of strain changes the distribution of charge on atomic bonds resulting in a net electrical polarization, **Figure 2.7** [73]. Thus, a relationship amongst the individual substrate variable i.e. mechanical, electrical and thermal, of a piezoelectric crystal structure could be mapped, as shown in **Figure 2.8** [74].

In 1885, the existence of elastic vibration on the surface of a solid material was first confirmed by Lord Rayleigh confirming the fact that such crystals, demonstrating the property of piezoelectricity, were important in sensing systems. More importantly, two important properties of piezoelectric crystals justify their application in sensor systems [75] [76].

- The presence of a distortion free interface, with low energy dissipation, due to the ideal coupling mechanism between the electrical and mechanical variables.
- The availability of a variety of angular cuts (with respect to the crystallographic axis) thus broadening their application to different sensing applications over a range of frequencies.

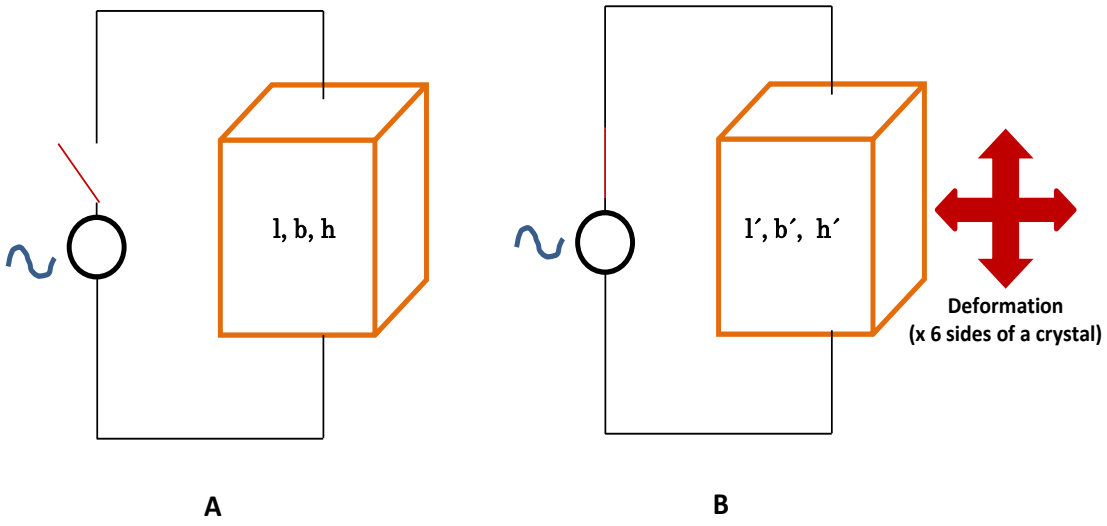

Figure 2.7: Concept of piezoelectricity – on application of an alternating electric field a crystal with dimensions l, b and h, changes to l′, b′, h′ due to the generation of stress on its faces.

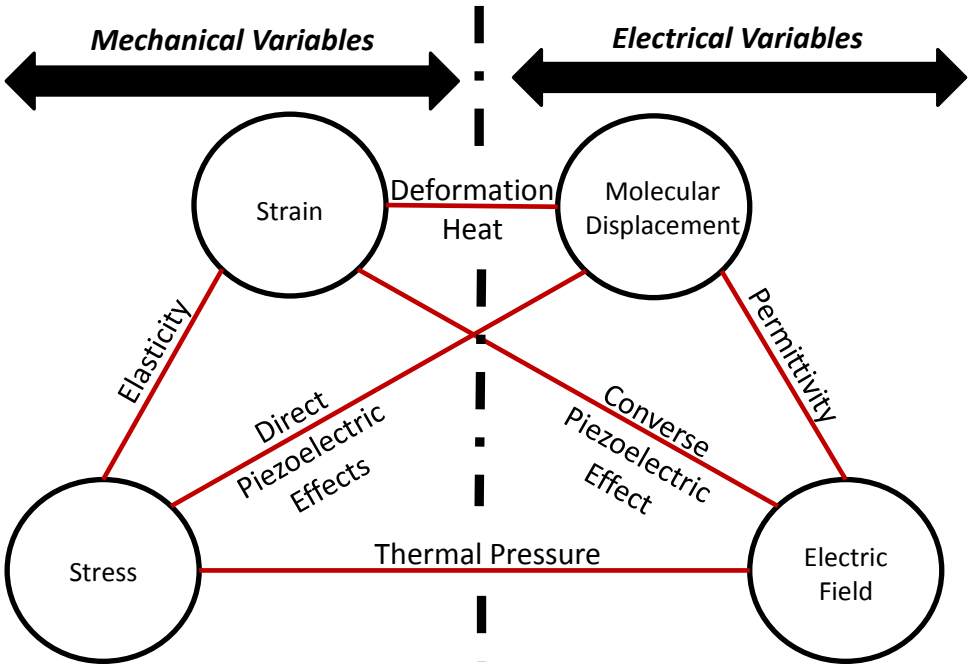

Figure 2.8: The different mechanical and electrical variable relating the stress and strain in a piezoelectric substrate [74].

2.2.3.1.1 Stress and Strain in an Elastic Solid

When an external force is applied on an elastic solid, the stresses and strain experienced by the solid exist in compressional and shear form which can be co-related, in one dimension, by Hook's law of elastic deformation **(Eq. 2.1)**, as shown in **Figure 2.9** [77].

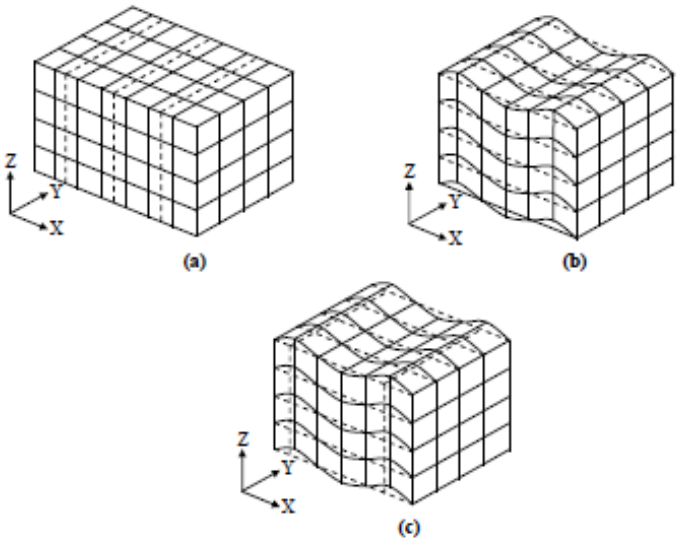

Figure 2.9: Different particle displacement profiles due to the stresses on a solid with (a) longitudinal while both (b, c) being shear .

Assuming that the stress and strain are along the same axis the relation can be expressed by a tensor equation:

$$[T] = [c]:[S] \qquad \text{Eq. 2.1}$$

where c is the elastic stiffness coefficient (Young's Modulus) and S being the strain (dimensionless) suffered by the solid. The tensor equation can then be reduced to the matrix equation taking into account all the other components, as a tensor relates parameters which are dependent on more than one set of co-ordinate axis. On re-dimensioning [T] and [S], we get :

$$[T] = [c] : [S] \qquad \text{Eq. 2.2}$$

In **Eq. 2.2** the elastic stiffness constant, [c], is a 6 x 6 matrix [c] with 36 independent values relating six (reduced) components of stress to six (reduced) components of strain (due to their symmetry properties) thus making only six of the nine elements unique. Out of the 36 independent terms, considering the energy and symmetry, only 21 terms are considered for most crystal structures. Further reduction to the above matrix depends on the choice of appropriate crystal substrate symmetry.

When an electric field (E) is applied to a simple dielectric, e.g. a capacitor, the field causes a distortion of the molecular charge (which is neutral) distribution in the non-conductor resulting in surface charge accumulation which can be related according to **Eq. 2.3**

$$D = \varepsilon_r \varepsilon_0 = eE \qquad \text{Eq. 2.3}$$

where ε_r and ε_o are the relative and permittivity of free space in **Eq. 2.3**. This relation depicted in **Eq. 2.3** does not hold true for piezoelectric dielectrics. The coupling between electrical and mechanical parameters on application of an electric field gives rise to mechanical deformation and vice-versa thus the earlier equation can be modified in terms of a piezoelectric constant matrix [e] such that the charge density by the matrix is given by :

$$D = [e][S] + [e]E \qquad \text{Eq. 2.4}$$

where [S] is the strain and E the magnitude of the electric field. In addition to this, for piezoelectric materials the mechanical stress relationship can be extended to:

$$[T] = [c][S] - [e']E \qquad \text{Eq. 2.5}$$

where e′ is a 3 x 6 matrix and is the transpose of the piezoelectric constant [c]. The value of [e] is dependant of the piezoelectric crystal. For example the following are the values of [e] for different piezoelectric substrates materials:

$$\text{Lithium Tantalate} = \begin{pmatrix} 0 & 0 & 0 & 0 & e_{15} & -e_{22} \\ -e_{22} & e_{22} & 0 & e_{15} & 0 & 0 \\ e_{31} & e_{31} & e_{33} & 0 & 0 & 0 \end{pmatrix} \quad \text{Eq. 2.6}$$

$$\text{Quart} = \begin{pmatrix} e_{11} & -e_{11} & 0 & e_{14} & 0 & 0 \\ 0 & 0 & 0 & 0 & -e_{14} & -e_{11} \\ 0 & 0 & 0 & 0 & 0 & 0 \end{pmatrix} \quad \text{Eq. 2.7}$$

$$\text{Gallium Arsenide} = \begin{pmatrix} 0 & 0 & 0 & e_{14} & 0 & 0 \\ 0 & 0 & 0 & 0 & e_{14} & 0 \\ 0 & 0 & 0 & 0 & 0 & e_{14} \end{pmatrix} \quad \text{Eq. 2.8}$$

The piezoelectric coefficient k^2 the elastic constant c and the dielectric permittivity e can then be related as:

$$k^2 = \frac{e^2}{ce} \quad \text{Eq. 2.9}$$

2.2.3.2 Acoustic Wave Propagation

2.2.3.2.1 The Wave Equation

The wave equation used for the numerical calculation of acoustic wave propagation was proposed by B. A. Auld in 1973 [78][79] can be depicted by **Eq. 2.10:**

$$\rho \ddot{u}_i = T_{i\,j,j} \text{ i, j} = 1,2,3 \quad \text{Eq.2.10}$$

in which ρ is the mass density and U_i the particle displacement. The tensor notation for the above can be written as:

$$T_{i\,j} = c^{E}_{i\,j\,k\,l}\, S_{kl} - e_{kij} E_k \qquad \text{Eq.2.11}$$

$$D_i = e_{ikl} S_{kl} + \varepsilon^{S}_{ik} E_k \qquad \text{Eq.2.12}$$

and the strain-mechanical displacement relation being:

$$c_{ijkl} S_{kl} = c_{ijkl} u_{l,k} \qquad \text{Eq.2.13}$$

In the absence of any intrinsic charge in the material, the wavelength (λ) of the generated elastic wave is much smaller than that of the electromagnetic wave. Thus, neglecting the magnetic effects of the material, it can be said that a [79] (**Eq. 2.14, 2.15)**

$$D_{j,j} = 0 \qquad \text{Eq.2.14}$$

$$E_k = -\varphi_{,k} \qquad \text{Eq.2.15}$$

Simplifying equation **Eq. 2.12** to the tensor form through substitution we are left with:

$$\rho \ddot{u}_{\iota} = c^{E}_{ijkl} u_{l,j\,k} + e_{k\,i\,j}\,\phi_{,jk} \qquad \text{Eq.2.16}$$

$$0 = e_{jkl} u_{l,jk} - \varepsilon^{S}_{j\,k} \phi_{j\,k} \qquad \text{Eq.2.17}$$

The surface acoustic wave is generated on a traction-free surface separating an infinitely thick solid from the free space thus setting $T_{i\,j}$, the mechanical stress second rank tensor component, to zero [80]. Assuming a surface wave which propagates parallel to the surface with a phase velocity (V_r) having amplitude which decays with distance travelled by the wave and assuming the direction of propagation of the wave taken as X_1 or the sagittal plane as shown in **Figure 2.10**

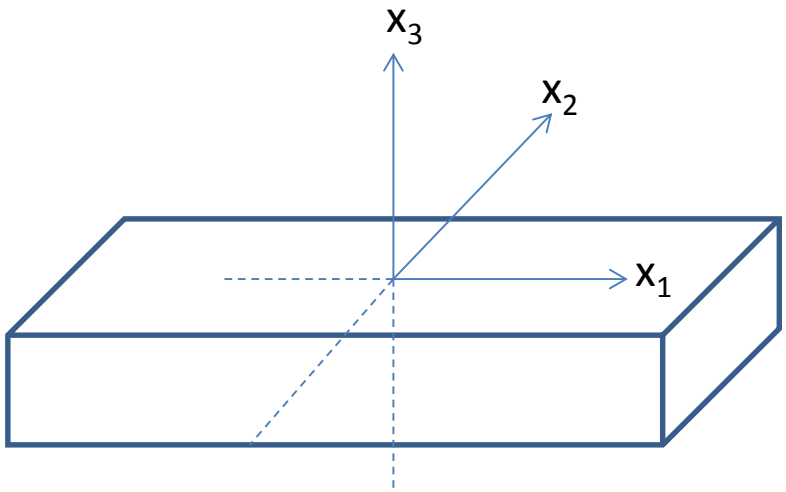

Figure 2.10: Propagation vector of the acoustic waves [78].

The elastic, piezoelectric and the dielectric constants can be substituted with the new coordinates referring to the rotated co-ordinate

system calculated through the transformation matrix. The solution of the surface wave can then be depicted in the form of a linear combination of partial waves which hold the form

$$u_i = A_i \exp(-kx_3)\, exp\left[-j\omega\,(t - {}^{x_1}/_{V_R}\right] \quad \text{Eq.2.18}$$

$$\phi = B \exp(-kx_3) \exp\left[-j\omega\,(t - {}^{x_1}/_{V_R}\right] \text{ as } x>0 \quad \text{Eq.2.19}$$

with ω is the angular frequency of the electrical signal , k being the wave number and λ the wavelength [80].

With the crystal symmetry and the additional boundary, electrical and mechanical, conditions levying a further constraint on the partial wave equation X_1 thus assuming that the sagittal plane is considered as the plane of symmetry of the crystal making X_1 the pure-mode axis for the surface wave and involves only the potential and the sagittal-plane component of the displacement [78] [80]. The Rayleigh wave has no displacement vector component in the X_2 direction. Assuming displacement U_1 and U_3 to have the form of [65] [67] :

$$A\, exp(-bx_3) \exp[jk(x_1 - ct] \quad \text{Eq. 2.20}$$

$$B\, exp(-bx_3) \exp[jk(x_1 - ct)] \quad \text{Eq. 2.21}$$

and $u_3 = 0$. Where the elastic half-space $X_3 \leq 0$, B and A are unknown amplitudes, k is the wave number for propagation along the boundary $x_1 - axis$ and c is the phase velocity of the wave. Physical considerations require b to be a positive real complex part. Substituting the assumed displacement in the Navier-Stokes equation infers

$$\nabla . \tau - \rho \frac{\partial^2 u}{\partial t^2} = 0 \qquad \text{Eq. 2.22}$$

And using the generalised Hook's law for an isotropic elastic solid yields two homogenous equations in A and B [78]. The above equation is a generalised displacement solution equation. These displacements can be depicted as the ones shown in **Figure 2.11** [78]. It can be observed that u_3 is in phase quadrature with u1 thus creating a motional ellipse. At a depth of 0.2λ the sign of u1 changes with an ellipse described above and below this point. At the surface the motion can be described as retrograde and at the bottom the motion is described as propagate, **Figure 2.11** [78].

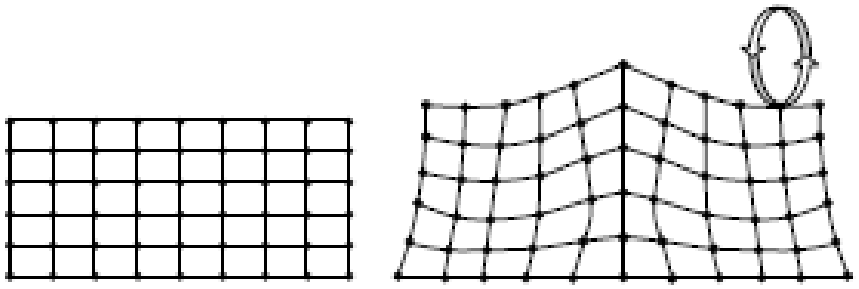

Figure 2.11: Sagittal plane view demonstrating the strain in a piezoelectric substrate due to the application of the field. It also depicts the particle displacement demonstrating the formation of a surface Rayleigh Wave.

This can then be described by the following equations:

$$u_1 = [A_1 \exp(-b_1 x_3) + A_2 \exp(-b_2 x_3)]\exp[jk(x_1 - ct)] \quad \text{Eq. 2.23}$$

$$u_3 = \left(\frac{-b_1}{jk}\right) A_1 \exp(-b_1 x_3) + \left(\frac{jk}{b_2}\right) A_2 \exp(-b_2 x_3) \exp[jk(x_1 - ct)] \quad \text{Eq. 2.24}$$

$$b_1 = k\left(1 - \frac{c^2}{v_l^2}\right)^{1/2} \quad \text{Eq. 2.25}$$

$$b_2 = k\left(1 - \frac{c^2}{v_t^2}\right)^{1/2} \quad \text{Eq. 2.26}$$

The longitudinal and transverse velocities v_l and v_t are given by:

$$v_l = \sqrt{\frac{\lambda+2G}{\rho}}, \quad \text{Eq. 2.27}$$

$$v_t = \sqrt{\frac{G}{\rho}} \quad \text{Eq. 2.28}$$

where the Lames' constant G is given by $E_m/2(1+\upsilon)$ and the wavelength λ is given by $\upsilon E_m/[(1+\upsilon)(1-2\upsilon)]$ with ν being the Poisson's ratio and E_m being the Young's modulus [78].

Acoustic or elastic waves can be described as a particle displacements in an infinite homogeneous medium caused due to an external disturbance, similar to a mass-spring system. The mass-spring system is described by a differential equation of time, displacement and mass, while the former involves a particle displacement which is a function of both time and position of the particle and requires the equation of motion to be more localised e.g. disturbance suffered by a particle at the surface of the medium will be different to the disturbance suffered by a particle deep inside the surface. Although the acoustic waves propagating in a medium is a planar wave, its characteristics are dependent on the properties of the medium. There are two types of planar waves namely the longitudinal and the shear wave with their respective characteristics depending on the polarisation and the propagation direction of the vibrating atom in the medium [79]. For longitudinal waves, the atoms of the crystal vibrate parallel to the direction of propagation, e.g. y-direction as shown in **Figure 2.10**, whereas shear wave is formed when the atoms of a medium vibrates in the x- and z- directions.

The propagating medium is considered as an infinite medium as it helps in the theoretically analysing the different solutions of the wave equation. When boundary conditions are applied to propagating medium, only a particular solution of the wave equation can be analysed, depending on the propagating medium itself, thus changing the nature of the travelling acoustic wave. Thus, different modes of the acoustic wave can be supported within a bounded medium. Of all the planar waves Surface Acoustic Waves are of the greatest interest as these waves travel along the surface of the medium with their amplitude decreasing exponentially away from the surface into the medium, thus they start travelling into the bulk of the substrate .

Due to the nature of the generation and detection of the surface wave, this particular type of microsensors offer sensitivity to different experimental parameter viz. mass, viscosity, density, conductivity and temperature, in real time with an option to extract the dynamic information regarding the kinetic of the bio-recognition layer. It is this property that helps in the realisation of cheap and a reliable alternative to other real-time optical techniques as they offer the same benefit as sensitive optical techniques e.g. SPR. [81] As mentioned earlier in this chapter, the detection of volatile organic compounds can occur by employing a chemical or a biologically derived coating. More specifically acoustic wave microsensors are a class of odour sensors which offer the

versatility to the user in terms of the operational or the experimental phase. This is because the user can choose the type of an acoustic microsensor based on the application or more simply put the operational phase. There are two main classes of acoustic wave devices which are employed for olfactory sensing or as odour sensors. They are the Bulk Acoustic Wave (BAW) and Surface Acoustic Wave (SAW) microsensors [82].

2.2.3.3 Bulk Acoustic Wave (BAW) devices

One of the most extensively employed microsensors of this family is the Quartz Crystal Microbalance (QCM) which consists of a thin disk of AT-cut quartz patterned with circular electrodes, made of gold, on both sides. Application of a potential difference between the electrodes cause the generation of an acoustic wave which travels within the bulk of the crystal, as shown in **Figure 2.12**.

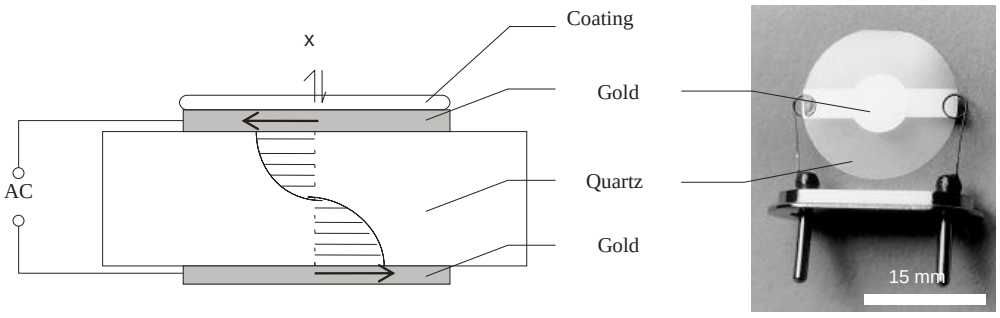

Figure 2.12: A Quartz Crystal Microbalance along with the wave generated shear wave.

Credit for employing QCM based microsensors first as chemical sensors goes to Sauerbray and King [83]. They employed an AT-cut QCM microsensor and observed that the shift in the resonant (design) frequency of the crystal could be co-related to additional or a removal of mass from the device surface. Thus, a mathematical relation describing this relation came to be known by the Sauerbray's equation, represented by **Eq. 2.29** [83].

$$\Delta f \cong -\frac{2f_o^2}{A\sqrt{\mu_q \rho_q}}\, m_f \qquad \text{Eq. 2.29}$$

where f_o resonant frequency, A being the area of the quartz crystal resonator, $\rho_q \; and \; \mu_q$ are the density and the shear stiffness of the quartz, crystal. Perturbation (Δf) to the resonant frequency are measured as a change in the mass/unit area on the surface of the Quartz substrate.

The QCM microsensors have been extensively employed in the area of odour detection and are amongst the three most referred techniques, apart from SPR and FET. More importantly literature indicates that parts per billion (ppb) level odours have been detected by coating the microsensor surface with a variety of functional compounds which include, proteins, enzymes, lipid membranes and polymer coatings

[84] [85]. Polymer based QCM sensor arrays have also been employed in the area of olfaction and have demonstrated sensitivity but the concept of on-site selectivity available due to a biological coating outstrips any advantages which polymer based devices offer. More recently polymer coated QCM microsensors have had more success in the detection of odorants from food, beverages and oils sparking extensive interest in building an olfactory systems which mimics a mammalian counterpart [86].

QCM microsensor arrays have found applications in the area of olfaction because of their ability to sense mass changes on their surface – as governed by the Sauerbray's equation. Literature indicated that the microsensor surface has also been modified by applying different biologically derived coatings which include crude membrane extracts containing olfactory receptors (ORD10), HEK-293 whole cells transfected with ORI7. Such setups have usually been exposed to different odorants such as octanal vapours and concentration dependant experiments have also been successfully demonstrated [38]. Wu et al. in 1999 further demonstrated this concept successfully by immobilizing crude bull frog cilia preparations onto a piezoelectric substrate through which trace levels of odorants were detected. Additionally, the microsensor surface was immobilized partial with fractions olfactory receptors from cilia preparations creating an array of six sensors, in essence a bioelectronics

nose, each consisting of different cilia fractions. This was done to detect the binding of odorants to their associated receptors [87]. Other authors such as Sung et al., (2006) have also coated QCM surfaces with E. coli membrane extract which express ODR-10 receptor and have demonstrated a linear dose-dependent response to an associated ligand diacetyl [88]. Specifically as the application of whole cell based microsensors have attracted special interest in the area of olfaction e.g. HEK293 cells, Sf9 cells, yeast, the use of QCM based microsensors has increased. QCM based microsensors have extensively been employed in several studies to characterise the dynamic process of whole cell coatings [89]. Wegener et al. in 2000 employed a QCM- setup to investigate the time properties of MDCK strains I and II and Swiss 3T3-fibroblasts cell attachment and spreading as a function of seeding density [90]. They reported frequency shifts associated of ~240 – 530Hz (depending on cell type) [91].

QCM's were the first devices manufactured that were relatively simple, supported a thickness shear mode (TSM) and fabricated frequencies ranging between 5 and 30MHz. When using acoustic wave microsensors, it is usually an increase in the central frequency of the microsensor which helps in increasing the sensitivity of the device but this is limited in the case of QCM microsensors. Thus, in order to increase the resonant frequency of the QCM, one would need more

thinner and fragile substrates which is where the potential downside to this technology still remains. For applications requiring higher sensitivities, usually Surface Acoustic Wave (SAW) microsensors have been employed.

2.2.3.4 Surface Acoustic Wave (SAW) devices

The principle of operation of SAW microsensors is conceptually simple as the generated acoustic wave is confined to the surface of a piezoelectric substrate. There are essentially two types of planar waves namely the longitudinal and the shear wave with their respective characteristics depending on the polarisation and the propagation direction of the vibrating atom in the medium. There are different modes of the acoustic waves that can be supported within a bounded medium and the following section will briefly review them.

2.2.3.4.1 Rayleigh Wave

The Rayleigh wave, names after its discoverer Lord Rayleigh (1887) , a British scientist discovered this form of surface acoustic wave. These waves has their energy confined to the surface of a propagating solid [92]. This wave is composed of a longitudinal component that has a

particle displacement parallel to the propagation direction and a transverse component with a particle displacement normal to the surface, as shown in **Figure 2.13** [92].

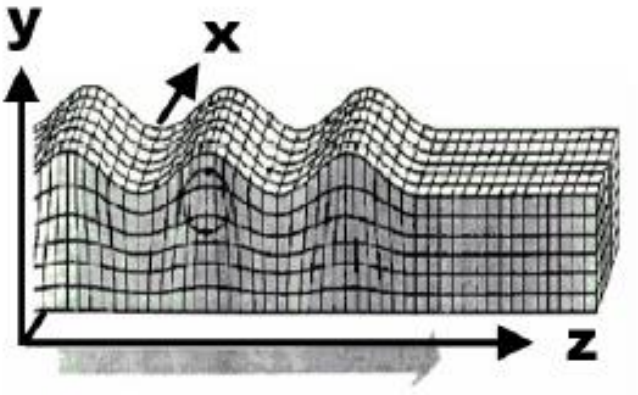

Figure 2.13: Shown is the Rayleigh mode propagation [93].

This particular mode has been extensively employed in chemical and vapour phase sensing applications with later applications in the area of biosensors and immunosensors. This was because of the particle polarisation which was found to be elliptical with the focus on the y-axis [94].

2.2.3.4.2 Shear Horizontal –Surface Acoustic Wave

Traditionally, the term "SAW" has been associated with this particular mode but there are other modes with different particle polarisations as well. The SH-SAW demonstrates little attenuation in

propagation under liquid loading environment and thus leads to better signal to noise ratio and system stability [95]. This is because this particular type of wave has a horizontal polarization in the direction normal to the propagation direction parallel to the substrate, the SH-SAW energy is less radiated into the liquid [96].

This particular particle polarisation has been found to appear in several substrates e.g. lithium tantalate, quartz and Langasite, but for sensing applications in the liquid phase SH-SAW on lithium tantalate substrate is often employed [96][97][98][99] . This helps in the detection of density and viscosity products, along with relative permittivity and conductivity of the liquid [96].

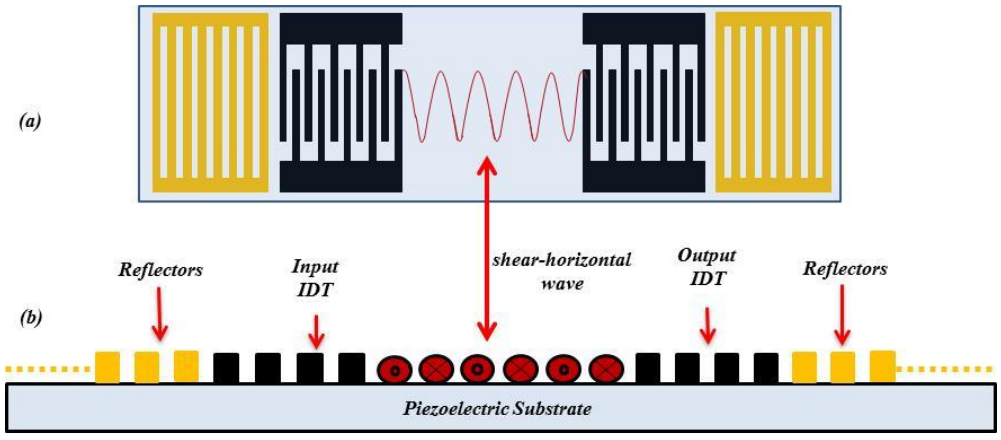

Figure 2.14: A surface acoustic wave microsensor (a) with the generated SH-mode (b).

The first measurements of the adhesion of mammalian cells to microsensor surfaces indicated the usefulness of SAW sensors for the characterization of advanced binding processes [100]. Since then interests in the application of SH-SAW biosensors in the liquid phase to understand ligand-receptor interactions using whole-cells as biological coatings has increased significantly. This is because of their ability to be sensitive to mass changes but also viscoelastic changes. Saintakis et al. employed a 110MHz a shear acoustic wave biosensor based on a Love waveguide configuration to monitor the binding of cells expressing class I Major Histocompatibility Complex (MHC) molecules, to a specific monoclonal antibody that were initially immobilized on the sensor surface, thus in effect demonstrating a label-free biosensor technique [101]. The same author also has performed a comparative analysis between the QCM and SAW microsensors examining and comparing the acoustic signals due to the binding of HLA-A2 molecules to the cell immobilized sensor surface [89].

2.2.3.4.3 Love Wave (SAW) devices

A love wave SAW microsensors are shear horizontal polarized acoustic wave microsensors with a waveguide modes. They are based on

a layered substrate combination with the waveguide layer having a lower shear phase velocity than the substrate, **Figure 2.14**.

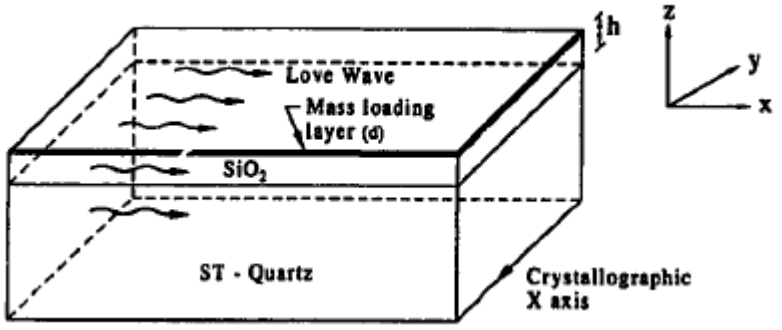

Figure 2.14: A Love wave SAW microsensors consisting of a waveguide on a piezoelectric substrate.

It is this particular property which helps in confining the acoustic wave energy to the surface. These types of microsensors have proven very promising for liquid phase sensor applications as they can be employed to detect the liquid density and viscosity more accurately. Substrate combinations employed for liquid based applications include SiO2/36◦YXLiTaO3 [102] and ZnO/ST-quartz [102] [103] with sensitivities of 6000Hz mm^2/ng being achieved. Traditionally these microsensors were made out of quartz substrate but temperature stability was the key aspect which they lacked. Thereafter different substrates started being employed in this area which included lithium tantalate and lithium niobate [68].

2.3 Conclusions

This chapter provided a brief review of the mechanism of odour detection in insects. The chapter also reviewed the field of olfactory biosensing and demonstrated how different transducer techniques have, employed in this area, evolved along with the different applications. More importantly acoustic sensing techniques have been reviewed providing the user with introductory knowledge to the principle of piezoelectricity, BAW and SAW microsensors. The next chapter demonstrates how quartz crystal microbalance (QCM) a class of BAW microsensors have been employed as a part of a prototype infochemical communication system to detect volatile organic compounds.

Chapter 3
Detection of Volatile Organic Compounds using TSM microsensors

3.1 Introduction

Chapter 2 introduced the basics of olfaction and reviewed the various techniques which have been traditionally employed in the area of cell and tissue level biosensing. Also, explained in Chapter 2 were the concepts of the receptor-ligand interaction and the mechanism of how an odour molecule detected only in a specific orientation can trigger downstream reactions. Thus, *sensitivity* and more importantly a *selective* odour orientation were the key elements which help's insects survive.

Similar to the mechanism of odour emission and detection in insects, a laboratory based prototype infochemical system was developed and has been demonstrated as a part of this chapter. It should be highlighted that this was not an attempt to mimic the natural process of detection with molecular precision, but to test the concept of odour emission and detection in a laboratory (controlled environment) based setting. Mimicking the

process of odour detection in a laboratory setting comes with its sets of challenges. One of the many constraints was cost - in a real environment, insects employ pheromones to communicate social messages but due to the high cost of acquiring real pheromones, volatile organic compounds or fruit volatiles have been used in the current system. The volatiles employed have been found to be detected by most insects and were thus suitable for the experiments to be performed in this chapter [7]. They were cheap, could be acquired easily and in high (milli-litre to litre) volume content.

This chapter introduces the reader to a prototype infochemical communication system and begins by introducing the background theory of a class of Bulk Acoustic Wave (BAW) microsensors – the Quartz Crystal Microbalance (QCM). QCM microsensors have been employed in an array format in the current system. The QCM microsensors were coated with sub 100nm thin organic polymer films in order to elevate their sensitivity. The principle underpinning the selection of the organic polymer coating has been outlined and described in details from first principle. The coated QCM array was then integrated into a prototype infochemical communication system which consisted of a chemoemitter unit and an odour chamber. Initial experiments performed were to characterise the polymer coating and choose the most responsive to the fruit volatiles. Being a prototype communication system, it should be noted that the orientation of the volatile molecules cannot be mimicked and thus instead the volatile organic

compounds were emitted in volumetric ratio pairs (3:1 i.e. 300ml of volatile 1:100ml of volatile 2). This ratiometrically emitted volatile organic compounds were then detected with using the polymer coated QCM microsensor array.

3.2 Quartz Crystal Microbalance

The detection of odorants by employing piezoelectric devices was first proposed by W.H. King in 1964 with researchers adopting and demonstrating the concept later on [104] [105] [106]. Moreover, over the last decade the concept of "electronic nose" has been adopted in order to detect odorant with some research groups adopting an array of piezoelectric devices with pattern recognition techniques [107]. In the field of odour detection TSM based piezoelectric microsensors have been employed extensively as they are highly sensitive to changes in mass and the most widely employed sensors for such an application is the Quartz Crystal Microbalance (QCM) microsensors.

Although, QCM microsensors are sensitive to mass loading effects, in most odour sensing applications, the sensitivity is traditionally increased by the help of organic coatings. There have been various materials proposed which span from monolayer coatings, surface attached molecules to thin polymeric films but it is the latter which has attracted most attention in this area. In addition to increasing the sensitivity the

polymeric coatings also reduces the response time of the microsensor [108]. The following section will outline the polymer selection principle and the protocol followed in order to choose the most sensitive polymer coatings which have been employed for the research presented in this part of the thesis.

3.2.1 Polymer Selection

There are different types of polymer coatings available to the user e.g. polymeric films which work at higher temperatures, soft and rubbery polymers, glassy polymers, but the overall sensitivity of a coating to a volatile depends not just on the nature of the polymeric film but also on the transduction process involved [82]. In order to choose an appropriate organic or inorganic coating which is both sensitive and selective to the target odorant, it becomes crucial to quantify the individual sorbent properties of the polymers themselves [109]. Thus, in equilibrium the sorption of vapour molecules inside the polymeric films can be described by the partition coefficient, K_p, which is a measure of the equilibrium distribution of vapour molecules in the polymer and in the vapour phase, **Figure 3.1** [82] [109].

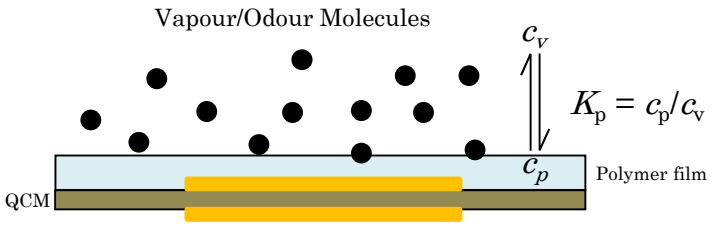

Figure 3.1: Schematic diagram illustrating the absorption of vapour into a polymer layer [109].

These partition coefficients can then be calculated by correlating the properties of the polymeric film to that of the adsorbing vapour molecules using the Linear Solvation Energy (LSER) relationship [110]. The overall solvation process between the vapour molecules and the polymeric films takes place in two distinct steps [111]. The first step is endothermic and involves the formation of cavities on the surface of the polymeric films [111]. This occurs due to the breakage of non-covalent bonds between the polymeric chains and the odour molecules [111]. The second step which is exothermic in nature involves the odour molecules entering the cavity by forming new covalent interactions with the polymeric film [111]. Based on partial co-efficient values reported in literature, obtained by gas-liquid chromatography, the LSER relationship can be constructed which relates the log of the partial coefficients to the parametric properties of the polymer coating +/- solute [111] [112] :

$$\log K_p = k + rR_2 + s\pi_2^H + a\alpha_2^H + b\beta_2^H + llogL^{16} \quad \text{Eq. 3.1}$$

where k is a constant, R_2 is the excess molar refraction, π_2^H is the dipolarity/ polarizability, α_2^H is the hydrogen-bond acidity, β_2^H is the hydrogen-bond basicity, and L^{16} is the gas-liquid partition coefficient on hexadecane at 298 K, while *r*, *s*, *a*, *b*, and *l* are parameters related to the polymer [109] [111]. The observable frequency shift of the QCM due to vapour or gas sorption is directly proportional to K_p through the following relationship:

$$\Delta f \propto K_p C_{vapour} \quad \text{Eq. 3.2}$$

and therefore, for a given odour, the goal is to find a polymer coating (with parameters *r*, *s*, *a*, *b*, and *l*) that maximizes the value of K_p [111]. In typical applications, K_p can be an amplification factor of 10 to 1,000. Typical values are shown in **Figure 3.2.**

It should be noted that solvation behaviour does not at all times dictate the selection of polymeric films. In addition to the theoretical arguments, practical usability should also be taken into account e.g. a

polymeric films should saturate the surface on which it is being applied. Care was taken to select the polymer coating based on practically available resources e.g. it would be helpful to choose coatings which are soluble in commonly available solvents - toluene. Additionally, care was also taken to choose coatings which were immune to changes in their physical state e.g. some polymer films behave as soft, rubbery polymers at low frequencies but behave as glassy polymers at ultrasonic frequencies. For the current work a set of polymeric films were chosen that took into account the above factors [82].

Solute	Structural formula	R_2	π_2^H	α_2^H	β_2^H	$\log L^{16}$
water	H_2O	0.000	0.45	0.82	0.35	0.260
methanol	CH_3OH	0.278	0.44	0.43	0.47	0.970
ethanol	CH_3CH_2OH	0.246	0.42	0.37	0.48	1.485
propanone	CH_3COCH_3	0.179	0.70	0.04	0.49	1.696
butanone	$CH_3CH_2COCH_3$	0.166	0.70	0.00	0.51	2.287
benzene	C_6H_6	0.610	0.52	0.00	0.14	2.786
toluene	$C_6H_5CH_3$	0.601	0.52	0.00	0.14	3.325
n-hexane	$CH_3(CH_2)_4CH_3$	0.000	0.00	0.00	0.00	2.668
n-octane	$CH_3(CH_2)_6CH_3$	0.000	0.00	0.00	0.00	3.677
ammonia	NH_3	0.139	0.35	0.10	0.62	0.680

Linear solvation energy relationships (LSER) regression coefficients for selected polymers at 25 °C:

Polymer	*k*	*r*	*s*	*a*	*b*	*l*
SXFA	-0.08	-0.42	0.60	0.70	4.25	0.72
FPOL	-1.21	-0.67	1.45	1.49	4.09	0.81
SXPYR	-1.94	-0.19	2.43	6.78	0.00	1.02
PEI	-1.60	0.50	1.52	7.02	0.00	0.77
SXCN	-1.63	0.00	2.28	3.03	0.52	0.77
PEM	-1.65	-1.03	2.75	4.23	0.00	0.87
SXPH	-0.85	0.18	1.29	0.56	0.44	0.89
PIB	-0.77	-0.08	0.37	0.18	0.00	1.02
OV2O2	-0.39	-0.48	1.30	0.44	0.71	0.81
PECH	-0.75	0.10	1.63	1.45	0.71	0.83

(Data from McGill et al. 1994)

Figure 3.2: The different properties of the polymer and their corresponding solute according to the LSER relationship [82].

Polymer	Polymer Acronym	Solvent Mix
Poly(styrene-co-butadiene)	PSB	Toluene
Poly(ethylene-co-vinyl acetate)	PEVA	Toluene
Polycaprolactone	PCL	Toluene
Poly(methyl methacrylate)	PMMA	Toluene
Poly(ethylene glycol)	PEG	Toluene
Poly(4-vinylphenol)	PVPH	Ethanol
Polyvinylpyrrolidone	PVPD	Ethanol
Poly(Bisphenol A carbonate)	PBA	Dichloromethane
Polysilfone	PSF	Dichloromethane

Table 2: Polymers selected to coat the QCM microsensors

3.2.2 Polymer Preparation and Deposition Procedure

In order to deposit the polymer solution various methods are available to the user which include, dip coating, spin coating etc. but for the research carried out in this thesis drop coating method was employed due to its simplicity and ease of use [113]. The polymers were deposited according to the procedure outlined in **Figure 3.2** creating a sub-100 nm thick gas sensitive polymer layers [(thickness calculated by using the Sauerbray's Equation). Care was taken to make sure that only the surface which was coated with the polymer was kept up at all times in order to achieve detection consistency [114].

The coated sensors were heat treated to completely removal any residual solvents. The polymer coated QCM's were employed as a part of a prototype infochemical communication system as described below.

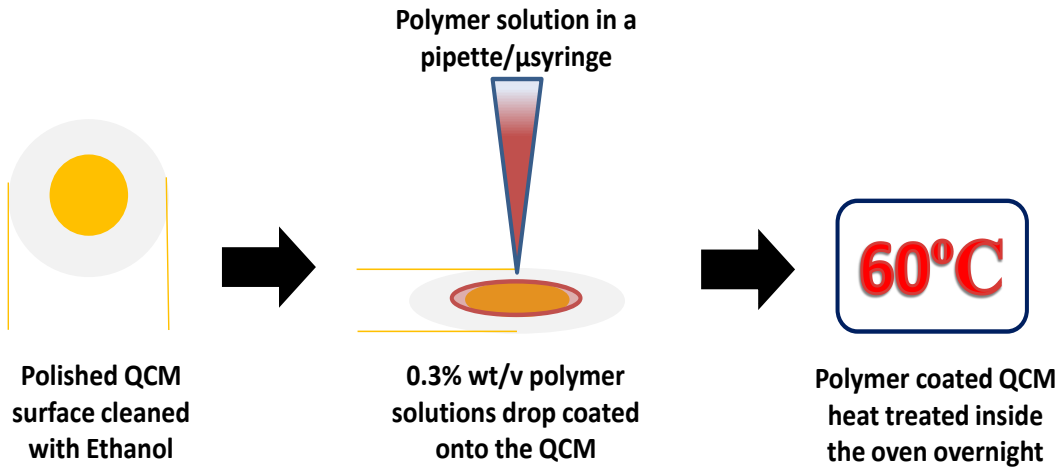

Figure 3.3: Polymer deposition procedure

The polymer coated QCM sensors were integrated into the prototype communication system. The following section describes the system in details.

3.3 The Prototype Infochemical Communication System

The prototype communication system developed in-house and consisted of a chemoemitter, an odour chamber and a chemoreceiver unit

3.3.1 The Chemoreceiver Unit

The prototype chemoreceiver setup consists of a 4 channel commercial available JLMQ USB interface (acquired by JLM Innovation, Tübingen, Germany) board. The board consists of a 4 channels input and a data port which acts as the output. **(Figure 3.4)** The polymer coated QCM's were attached to 3 of the 4 channels with an uncoated QCM attached to the 4th channel. A complementary software package accompanying the JLMQ board – Multisens, was acquired to plot the frequency response of the polymer coated QCM microsensors.

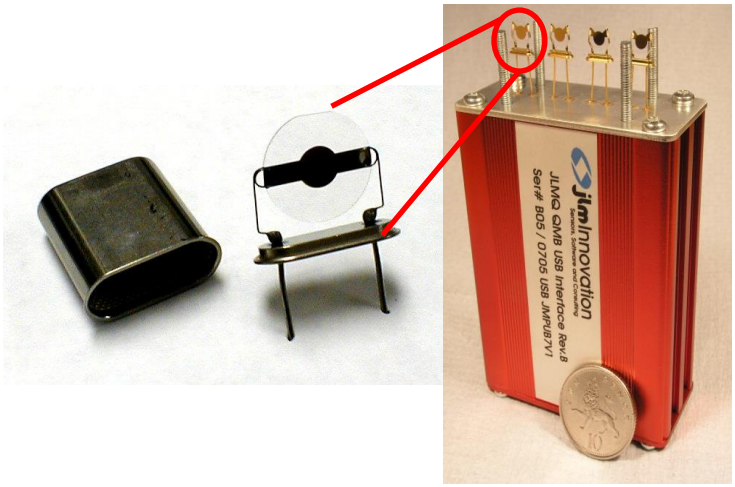

Figure 3.4: The four channel JLMQ USB Interface Board (courtesy JLM Innovation, Tübingen, Germany)

3.3.2 The Chemoemitter Unit

The chemoemitter consists of an automated syringe pump capable of delivering µl volume of the volatile mixtures. The unit consists of a pair of µl (Hamilton 0.5µl and SGE 0.1 µl) syringes attached to a commercially available neMESYS syringe pump platform. **(Figure 3.5)**

Figure 3.5: A 5 channel neMYSYS automated syringe pump platform.

The most critical component of the chemoemitter setup were the fruit volatiles mixtures that would form the content of the syringe pump. For the research presented in this thesis fruit volatiles were chosen as a substitute for real pheromones because of the cost effectiveness of the mixtures and the ability to get them commercially. The volatiles chosen for the work presented in this thesis formed the major components of apple hawthorn and dogwood volatile blends were used in the present study, **Figure 3.5**.

This selection of fruit volatiles was recommended by iCHEM project partners. The four important volatiles made up 81 and 97.3% all the 3 chosen components which were detected by most insect species. These include:

- Ethyl Acetate,
- 3 –Methylbutan-1-ol
- Butyl hexanoate
- Hexyl butanoate

Chemical	GC (%)
Apple	
butyl hexanoate	37
pentyl hexanoate	5
propyl hexanoate	4
butyl butanoate	10
hexyl butanoate	44
Hawthorn	
butyl hexanoate	0.01
3-methylbutan-1-ol	4
isoamyl acetate	1.5
4,8-dimethyl-1,3(E),7-nonatriene	0.09
ethyl acetate	94.3
dihydro-β-ionone	0.10
Dogwood	
β-caryophyllene	5.8
3-methylbutan-1-ol	27.5
isoamyl acetate	0.9
1-octen-3-ol	9
ethyl acetate	54.9
dimethyl trisulfide	1.9

Figure 3.6: The different volatile components of Apple, Hawthorn Dogwood [115].

3.3.3 The Combined Communication System

The polymer coated QCM arrays were attached to the chemoreceiver unit which was then fitted to the odour chamber. The baseline was recorded after polymer coating was deposited onto the QCM microsensors. At discrete intervals the volatiles were released (in pre-defined volumes) into the odour chamber which after travelling through the chamber, were detected by the polymer coated QCM array, integrated with the odour chamber, as shown in **Figure 3.8**. After each injection the odour chamber was vented using an air pump which was located diagonally opposite to the syringe pump inlet **(Figure 3.8)**. The constant air circulation facilitated by the pump facilitated in removing the residual odours after each measurement. The combined prototype infochemical communication system was shown in **Figure 3.7**.

Previously experiments were carried out, by other group members, at the University of Warwick in order to classify the four volatile components. The experiment entailed injecting the four volatile components into the odour chamber **(Figure 3.7)** in three random ordered sequences. The injected volatile components were then detected by polymer coated QCM array (setup exactly the same as in **Figure 3.8**). The change in mass/unit area at the polymer coated QCM surface resulted in a shift in the QCM's resonant frequency, according to the

Sauerbray's equation. The extracted frequency shifts were classified using Linear Discriminant Analysis (LDA), shown in **Figure 3.8**

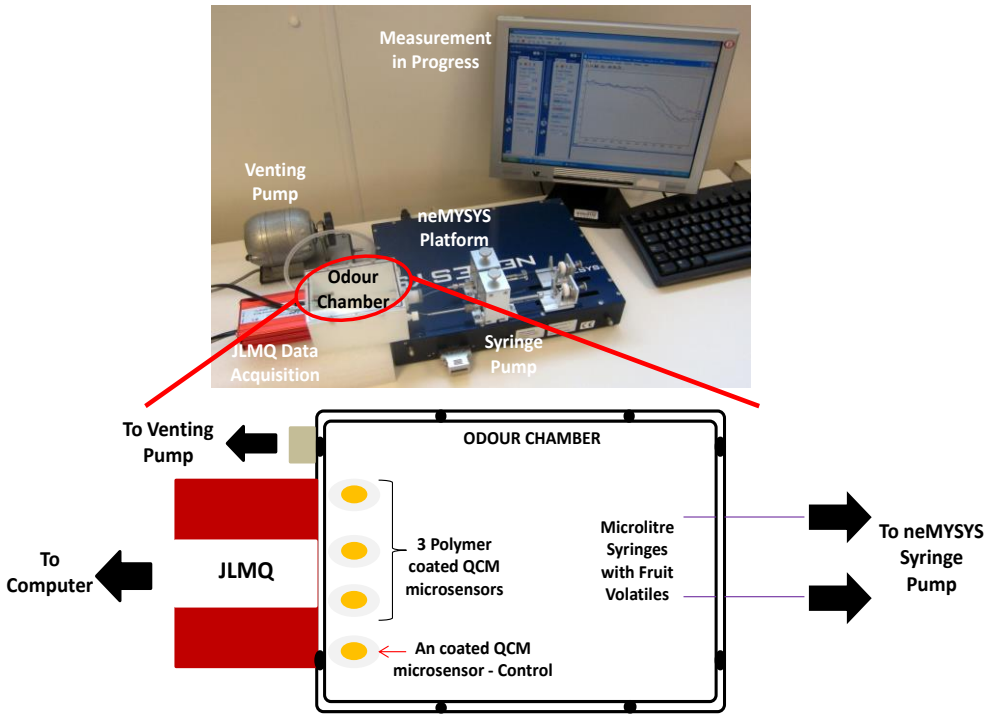

Figure 3.7: The prototype infochemical communication system also showing the exploded view of the odour chamber.

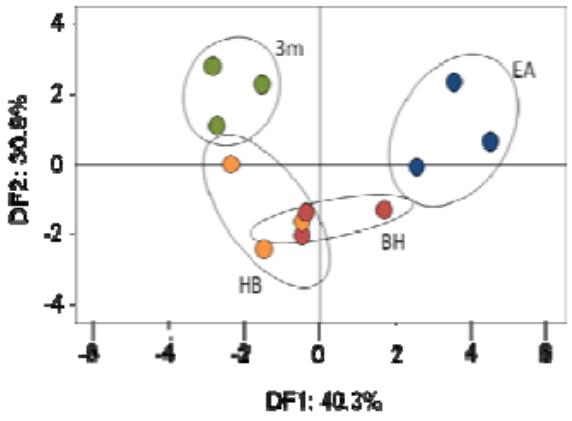

Figure 3.8: Linear Discriminant Analysis (LDA) of the four fruit blends, 3 – Methylbutan-1-ol (3M), ethyl acetate (EA), hexyl butanoate (HB) and butyl hexanoate (BH) [10].

It can be observed from **Figure 3.8** that out of the four blends, ethyl acetate and 3 –Methylbutan-1-ol could be linearly separated while attempts to separate hexyl butanoate and butyl hexanoate failed. This result can also be attributed to the chemical group similarity between hexyl butanoate and butyl hexanoate and vice-versa for ethyl acetate and 3 –Methylbutan-1-ol. Thus, instead of employing all the four volatile components, only ethyl acetate and 3 –Methylbutan-1-ol were used in all future experiments.

After characterising the volatile organic components, sensitivity analysis of the different polymer coating was carried out.

3.4 Polymer Sensitivity Analysis

3.4.1 Experimental Methodology

The main aim of this particular experiment was to characterise the sensitivity of all the nine different coatings. Finally, the three most sensitive polymer coatings would be chosen for future experiments. At this juncture an argument can be made for the use of all the nine coatings in a single experiment, but for the work presented here the ability of the JLMQ data acquisition card was the constraining factor as it provided only four output channels **(Figure 3.4, 3.7)**. Thus, the final system was envisioned to consist of an array of four QCM microsensor

with three of four coated with a sensitive polymer coating while one left uncoated (act as a control).

Nine different polymers coated QCM's were sorted into three groups, as shown in **Table 2**. No particular sorting methodology was employed although attempts were made to make the group as varied as possible i.e. based on the solvent employed to prepare the 2% wt/v polymer solution. For each experiment the volatile organic components were injected into the testing chamber in two random sequences and in a volumetric ratios of 100nl:0 and 0:100nl i.e. 100nl of ethyl acetate (100:0) and 100nl of 3 –Methylbutan-1-ol (0:100). As this was a sensitivity measurement, the volume of volatiles was kept as low as possible – again limited by the setup.

QCM/ Batch	QCM I	QCM II	QCM III	QCM IV
I	PSF	PSB	PVPH	Uncoated
II	PCL	PVPD	PBA	Uncoated
III	PEVA	PEG	PMMA	Uncoated

Table 3: Three batches of 9 polymer coatings with an uncoated QCM microsensor as a reference

3.4.2 Experimental Results

A typical response of a batch of QCM microsensors has been provided in **Figure 3.9** with each measurement repeated twice. The figure shows shift in the QCM resonant frequency **(Figure 3.9 a)** at the instant when the volatiles were injected and the system was ventilated.

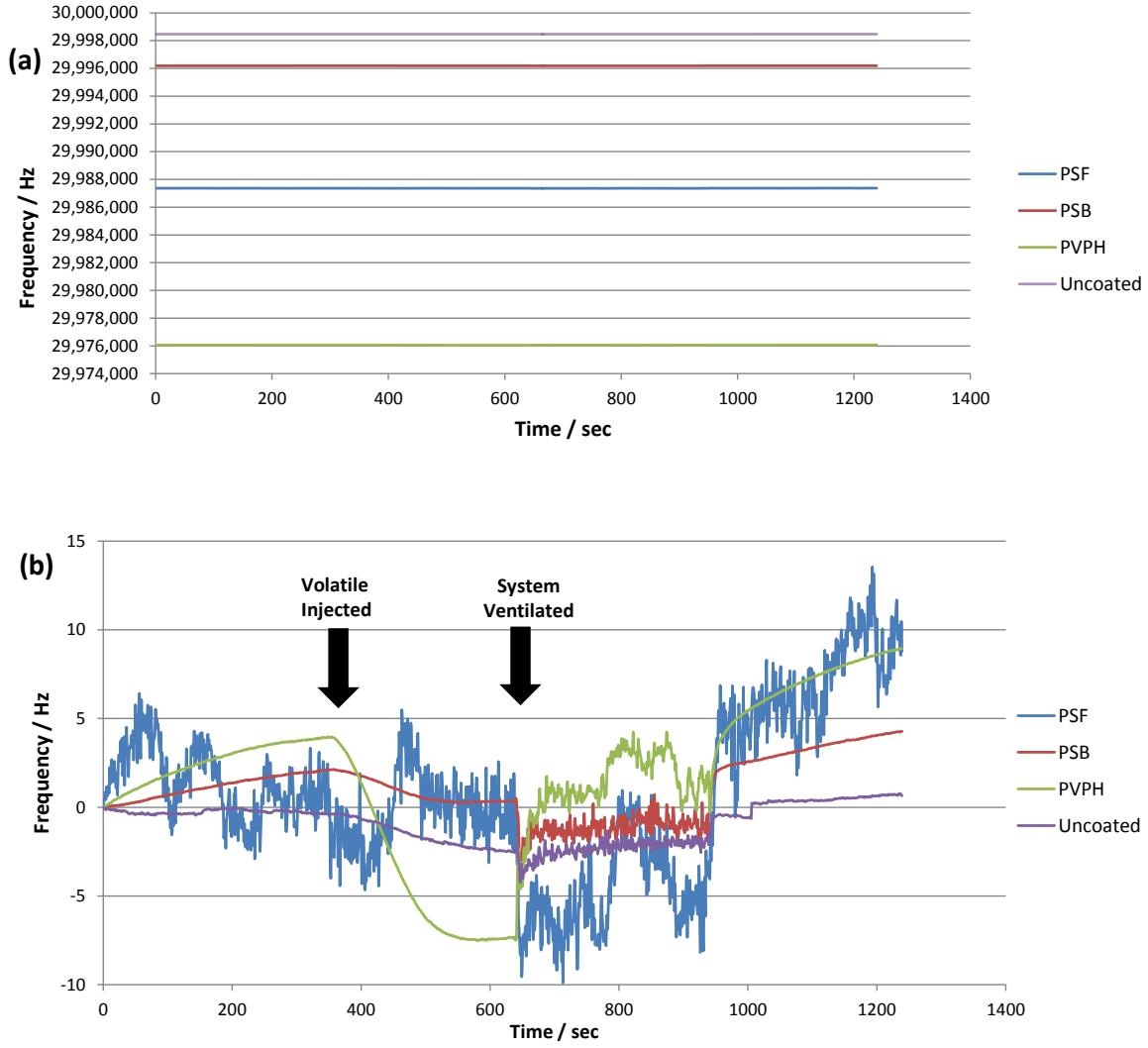

Figure 3.9: Frequency response of the polymer coated QCM microsensors (a) the resonant frequency shown (b) the offset removed plot showing the response with better resolution

Parts per million frequency changes are not visible when the resonant frequency plot is viewed **(Figure 3.9 a)**. Therefore, offset was removed (which entails subtracting the frequency values from the starting value) from the plot in order to better the resolution and thus showing the shift in the resonant frequency, **Figure 3.9b**. **Appendix A** provides the list of plots of each of the six experiments while **Table-4** provides the extracted values.

	QCM 1	*QCM 2*	*QCM 3*	*QCM 4*
	Frequency Response / Hz			
Batch I	**PSF**	**PSB**	**PVPH**	**Uncoated**
3-methylbutan-1-ol	**Noisy**	**3.2**	**3.7**	**1.8**
ethyl acetate	**Noisy**	**0.5**	**0.5**	**- 0.6**
II	**PCL**	**PVPD**	**PBA**	**Uncoated**
3-methylbutan-1-ol	**17.8**	**2.4**	**5.2**	**2.2**
ethyl acetate	**0**	**0**	**0**	**0**
III	**PEVA**	**PEG**	**PMMA**	**Uncoated**
3-methylbutan-1-ol	**6.1**	**6.3**	**3.3**	**3.1**
ethyl acetate	**0**	**0**	**0**	**0**

Table 4: Frequency response of various polymers to 3-methylbutan-1-ol (3M) and ethyl acetate (EA)

From **Table-4** it can be inferred that PEG, PCL, PEVA and PVPH produced the greatest frequency shifts in response to 3-methylbutan-1-ol while the responses of PSF, PSB, PVPD and PMMA coated QCMs were similar to that of the experimental control. The response to ethyl acetate was within the error of the measurement for all polymers. After

extracting the shifts in the resonant frequency, it was inferred that out of the nine available polymers PSB, PEG and PCL were the most sensitive in their response to the injected blends.

Thereafter, in order to test the concept of chemo-transmission and reception, the selected coatings were exposed to different (1:3, 3:1, 1:1) volumetric ratios of the fruit volatiles (ethyl acetate and 3 methyl butanol).

3.5 Infochemical Communication

As explained earlier, the main aim of this chapter was not to mimic nature but to test the concept of chemo-transmission and reception. In order to study this effect, in a laboratory based setting, volumetric concentration of fruit volatiles were tested. In real world the orientation of the pheromone determines the type of information transmitted or received but for the experiments carried out in this thesis, different volumetric ratios (1:3, 3:1, 1:1) of blends were transmitted and detected by the polymer selected from the sensitivity analysis.

3.5.1 Experimental Methodology

Nine different mixtures (volumetric) of 3-methylbutan-1-ol and ethyl acetate of varying concentrations (1, 2 and 3 units, 1 unit = 100nl)

and ratios (3:1, 1:1 and 1:3) were prepared. In order to eliminate the effects of various unaccounted factors e.g. memory effects of the polymers, system, the injection sequence was repeated four times (different run's) with each individual injection order being randomised i.e. 36 injection sequence were randomised regardless of groups and ratio's. It was expected that the injection at the given ratio would produce a corresponding frequency change. By plotting the frequency changes of a polymer coated QCM against another (ideally uncorrelated) one can rev create nine well-defined clusters each corresponding to a concentration ratio as shown in **Figure 3.10**.

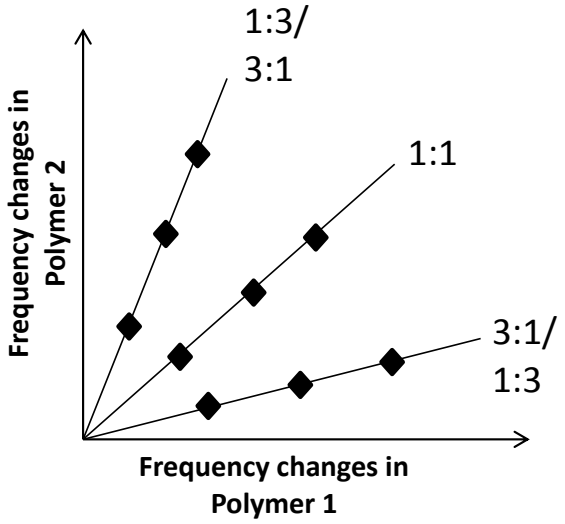

Figure 3.10: Expected response to the injected volumetric ratio's

3.5.2 Experimental Results

Although, the polymer coated QCM's were able to detect the fruit volatile injections, ratiometric information could not be extracted. The degree of clustering which could be observed was not enough to separate the injected fruit blends. **Figure 3.11** relates the frequencies of the two polymer coatings – PSB and PCL. The information from only these two polymer coatings was extracted as the third coating demonstrated a highly noisy signal. This particular experiment proved that although such a system could transmit volumetric ratio of blends, their detection was highly correlated due to the overlapping sensitivities of the polymer coatings.

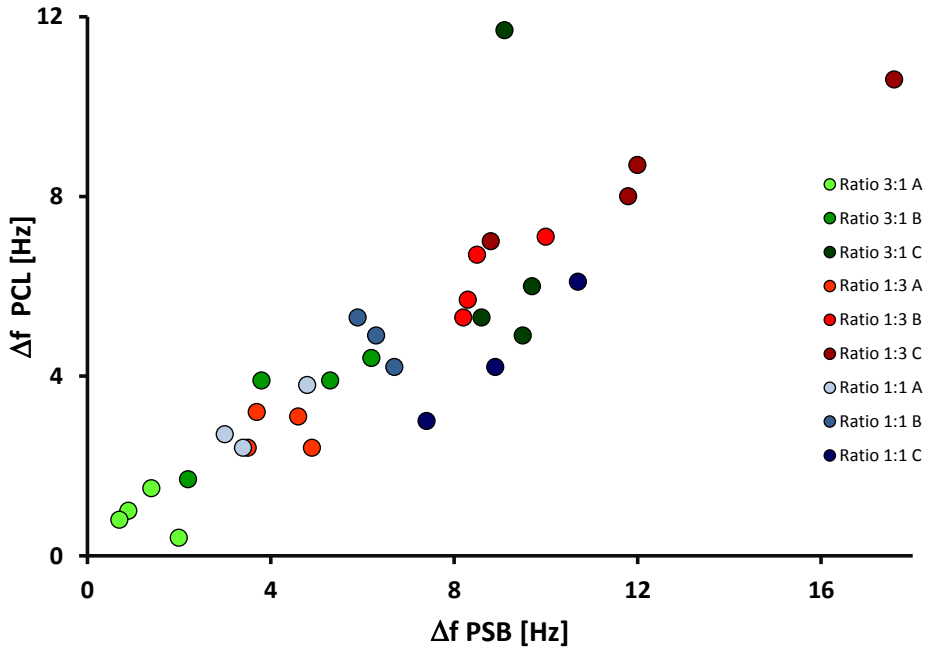

Figure 3.11: Ratiometric information decoded

3.6 Conclusions

The current chapter demonstrated the concept of semiochemical detection by the help of a novel prototype infochemical communication system consisting of a chemoemitter unit (syringe pump, fruit volatiles) and a chemoreceiver unit (polymer coated QCM's). An odour flow chamber form the environment of this communication system through which the emitted volatiles flowed towards the chemoreceiver unit comprising of polymer coated quartz crystal microbalances (QCM). Experiments to characterise the polymer coating were successful and helped in the selection of the three most sensitive coatings.

In order to test the concept of infochemical communication, experiments were carried out in which ratiometrically encoded fruit blends were transmitted. The encoded blends were detected using the polymer coated QCM's. Although attempts were made to correlate the measured frequency responses to the injected fruit volatile concentration ratios were successful, the decoding of ratiometric information in the form of volatile fruit blends had limited success.

Chapter 4
Acoustic Wave Microsensors – wave perturbation and detection mechanisms

4.1 Introduction

The previous chapter demonstrated a prototype system which was able to dispense and detect volatile organic compounds. Although, the emitted volatiles could be detected by the help of polymer coated QCM array, sensitivity and selectivity was found to be the main points of concern. There are numerous ways by which the sensitivity of a system can be elevated. Traditionally, they have been increased by fabricating microsensor at higher resonant frequencies. Such a step wouldn't be feasible for the current setup as this would entail fabricating electrodes on thinner and more fragile layers of quartz substrate in-turn raising

the point of practicality and handling efficiency. Another way would be to completely replace the QCM microsensor array with another family of acoustic wave microsensors - the Surface Acoustic Wave (SAW) sensors.

Historically, SAW microsensors have been designed and employed for the detection of chemical components e.g. toxins vapours, and have shown to demonstrate a higher mass sensitivity compared to QCM array's [114] [117]with recent applications also involved in detecting toxin's in liquid phase [118]. One of the many advantages of employing this class of microsensor is the flexibility offered to the designer to fabricated microsensors with higher operational frequencies without compromising the substrate thickness. This class of microsensors also offer sensitivity to different electrical and mechanical parameters viz. viscosity, density, permittivity and conductivity.

This chapter aims to examine the various detection mechanisms involved in the SAW microsensors employed for liquid phase applications.

4.2 Surface Acoustic Wave (SAW)

4.2.1 Properties

In order to understand and explain the basic operational mechanisms of acoustic wave microsensors the generation and detection

of the acoustic wave first needs to be understood. This knowledge can then be combined along with the different available designs and configurations to understand the acoustic wave perturbation and other mechanism involved during the operation of the microsensors.

SAW's are guided waves that are generated on a piezoelectric solid surface. This was first demonstrated by Lord Rayleigh in 1885 [75]. These waves later came to be known as the Rayleigh waves and had a particle displacement profile normal to the substrate surface with the trajectory being elliptically polarised, **(Figure 4.1 a).** Their application in sensing various vapours (octane and tetrachloroethlelene) and toxins has been reported by several authors [119] [120]. But, when loaded with liquid they were found to radiate a longitudinal wave triggering an actuation process [121].

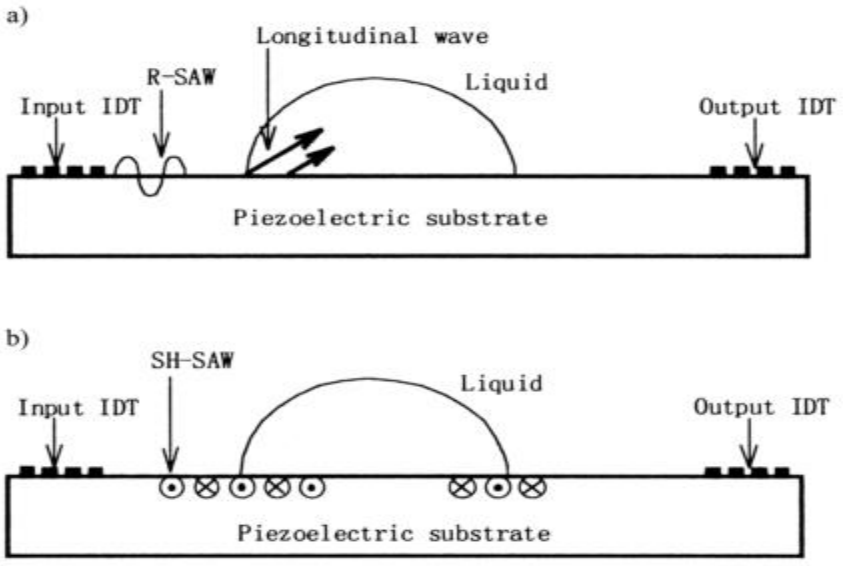

Figure 4.1: Schematic illustration of the Rayleigh (a) and SH SAW (b) [121].

Due to this the wave energy of the Rayleigh mode is lost into the liquid and causing the surface wave to suffer from higher attenuation [122]. In contrast to the Rayleigh SAW mode the Shear Horizontal SAW (SH-SAW) mode was able to function at the interface between the liquid and substrate, with minimal wave attenuation, as the wave had a shear horizontal polarisation, **(Figure 4.1 b).** This mode was reported in 1977 by Nakamura et al. with their first application in a liquid sensor reported by Moriizumi et al. in 1987 based on 36° rotated Y-cut X-propagating lithium tantalate substrate material [123].

The next section provides an overview of the various geometry of a SAW microsensor and how different available configurations support the generated acoustic wave.

4.2.2 Operational Configurations

Variations in the different acoustic wave microsensor configurations stem from the basic fact that different sensing (biological or chemical) applications require one or more optimised aspect of a sensor design. Initial distinctions on the overall design of a SAW microsensor can be made according to the number of connections or "ports" that are present on the sensor surface. A one port microsensor consist of a single pair of electrodes which acts as both the input and output transducer, while a dual or two port microsensor design consists

of two pairs of electrodes with one acting as an input transducer, which generates the acoustic wave, while the other acting as the output transducer, which detects the generated acoustic wave, **Figure 4.2** [73].

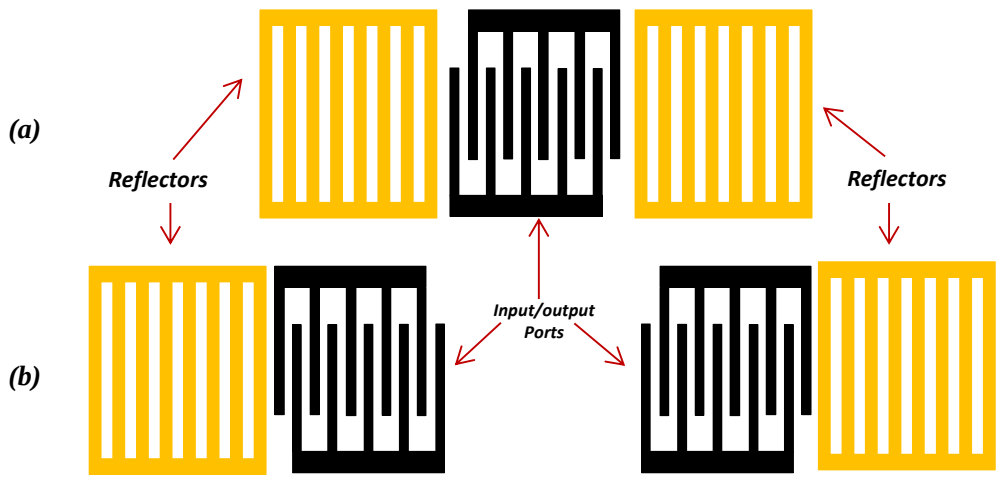

Figure 4.2: Single port SAW sensor (a) and a dual or two port SAW sensor (b)

There are essentially two different classes of SAW microsensor designs. They are the delay-line, **Figure 4.3 a,** and a resonator, **Figure 4.2**. In a delay-line design, the SAW microsensor consists of a pair of interdigitated transducer's (IDT's), which are comb-shaped and are placed in an alternating polarity arrangement, separated by a delay path. On application of a time-varying potential, the IDT's, through the phenomenon of piezoelectricity, generate an acoustic wave that propagates on the surface of the piezoelectric substrate and after travelling through the delay-path or the sensing area, is detected by the

second pair IDT's or the output port that are responsible for converting this acoustic impulse into a readable electrical signal, **Figure 4.3 a**. Thus, the name delay-line as generated acoustic wave is detected after a time-delay.

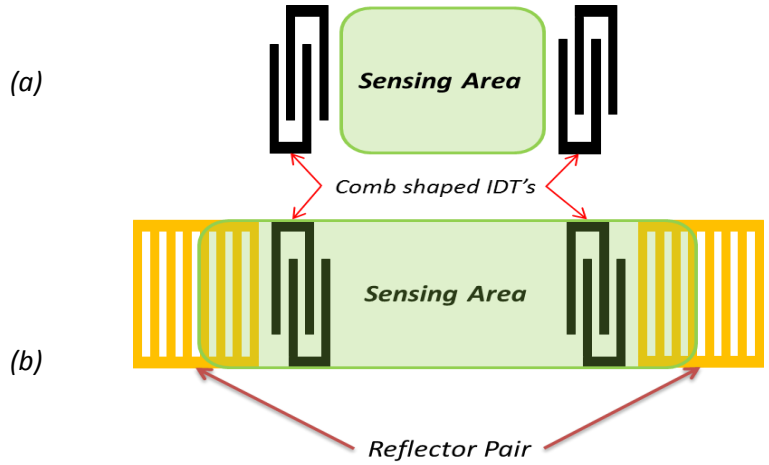

Figure 4.3: A SAW delay line sensor (a) and a SAW resonator sensor (b)

In a resonator design, in addition to a set IDT's, a set of acoustic grating known as reflectors or acoustic mirrors are placed on either side of the transducers to form a closed acoustic cavity, as shown in **Figure 4.2, Figure 4.3b**. Traditionally, they are either grooved inside or patterned on the piezoelectric substrate surface. Their function is to help in the construction of a standing wave pattern by confining and successively reflecting the generated acoustic wave [1] [124]. This particular property of a SAW resonator helps in increasing the Q factor

(or quality factor) of the microsensor when compared to a delay-line design [125].

4.3 Acoustic Wave Perturbation

The travelling acoustic wave, between the input and the output IDT's is perturbed by variation in the properties of the sensing area which could be loaded with either liquid or a biological coating. In order to monitor the different properties of the loaded liquid or the biological layer, the inherent properties of the delay path also plays a crucial role. The delay path can either be electrically shorted by applying a metallisation layer or left electrically free (non-metalised), **Figure 4.4.**

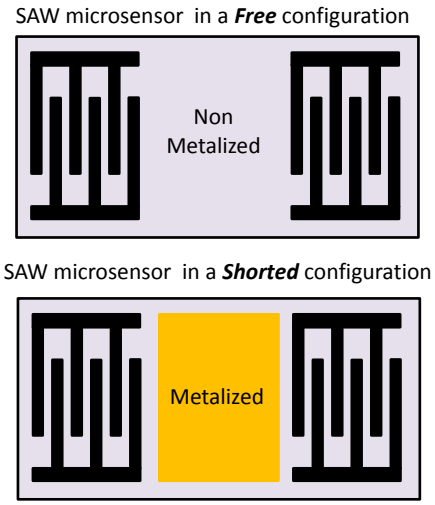

Figure 4.4: Two different operational configurations of SAW sensors

4.3.1 Detection Mechanisms

For liquid phase application, an associated factor which needs to be considered while calculating the resonant frequency of the microsensor is the acoustic wave penetration depth (δ). The acousto-electric potential associated with the generated SH-SAW on the surface of the lithium tantalate extends into the adjacent liquid. It is the extent of the penetration of this potential that determines how far into the liquid a measurable change can be detected using the SH-SAW microsensor. Thus, a generated SH-SAW on the lithium tantalate surface covered with water has a normalised acousto-electric potential. This extension or the potential skin depth was calculated by Kondoh et al., to be approximately 1/7th of the wavelength of a SH-SAW for a free surface (thus monitoring electric or acousto-electric perturbations) and zero for the SH-SAW travelling on a shorted surface [126] (**Figure 4.5**).

Since the wave potential is zero, the surface wave particles of the SH-SAW wave travelling on the shorted surface only interacts with the adjacent liquid/biological coating (monitoring only mechanical perturbations). The acoustic penetration depth for mechanical perturbation can be monitored by employing the formulae

$$\sigma = \sqrt{\eta / \pi f_0 \rho} \qquad \text{Eq. 4.1}$$

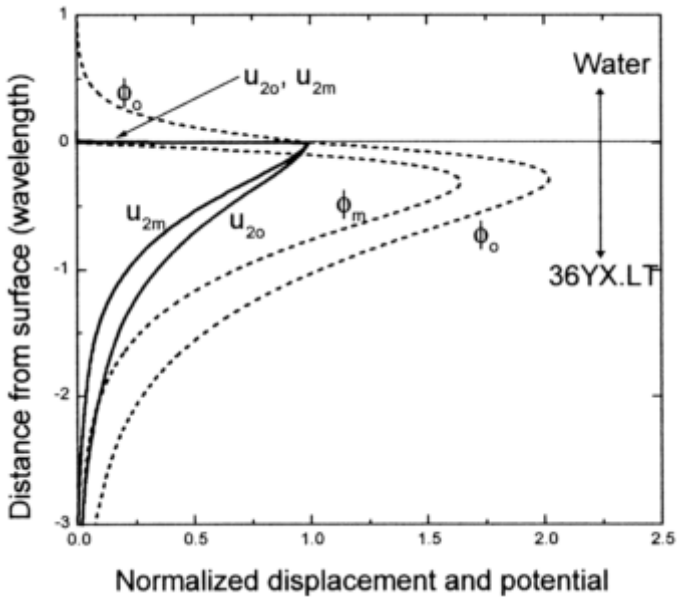

Figure 4.5: Normalized particle displacement (u) and acousto-electric potential (ϕ) profiles at the crystal/water interface for metalized (m) and metal free surface (f).

In **Eq. 4.1**, σ corresponds to the acoustic penetration depth of the acoustic wave, η is the viscosity of the liquid, ρ is the density and f is the central frequency of the SH-SAW microsensors [127].

Although, the acoustic wave particle velocity on both the metallised and unmetalized path differs [unmetalized or free (4161.5m/s) and a metallized or electrically shorted surface (4110.8 m/s)] the significance of considering both the above mentioned profiles is crucial in order to understand the different mechanical and electrical perturbation parameters. Thus in order to quantify them an approximate theory can be developed using the perturbation theory [123] [122].

4.3.2 Mechanical Interactions

The unperturbed mechanical characteristics of a coating e.g. a biological coating can be expressed by referring to the acoustic impedance of the generated surface wave Z_a. Changes to the properties of the acoustic wave due to mechanical interactions between the travelling wave and the coating can then be expressed by the complex equation

$$\frac{\Delta\beta}{k} = -\frac{jV}{4\omega P}\left(v^*.Z'_{a1}.v + v.Z^*_{a1}.v^*\right) \qquad \text{Eq. 4.2}$$

where k is the wavenumber, V the phase velocity, ω the angular frequency, P the power flow per unit width, v being the particle velocity and $j = \sqrt{-1}$. The prime (') denotes the perturbed quantity while the * denotes the complex conjugate. In the **Eq. 4.2,** $\Delta\beta$ is the perturbation quantity of the complex perturbation constant β and both can be relate to the wavenumber k and the attenuation α and velocity ratio ΔV/V of the propagating acoustic wave by

$$\beta = k - j\alpha \qquad \text{Eq. 4.3}$$

$$\therefore \quad \frac{\Delta\beta}{k} = -\frac{\Delta V}{V} - j\frac{\Delta\alpha}{k} \qquad \text{Eq. 4.4}$$

By substituting **Eq. 4.3 in Eq. 4.4**, the variation in the complex propagating constant as a function of the variation of the wave velocity and attenuation can be estimated and is represented by

$$\frac{\Delta V}{V} = -\frac{V}{4\omega P}\left(v^*.Z'_{a1i}.v - v.Z^*_{a1i}.v^*\right) \qquad \text{Eq. 4.5}$$

$$\frac{\Delta \alpha}{k} = \frac{V}{4\omega P}\left(v^*.Z'_{a1r}.v + v.Z^*_{a1r}.v^*\right) \qquad \text{Eq. 4.6}$$

where the subscripts r and i, in **Eq. 4.5** and **Eq. 4.6**, denote the real and imaginary parts of the wave, respectively. For the work presented in this thesis a liquid phase whole cell based biosensor has been realised and to that effect different coupling parameters need to be understood.

4.3.3 Viscous Coupling

In most biosensing sensing applications the physiological changes to the biological layer is caused by an analyte or a ligand flowing over the biosensitive layer. Assuming a SAW microsensor is coated with a biosensitive coating, the properties of the analyte flowing as incompressible, i.e. a Newtonian fluid, we can now substitute the impedance terms of **Eq. 4.7** and **Eq. 4.8** yielding [128],

$$\frac{\Delta V}{V} = -\frac{V v_2^2}{4\omega P}\left(\sqrt{\frac{\omega\eta'\rho'}{2}} - \sqrt{\frac{\omega\eta\rho}{2}}\right) \quad \text{Eq. 4.7}$$

$$\frac{\Delta \alpha}{k} = -\frac{V v_2^2}{4\omega P}\left(\sqrt{\frac{\omega\eta'\rho'}{2}} - \sqrt{\frac{\omega\eta\rho}{2}}\right) \quad \text{Eq. 4.8}$$

where η, ρ denote the liquid viscosity and density and v_2 the SH-mode particle velocity, respectively.

4.3.4 Effects of Mass Loading

Acoustic wave sensors, both SAW and TSM, are traditionally referred to as mass sensors as the propagating acoustic wave is perturbed when mass is added or removed from the microsensor surface. The addition and removal of mass varies from application to application with the simplest being adding/removing e.g. a DNA, RNA strands to complex processes e.g. measuring the changes in surface mass of a biological cell due to the sorption or interactions between a receptor-ligand, ligand-enzyme. In order to co-relate the mass detection mechanism of SAW microsensors, the density of the loaded sample on the sensor surface is considered to be unchanging and therefore the absolute mass sensitivity depending on the different device parameters are measured. In the vapour phase applications the Sauerbray's equation is employed co-relating the frequency shift to the applied mass

on the sensor surface. A similar relationship was described by Tiersten and Sinha, **Eq. 4.9**, which derived the SAW velocity perturbation as a result of coating the sensor surface with an acoustically thin film [94].

$$\frac{\Delta V}{V} = -\omega h\left[C_1\left(\rho - \frac{\mu}{V^2}\right) + C_2\rho + C_3\left(\rho - \frac{4\mu}{V^2}.\frac{\lambda + \mu}{\lambda + 2\mu}\right)\right] \qquad \text{Eq. 4.9}$$

where:

Equation Variable	Definitions
Ω	Angular Frequency
H	Film thickness
P	Film Mass density
μ	Lamé constant
V	SAW Phase Velocity
C_i	SAW particle velocity (directional)

In the case of a SH-SAW microsensor, the wave polarisation is in one direction i.e. C_1 (horizontally polarised) thus nullifying the contributions of C_2 and C_3. Simplifying **Eq. 4.10** by equating C_2 and C_3 to zero leads us to:

$$\frac{\Delta V}{V} = -\frac{Vhv_2^2}{4P}\left(\rho' - \frac{\mu'}{V^2}\right) \qquad \text{Eq. 4.10}$$

$$\frac{\Delta\alpha}{k} = 0 \qquad \text{Eq. 4.11}$$

By analysing **Eq.4.10** and **Eq.4.11** one can infer that for a wave propagating on a metallised sensor surface the wave velocity is only perturbed while the attenuation of the wave does not change (assuming that the properties of the sample flowing constant remains the same). Another set of interactions which need to be considered is the acoustoelectric interactions.

4.3.5 Acoustoelectric Interactions

In addition to the density and viscosity, electrical properties can also be represented by the relative permittivity ε_t and conductivity σ_t. In order to derive an approximate theory quantifying the acoustoelectric interactions, the sample flowing on reference sensors is assumed to be non-conductive. This can be represented by the relative permittivity equation:

$$\varepsilon_{rl} = \varepsilon_r \varepsilon_o \qquad \text{Eq. 4.12}$$

where ε_{rl}, ε_r, ε_o are the permittivity of the liquid, in question, relative to the free space. The electrical properties of the sample can then be expressed by **Eq. 4.13** relating the complex permittivity:

$$\varepsilon_l' = \varepsilon_r'\varepsilon_o - j\frac{\sigma'}{\omega} \qquad \text{Eq. 4.13}$$

Thus, any changes to the electrical properties of the liquid causes the velocity and the attenuation of the propagating SH-SAW, on a free surface, to change which can again be represented like the metallised case by the following equations:

$$\frac{\Delta V}{V} = -\frac{K_s^2}{2}\frac{\left(\frac{\sigma'}{\omega}\right)^2 + \varepsilon_o(\varepsilon_r' - \varepsilon_r)\left(\varepsilon_r'\varepsilon_o + \varepsilon_p^T\right)}{\left(\frac{\sigma'}{\omega}\right)^2 + \left(\varepsilon_r'\varepsilon_o + \varepsilon_p^T\right)^2} \qquad \text{Eq. 4.14}$$

$$\frac{\Delta\alpha}{k} = -\frac{K_s^2}{2}\frac{\left(\frac{\sigma'}{\omega}\right)\left(\varepsilon_r\varepsilon_o + \varepsilon_p^T\right)}{\left(\frac{\sigma'}{\omega}\right)^2 + \left(\varepsilon_r'\varepsilon_o + \varepsilon_p^T\right)^2} \qquad \text{Eq. 4.15}$$

where K_s^2 is the electromechanical coupling coefficient of the substrate. When the free surface of the sensor is loaded with a liquid with an effective permittivity of the crystal ε_p^T. The velocity ratios and the attenuation are seen to be proportional to the square of electromechanical coupling of the substrate. Therefore substrates with a higher electromechanical coupling coefficient will produce a high sensitivity. For the work employed in this thesis 36° rotated Y cut X propagating lithium tantalate crystal is employed which has a K_s^2 of

4.5% and ε_p^T of approximately $4.6.10^{-10}$ F/m. The wave velocity shift and changes to the attenuation can be obtained from experiments and the electrical properties of the liquid can then be estimated. The estimation of conductivity and permittivity from the above equation

$$\frac{\Delta V}{V} + \frac{K_s^2}{4}\,\frac{\varepsilon_o(2\varepsilon_r' - \varepsilon_r) + \varepsilon_p^T}{\varepsilon_r'\varepsilon_o + \varepsilon_p^T} + \left(\frac{\Delta\alpha}{k}\right)^2 = \left(\frac{K_s^2}{4}\,\frac{\varepsilon_o\varepsilon_r + \varepsilon_p^T}{\varepsilon_r'\varepsilon_o + \varepsilon_p^T}\right) \qquad \text{Eq. 4.16}$$

$$\left(\frac{\Delta V}{V} + \frac{K_s^2}{4}\right)^2 + \left(\frac{\Delta\alpha}{k} - \frac{K_s^2}{4}\,\frac{\varepsilon_o\varepsilon_r + \varepsilon_p^T}{(\sigma'/\omega)}\right)^2 = \left(\frac{K_s^2}{4}\,\frac{\varepsilon_o\varepsilon_r + \varepsilon_p^T}{(\sigma'/\omega)}\right) \qquad \text{Eq. 4.17}$$

Therefore, changes to the SAW velocity and attenuation to the physiological changes to the liquid/biological coating parameters, viscosity—η, density—ρ, electrical conductivity—σ, electric permittivity—ε and temperature—T of the biological coating that can be expressed by

$$A, \Phi = f(\eta, \rho, \sigma, \varepsilon, T) \qquad \text{Eq. 4.18}$$

In addition to a high degree of versatility on the range of parameters, as represented in **Eq.4.18**, which perturb the acoustic wave the question of cross-sensitivities also arises, as many different

parameters and processes could be responsible for the generated acoustic signal. It is difficult to resolve such a broad range of parameters although one can minimise the set and focus on the important ones. For the purpose of the work presented in this thesis, the issue of cross sensitivities was addressed by adopting different SAW microsensor configurations i.e. free and shorted, **Figure 4.6.**

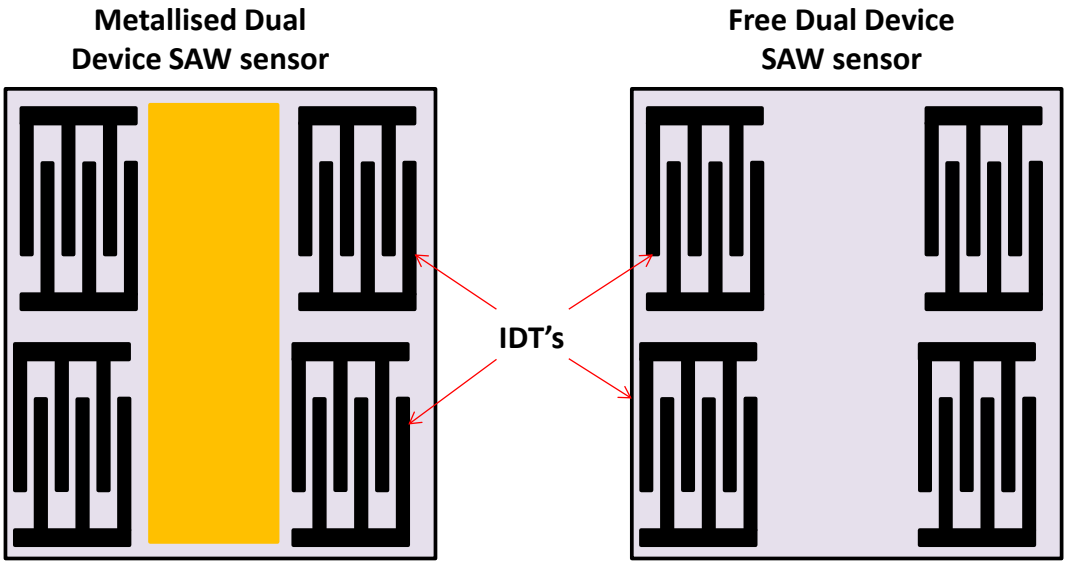

Figure 4.6: SAW microsensors in a dual device configuration

4.3.6 Additional Parameters: Temperature

The propagating acoustic wave is affected by temperature. Additionally all the liquid/biological coating parameters i.e. viscosity—η, density—ρ, electrical conductivity—σ, electric permittivity—ε are also temperature dependant. One way of mitigating such cross sensitivity issues is by adopting a differential measurement approach**, Figure 4.6.**

For the work presented in this thesis, both the methods have been adopted. Based on the different mechanisms examined in this chapter one can build a generalised model which explains the variation in the SAW frequency as a function of changes in the properties of the over-layer.

4.4 Generalised Model

As described previously, the acoustic wave propagating on the free surface of a piezoelectric crystal has an associated electric field that extends several micro-meters within the liquid. Thus, in addition to the mechanical interactions of the over-layer, electrical interaction (referred to as acoustoelectric interactions) also perturb the velocity and attenuation of the surface acoustic wave [129]. When the acoustic wave is travelling on an electrically shorted surface e.g. a grounded gold surface, only changes in the mechanical properties of the over-layer perturb the propagating wave, as the piezoelectric potential becomes zero [130]. Furthermore for each designs i.e. the free and shorted we can separate out the variable which are in question such that:

$$\left(\frac{\Delta V}{V}\right)_{Free} = \psi(\rho, \mu, \sigma, \varepsilon, T) \qquad \text{Eq. 4.19}$$

$$\left(\frac{\Delta V}{V}\right)_{Shorted} = \psi(\rho, \mu, T) \qquad \text{Eq. 4.20}$$

Thus, the perturbed acoustic velocity can then be described as a function of the partial change to the associated parameters with respect to its full differential thus leading us to combine **Eq.4.19** and **Eq.4.20** to a generalised equation

$$\frac{\Delta v}{v} \cong \frac{1}{v}\left\{\frac{\partial v}{\partial \rho}\Delta\rho + \frac{\partial v}{\partial \mu}\Delta\mu + \frac{\partial v}{\partial \sigma}\Delta\sigma + \frac{\partial v}{\partial \varepsilon}\Delta\varepsilon\right\} \qquad \text{Eq. 4.21}$$

Both these relationships can be related to the ratio of the change in the wave velocity or the change in the resonant frequency (Δf) of the SH-SAW sensor [131]. As the wave velocity is related to the frequency by the equation $v = \lambda . f$, the L.H.S of **Eq. 4.21** can be replaced by the ratio of frequency giving [132]

$$\Delta f \cong \left\{\frac{\partial f}{\partial \rho}\Delta\rho + \frac{\partial f}{\partial \mu}\Delta\mu + \frac{\partial f}{\partial \sigma}\Delta\sigma + \frac{\partial f}{\partial \varepsilon}\Delta\varepsilon\right\} \qquad \text{Eq. 4.22}$$

For the work presented in this thesis, a frequency measurement system has been adopted and therefore only changes to frequency will be referred to from hereon.

A simple theoretical model can be derived leading from **Eq.4.22** which encompasses the various experimental conditions for the free (Δf_f) and the shorted (Δf_s) SAW sensors. This can be represented by:

$$\Delta f_f \cong \left\{\frac{\partial f}{\partial \rho}\Delta\rho + \frac{\partial f}{\partial \mu}\Delta\mu + \frac{\partial f}{\partial \sigma}\Delta\sigma + \frac{\partial f}{\partial \varepsilon}\Delta\varepsilon\right\} \quad \text{Eq. 4.23}$$

$$\Delta f_s \cong \left\{\frac{\partial f}{\partial \rho}\Delta\rho + \frac{\partial f}{\partial \mu}\Delta\mu\right\} \quad \text{Eq. 4.24}$$

where Δf_f and Δf_s refer to the changes in the resonant frequency of the free and the shorted SAW sensors. **Eq. 4.23** and **Eq. 4.24** can then be modified to according to the different experimental scenarios and device configuration e.g. as a dual device setup has been adopted here, the control sensor will have no immobilization and thus the frequency shift ($\Delta f_{control}$) is a function of the sum of the changes in the over-layer (air, liquid) density, viscosity, conductivity etc., **Figure 4.7** :

$$\Delta f_{control} \cong \left\{\frac{\partial f_{liquid}}{\partial \rho_{liquid}}\Delta\rho_{liuid} + \frac{\partial f_{liquid}}{\partial \eta_{liquid}}\Delta\eta_{liquid} + \frac{\partial f_{liquid}}{\partial \delta_{liquid}}\Delta\delta_{liquid} + \frac{\partial f_{liquid}}{\partial \varepsilon_{liquid}}\Delta\varepsilon_{liquid}\right\} \quad \text{Eq. 4.24}$$

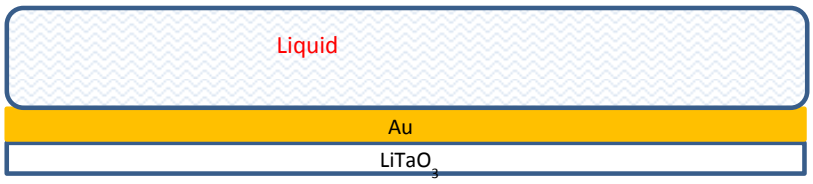

Figure 4.7: Sagittal view of the sensing area of a SAW sensor

The **Eq. 4.24** can be refined for according to the configuration which is being employed in the experiment i.e. free ($\Delta f_{f\,c}$) or shorted ($\Delta f_{s\,c}$) case:

$$\Delta f_{f\,c} \cong \left\{\frac{\partial f_{liquid}}{\partial \rho_{liquid}}\Delta\rho_{liuid} + \frac{\partial f_{liquid}}{\partial \eta_{liquid}}\Delta\eta_{liquid} + \frac{\partial f_{liquid}}{\partial \delta_{liquid}}\Delta\delta_{liquid} + \frac{\partial f_{liquid}}{\partial \varepsilon_{liquid}}\Delta\varepsilon_{liquid}\right\} \quad \text{Eq. 4.25}$$

$$\Delta f_{s\,c} \cong \left\{\frac{\partial f_{liquid}}{\partial \rho_{liquid}}\Delta\rho_{liuid} + \frac{\partial f_{liquid}}{\partial \eta_{liquid}}\Delta\eta_{liquid}\right\} \quad \text{Eq. 4.26}$$

One can now examine the case when one of the dual devices is coated with a biological/biosensitive film, **Figure 4.8**. As only one of the sensors (experimental sensor) has been functionalised with a whole cell biological coating, while the other sensor left bare (control sensor) the response of the free and shorted sensor to the immobilization can be represented as:

$$\Delta f_{f\,cell} \cong \left\{\frac{\partial f_{cell}}{\partial \rho_{cell}}\Delta\rho_{cell} + \frac{\partial f_{cell}}{\partial \eta_{cell}}\Delta\eta_{cell} + \frac{\partial f_{cell}}{\partial \delta_{cell}}\Delta\delta_{cell} + \frac{\partial f_{cell}}{\partial \varepsilon_{cell}}\Delta\varepsilon_{cell} + \frac{\partial f_{cell}}{\partial \mu_{cell}}\Delta\mu_{cell}\right\} \quad \text{Eq. 4.27}$$

$$\Delta f_{s\,cell} \cong \left\{\frac{\partial f_{cell}}{\partial \rho_{cell}}\Delta\rho_{cell} + \frac{\partial f_{cell}}{\partial \eta_{cell}}\Delta\eta_{cell}\right\} \quad \text{Eq. 4.28}$$

Eq. 4.27 and Eq. 4.28 can then be modified to take into account that ideally a 100% coverage area is not possible due to manual and instrumental errors. Thus, we assume that cells only cover a fraction (f_c) of the sensing area and that this area is within the volume of the acoustic penetration depth. As the cell are in a liquid environment, the changes in the resonant frequency of the control sensor will occur due to the acoustic wave being perturbed by the liquid plus contributions from the experimental sensor due to the fractional coverage $(1 - f_c)$ area of the cells. Thus **Eq. 4.27**and **Eq. 4.28** can then be modified to show the frequency shift for the control sensor for a free ($\Delta f_{f\,c\,l}$) and shorted ($\Delta f_{s\,c\,l}$) operational configuration:

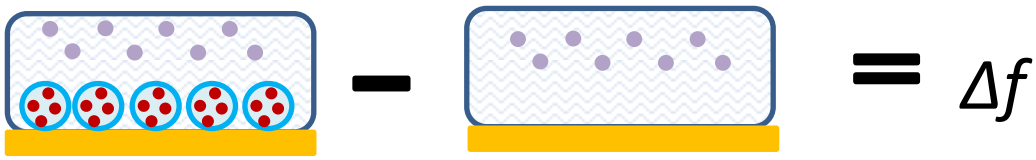

Figure 4.8: An experimental condition represented with one sensor coated with a biological coating and the other left bare with the differential signal shown.

$$\Delta f_{f\,c\,l} \cong f_c\left\{\frac{\partial f_{cell}}{\partial \rho_{cell}}\Delta\rho_{cell} + \frac{\partial f_{cell}}{\partial \eta_{cell}}\Delta\eta_{cell} + \frac{\partial f_{cell}}{\partial \delta_{cell}}\Delta\delta_{cell} + \frac{\partial f_{cell}}{\partial \varepsilon_{cell}}\Delta\varepsilon_{cell} + \frac{\partial f_{cell}}{\partial \mu_{cell}}\Delta\mu_{cell}\right\}$$
$$+ (1 - f_c)\left\{\frac{\partial f_{liquid}}{\partial \rho_{liquid}}\Delta\rho_{liuid} + \frac{\partial f_{liquid}}{\partial \eta_{liquid}}\Delta\eta_{liquid} + \frac{\partial f_{liquid}}{\partial \delta_{liquid}}\Delta\delta\right.$$
$$\left. + \frac{\partial f_{liquid}}{\partial \varepsilon_{liquid}}\right\} \qquad \text{Eq. 4.29}$$

$$\Delta f_{s\,c\,l} \cong f_c\left\{\frac{\partial f_{cell}}{\partial \rho_{cell}}\Delta\rho_{cell} + \frac{\partial f_{cell}}{\partial \eta_{cell}}\Delta\eta_{cell}\right\}$$
$$+ (1 - f_c)\left\{\frac{\partial f_{liquid}}{\partial \rho_{liquid}}\Delta\rho_{liuid}\right.$$
$$\left. + \frac{\partial f_{liquid}}{\partial \eta_{liquid}}\Delta\eta_{liquid}\right\} \qquad \text{Eq. 4.30}$$

where f_c is the volume fraction of the cell area covered. In order to quantify the frequency shift due to the whole cells, the contribution from the liquid i.e. the exposed areas on the experimental sensor need to be negated and thus:

$$\Delta f_{f\,c\,\,l} - (1 - f_c)\Delta f_{f\,l}$$
$$\cong f_c\left\{\frac{\partial f_{cell}}{\partial \rho_{cell}}\Delta\rho_{cell} + \frac{\partial f_{cell}}{\partial \eta_{cell}}\Delta\eta_{cell} + \frac{\partial f_{cell}}{\partial \delta_{cell}}\Delta\delta_{cell} + \frac{\partial f_{cell}}{\partial \varepsilon_{cell}}\,\Delta\varepsilon_{cell}\right.$$
$$\left. + \frac{\partial f_{cell}}{\partial \mu_{cell}}\,\Delta\mu_{cell}\right\} \qquad \text{Eq. 4.31}$$

$$\Delta f_{s\,c\,l} - (1 - f_c)\Delta f_{s\,l} \cong f_c\left\{\frac{\partial f_{cell}}{\partial \rho_{cell}}\Delta\rho_{cell} + \frac{\partial f_{cell}}{\partial \eta_{cell}}\Delta\eta_{cell}\right\} \qquad \text{Eq. 4.32}$$

Eq. 4.31 and Eq. **4.32** represent the shift in the resonant frequency of a free ($\Delta f_{f\,c\,\,l} - (1 - f_c)\Delta f_{f\,l}$) or shorted ($\Delta f_{s\,c\,l} - (1 - f_c)\Delta f_{s\,l}$) dual device SAW microsensor with only one of the dual devices immobilized with a whole cell coating. They also account for the fractional coverage area of the coating. Contributions from the control sensor can then be

subtracted from the experimental sensor to give the final shift in frequency. **Eq. 4.31** and **Eq. 4.32** will be revisited in Chapter 7 and the simple model developed here will be expanded and applied to explain the experimental results.

4.5 Conclusion

This chapter introduced the concept of SAW sensors providing the user with a detailed summary of the different device configurations and designs. The chapter also covered the different detection mechanisms involved in a SH-SAW, a type of acoustic wave microsensors. Details of the various interactions which perturb the properties of a travelling acoustic wave were examined w.r.t. the resonant frequency of the microsensor. The knowledge gained in this chapter will be employed to designing the acoustic wave microsensors presented in the next chapter and will also be revisited in order to explain the experimental results (in the liquid phase) presented in the later chapter.

Chapter 5
Design of Surface Acoustic Wave (SAW) microsensors for Liquid and Vapour Phase Applications

5.1 Introduction

The preceding chapter introduced the concept of SH-SAW microsensors and showed how they could be employed in the liquid phase with limited attenuation. This chapter introduces the design principle of the SAW microsensor covering key principles which aide in the achievement of an optimised layout. This chapter shows how different design parameters were calculated and also presents the final designs. In addition to designing SAW microsensors for liquid phase applications, the SAW microsensors have also been designed for vapour phase applications using the same principle and techniques outlined in this chapter.

5.2 Design Parameters

Subsequent sections of this chapter will discuss the key principles which aid in the achievement of a successful design of a SAW micro-device. They include selecting an optimised IDT, reflector geometry, calculating the spacing parameter between the IDT's and between the IDTs and reflectors and finally optimising the design which aid in the efficient population of a wafer.

5.2.1 Substrate Selection

Selecting an appropriate piezoelectric substrate is an important step as it defines the polarisation of the generated acoustic wave. As research in the area of SAW microsensors is an application driven area, knowledge of the environment of the application provides the first indications of the type of substrate required. Other factors which are influence by the substrate properties are the operational frequency, size and dimensions of the microsensors.

In order to run experiments in the liquid phase, the shear-horizontal component of the surface acoustic wave (SH-SAW) is preferred while in the vapour phase the Rayleigh mode is the preferred choice of acoustic mode. The shear horizontal mode has been found in particular to be ideal for liquid based sensing applications as the

acoustic wave has a horizontal polarisation to the normal propagation direction (parallel to the substrate) [96].

In 1977, Nakamura et al. demonstrated that a SH-SAW was supported by YX cut lithium tantalate ($LiTaO_3$) crystal on a rotated 36° angle but it was not until 1988 that Shiokawa et al., demonstrated the first liquid phase sensor employing this particular crystal cut[96] [124][96]. It was only in the early 1990's that SAW sensors operating in the liquid phase, designed on 36°YX LiTaO3, were first used for bio-sensing applications [125][133]. Other characteristics that make 36° YX LiTaO3 crystal a suitable substrate for the study presented here include a relatively low temperature coefficient of delay (TDC) (32 ppm/°C) and a high electromechanical coupling coefficient (4.7%) when compared to substrates like quartz and lithium niobate [134].

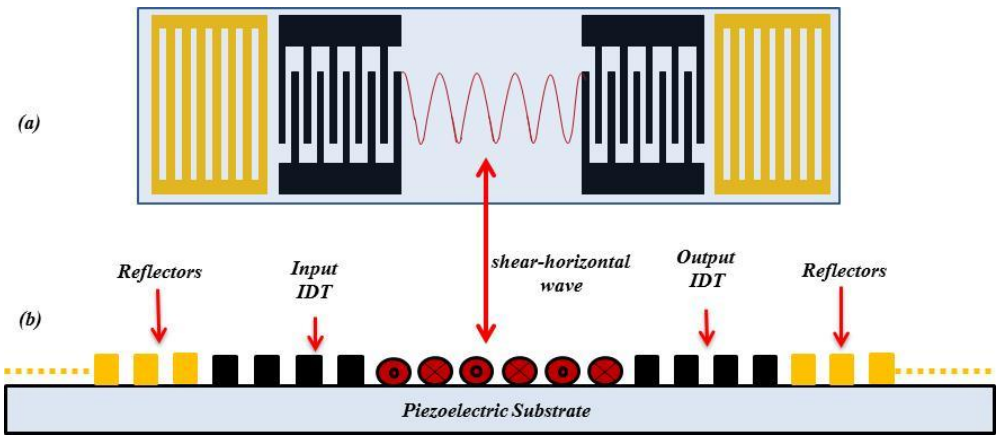

Figure 5.1: SAW Resonator with the generated SH wave top view (a) and side view (b).

For vapour phase applications the preferred substrate material which support the Rayleigh mode of the acoustic wave is the ST (42.75° rotated Y) Quartz material. In addition to supporting the Rayleigh cut of the acoustic wave, this substrate also offers excellent temperature stability theoretically zero (~0 ppm/°C). Although it offers a low electromechanical coupling coefficient (0.16%), the temperature stability helps experiments to be performed at higher temperatures in order to increase the sensitivity of the surface film (usually a chemical coating) [135] [120][133].

5.2.2 Frequency Selection

As the different structural parameters (IDT electrode spacing, width, acoustic aperture etc.) of a SH-SAW microsensor are functions of the acoustic wavelength λ of the generated SH-SAW the operational frequencies of the microsensor have been traditionally defined from the onset, regardless of phase of operation. For the work presented here, a whole-cell based SH-SAW microsensor was to be realised in order to carry out ligand receptor interaction studies. Therefore the final objective was to interrogate different regions within an immobilised whole cell in order to study the various chemical and mechanical reactions triggered when a ligand was detected **(Figure 5.2)**.

For the current study Sf9 whole cells would be immobilised onto the whole-cell surface **(Figure 5.2)**. In order to acquire the ability to interrogate different regions (demonstrated by the yellow arrows on **Figure 5.3**) within the immobilised Sf9 whole-cell the acoustic wave penetration depth or the wave skin depth would first need to be calculated.

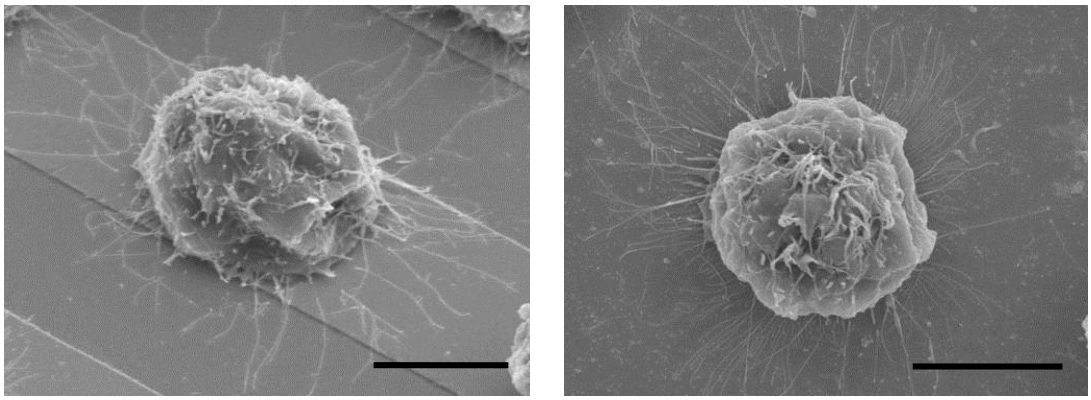

Figure 5.2: Electron Microscopy picture of an Sf9 insect cell (Scale bar: 10µm) (Courtesy: Electron Microscopy Lab, University of Leicester)

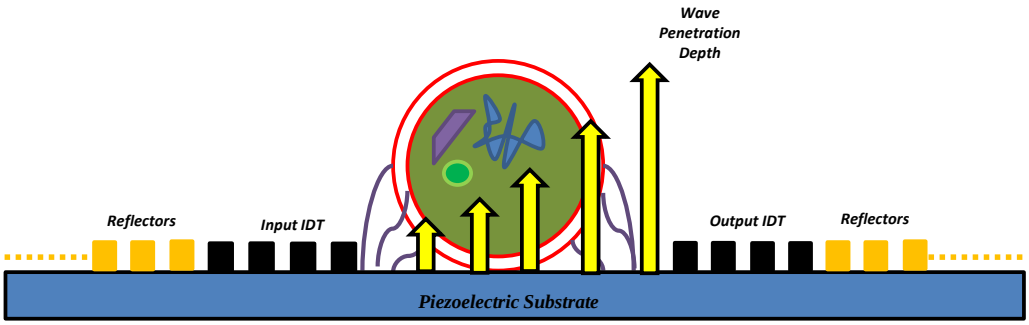

Figure 5.3: Shown the different penetration depths of the SH-SAW microsensors which are being probed.

When a SH-SAW wave is generated on a piezoelectric substrate (e.g. lithium tantalate) it has an associated acousto-electric potential that extends into the adjacent liquid **(Figure 4.5 – Chapter 4, page 83)**. It is the height of this wave penetration or the skin depth that determines how far into the liquid a measurable change can be detected.

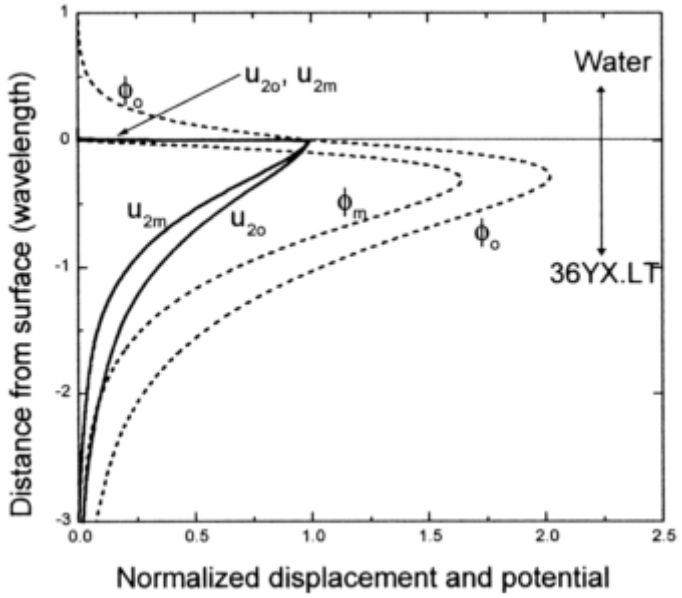

Figure 5.4: Normalized particle displacement (u) and acousto-electric potential (ϕ) profiles at the crystal/water interface for metalized (m) and metal free surface (f) on a 36° Y cut X propagating lithium tantalate piezoelectric crystal.

Depending on the nature of the surface i.e. metallised (shorted) or non-metallised (free), on which the SH-SAW wave is generated, the acoustic wave possesses a mechanical and an electrical skin depth. Kondoh et al. in 1993 calculated that the electrical skin depth was approximately 1/7th of the sensor wavelength [126].

Therefore in order to be able to interrogate different regions of the whole-cell e.g. the centre, the top cell membrane using different device types (metallised and non-metallised), acoustic wave microsensors would need to be designed at different operating frequencies.

For the work presented in this thesis, the SH-SAW resonant frequency was calculated by first setting the acoustic wave skin depth and then calculating the wavelength (λ) (as it is 7 x the skin depth). Therefore, for an electrical skin depth of 9.7 μm the wavelength was calculated to be 68 μm (67.9 μm normalised to first decimal) which gave a SH-SAW resonant frequency of 60.56MHz. Similar calculations were performed for the 228.79MHz SH-SAW microsensor. **Table 5** shows the frequencies of the different SH-SAW microsensors along with their associated electrical and mechanical penetration depths and the regions being probed.

SH-SAW Frequencies (MHz)	Wavelength λ (μm)	Electric Penetration Depth (μm)	Mechanical Penetration Depth (nm)
60.56	68	9.7	72
228.79	18	2.6	37.4

Table 5: Shown are the various SH-SAW frequencies with the associated wave penetration depths.

From Figure 4.5 one observe that the normalised wave particle displacement becomes zero on a metallised surface. Thus, the

mechanical skin depth, at the calculated frequencies of 60.56 and 228.79MHz, was calculated by employing the **Eq. 5.1** [127]:

$$\sigma = \sqrt{\eta / \pi f_0 \rho} \qquad \text{Eq.5.1}$$

where σ corresponds to the acoustic penetration depth of the acoustic wave, η is the viscosity of the liquid, ρ is the density and f is the central frequency of the SH-SAW microsensors. In order to calculate the acoustic penetration depth the viscosity and density of water at 20°C was considered i.e. η being 0.001 kg/m/s and ρ being 998.2071 $kg.m^{-3}$. The typical size of a cell is 10μm, **Figure 5.3,** and its weight equals 1ng. The density then calculated from the above values of mass and diameter was found to be 1910 $kg.m^{-3}$.

5.3.1 IDT Design

The IDT's are comb-like finger pairs, as shown in **Figure 5.4**, which are lithographically patterned on the surface of a piezoelectric crystal and are made of thin films of aluminium (Al) or gold (Au). They aid in the generation of the acoustic wave on the substrate surface when connected to a time varying voltage. This method of generating an acoustic wave by an IDT was first reported by White and Voltmer in

1965 [136] but the process by which lithographically patterned electrodes excite and detect a surface acoustic waves on a piezoelectric crystal, was first discovered by R. M. White at the University of California, Berkeley [137].

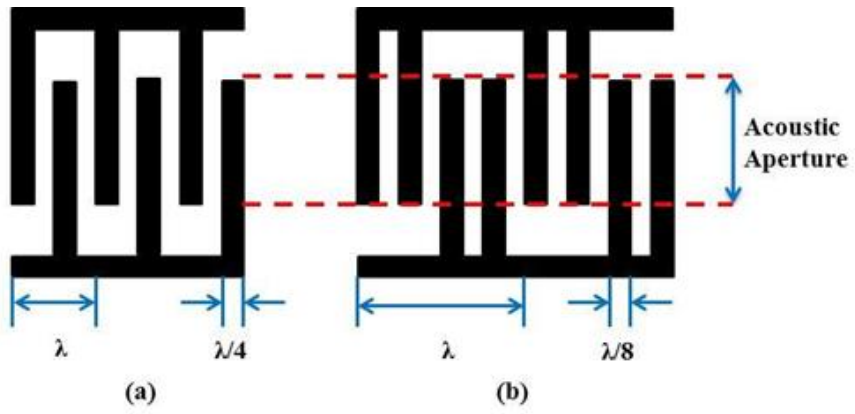

Figure 5.5: Different IDT structures namely the Split finger design (a) and the Solid finger design (b) along with the Acoustic Aperture

In general, an IDT has a constant period as the wavelength (λ) of the generated acoustic wave is defined by its periodicity [134]. In addition, factors such as the electromechanical coupling coefficient and dielectric permittivity of the substrate also affect the electrical impedance of the patterned IDT fingers.

Essentially two different types of IDT design configuration have traditionally been studied. These include the single electrode design and a split finger design. Variations to the above mentioned design configurations, which includes the use of single phase unidirectional

transducers (SPUDT) and circular IDT designs, have also been reported by various authors [138] [139]. For the present work, a split finger IDT configuration has been adopted.

Assuming a metallization ratio of 0.5, the width of an IDT finger in a single electrode design is λ/4 while that for a split-finger design is λ/8. Both the design configurations have their respective advantages and dis-advantages which range from the ease of patterning the electrodes onto the substrate surface to reducing any undesirable finger reflections caused when the propagating waves are reflected of the edge of the electrodes.

By examining the finger width of the IDT's, from **Figure 5.4**, it can be seen that to define a split finger geometry an increased lithography resolution will be required. The increased lithography resolution however this pays off in reducing the Bragg's reflection as the finger width is 4 times narrower than the pre-requisite condition of λ/2 according to the Bragg's equation. The transducer electrode material is one of the many important parameters that need to be considered, especially for bio-sensing applications, as increased re-usability of the sensor can be achieved by employing noble metals as electrode material. In this context, split-finger IDT geometry was adopted for the present work with the patterned electrode material being gold. Being a noble metal, Au offer superior performance in liquid sensing applications as it

is resistant to any corrosive effects of the liquid. For vapour phase applications, the devices were fabricated with Au and Al electrodes.

Other factors such as the electromechanical coupling coefficient of substrate material play a critical role in determining the function of a SAW sensor as substrate materials with a weak electro-mechanical coupling requiring a larger number of finger pairs to generate a coupled acoustic wave. As lithium tantalate, a substrate which has a high electromechanical coupling coefficient (4.5%) was chosen as the substrate material and considering that a resonator configuration has been adopted the number of IDT pairs was limited (2.5 finger pairs per IDT) in order for the electrodes to couple well to the acoustic cavity at the appropriate signal level. In addition, the numbers of IDT finger pairs are usually kept low as their number is inversely proportional to the bandwidth (BW α 1/ Np finger pairs) of the micro-device [1].

The IDT overlap region, or the acoustic aperture (AA) as shown in **(Figure 5.4)**, also plays a key role as a small aperture will make sure the propagating acoustic wave does not distort before reaching the output IDT. In the present work the acoustic aperture of the IDTs was kept large enough (≥50λ) to supress any diffraction effects of the acoustic beam [1].

5.3.2 Reflector Design

The reflector or acoustic mirrors, as they are known, help in the construction of a standing wave pattern by repeatedly reflecting the generated SAW in the acoustic cavity. The grating pattern can be described as periodically spaced discontinuities with a metallization ratio of 0.5. To achieve near total reflection of the acoustic wave, a number of reflector strips are required as the contribution of each metal strip adds constructively to give a high yield.

There are two available designs for the grating structures. The first design consists of etched grooves in the piezoelectric substrates that are filled with metal layers. The depth of the grooves would vary from 500Å to 2000Å for less dense metals like aluminium with this value being much thinner for denser electrode materials such as gold. The second design consists of electrodes patterned onto the piezoelectric substrate surface and can be divided into three sub-types such as Open Circuit (OC) reflector, Short Circuit (SC) reflector and Positive and Negative (P&N) reflector, **Figure 5.5.** There are four distinct types of reflection mechanism namely piezoelectric shorting, geometric discontinuities, electrical regeneration and mass loading, which contribute to the generation of the standing wave pattern. These include effects from effects of the reflector electrodes. Reflection effects due to

the piezoelectric shorting are normally found in substrate materials with large electromechanical coupling coefficient (K^2) e.g. lithium niobate, lithium tantalate, ZnO, AlN. Geometric discontinuities also contribute to the reflection process but to a lesser degree when thin metal strips are being considered on a substrate which has a strong electromechanical coupling coefficient. This has a more pronounced effect on weak piezoelectric substrates such as ST-Quartz. It should also be noted that the type of reflective strip used i.e. OC, SC or PNR also plays a key role in deciding this effect e.g. in SC type reflector strips are more effective than OC type reflector strips as there geometric discontinuity adds to the piezoelectric shorting phenomenon.

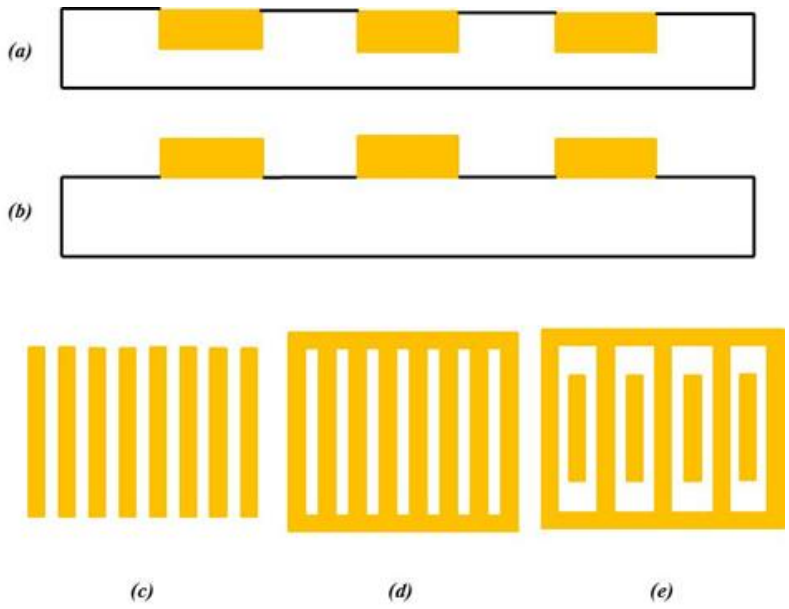

Figure 5.5: Different design of the acoustic grating showing the (a) Etched grooves on the substrate, (b) patterned electrodes on the substrate surface, (c) Open Circuit- OC reflectors, (d) Short Circuit – SC reflectors, (e) Positive and Negative – P&N reflectors grooved

During the process of reflection, acoustic waves are re-generated when a time varying electrical potentials are established, on the surface of the metal grating. This causes an electrically regenerated acoustic wave which adds to the reflective component thus playing a crucial role in the process of reflection from the grating pattern. Mass loading effects arise from the difference in densities and elastic properties between the metal strips and the substrate material. Therefore when substrates with weak electromechanical coupling coefficients e.g. ST-Quartz (0.16%), are patterned with reflectors made of dense material e.g. gold, this effects is more pronounced.

As two or more effects have the likelihood of occurring within a reflective structure simultaneously with none of their effects being negligible, it is important to determine each reflection coefficient phase. However, phase determination is complex process when different reflection mechanisms compete in a SAW resonator grating or tend to cancel each other. Thus the simplest of the reflector designs i.e. the SC designs was employed with reflector pair consisting of 100 metal strips.

5.3.3 Metallisation

In order to realise the IDT microstructures, a metal layer needs to be deposited on the piezoelectric substrate. Generally the two most employed metallisation used in the fabrication of IDT patterns in SAW micro-devices are Aluminium (Al) and Gold (Au).

Both the metal layers have their associated advantages and disadvantages. Aluminium has several associated advantages over gold as it adheres well to the piezoelectric substrate and this property offers significant advantage while fabricating SAW microsensors as an additional adhesive layer is not require (which is the case while depositing a Gold layers). The lower density of aluminium layer also contributes significantly in lowering the pass-band ripple which occurs in the frequency response of the SAW sensor and is caused by the edge reflections of the IDT's. However, with regards to the life-span of the sensor, aluminium is at a disadvantage to gold as it corrodes easily raising the question of data validity thus raising questions over the re-usability and thus repeatability of the results. Although in a more commercial setting aluminium passivation is usually carried out by depositing thin layers of silicon dioxide, silicon nitride or aluminium nitride but such steps are not suitable for a laboratory setting as SAW

sensors are sensitive to mass loading effects and this step will significantly increase the metallic [140].

Gold, on the other hand, is employed as the electrode material for many bio-chemical applications as it is a noble (inert) metal and is resistant to corrosion. Although it is 10 times denser and 17% more conductive and substantially softer than aluminium, its major drawback lies in its inability to adhere to the piezoelectric substrate [120]. In addition to this, gold is also a highly reflective material thus the magnitude of pass-band ripple in the frequency response of the SAW sensor also increases also affecting the device bandwidth [140]. Additionally, in order to pattern gold electrodes on a piezoelectric substrate, an initial seeding layer needs to be deposited which helps in increasing the adhesiveness of the gold electrode to the piezoelectric substrate. The metal for the seeding layer is usually chromium or titanium.

5.4 Design Procedure: Calculation of Spacing parameters

In order for the device to generate the acoustic wave constructively the various components need to successfully couple with the substrate and each other. Therefore in order to attain constructive interference the individual structures need to be placed at precise

distances from each other. In this section, the various spacing parameters have been calculated.

5.4.1 IDT-IDT Spacing

In order to calculate the separation distance between the IDTs, assuming a metallization ratio $\eta = 0.5$, the following procedure was adopted. Consider a standing wave pattern, as shown in **Figure 5.6**, the IDT fingers are placed above the maxima of the acoustic wave. In a synchronous resonator structure, the IDT's are symmetrically placed, thus according to the above condition a minimum offset value for placing the IDTs can be found. On examining the pattern of the generated acoustic wave this minimum offset value can be found to be $\lambda/4$. The IDT fingers can then be moved by 'x' integer wavelengths or half-a-wavelength with respect to a single IDT finger, according to **(Eq. 5.2)**

$$S_{IDT\text{-}IDT} = \lambda/4 + x\,\lambda/2 \text{ (with } x = 0, 1, 2, 3, 4 \ldots..) \qquad \text{Eq. 5.2}$$

Similarly, the separation distance between the IDT and the reflectors can be calculated with an added caveat, the consideration of an additional parameter i.e. the reflectivity of the grating.

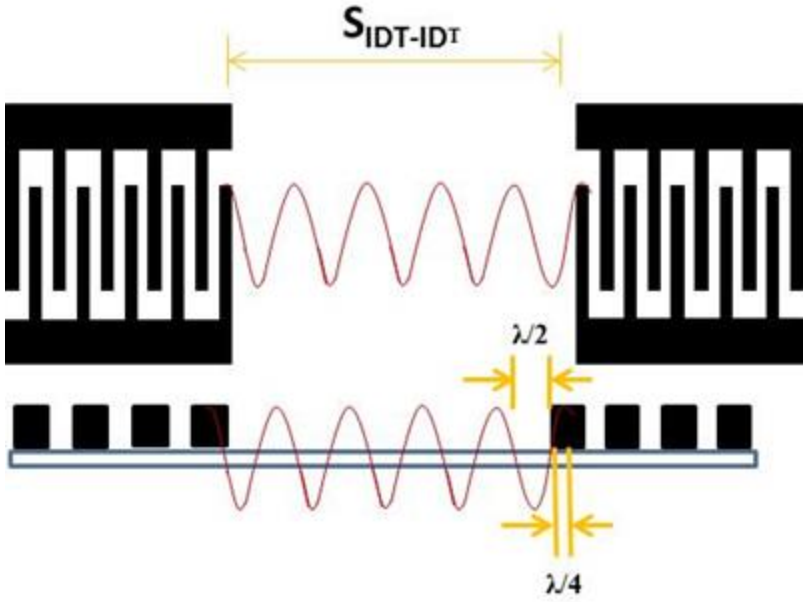

Figure 5.6: Standing wave pattern in the sensing area (between the IDTs)

5.4.2 IDT-Reflector Spacing

As the grating pattern was made of gold a high reflectivity noble metal edge reflection can be expected of the grating pattern. Plessky and Hartmann reported that the use of heavy metals (Au, Ti) as grating electrode material with thicknesses of 4% of the wavelength produced a reflectivity per wave in the order of 50%, although their work was based on a synchronous one port resonator [141]. For the present work, h/λ was kept relatively small (<1%) as two frequencies with different operating configurations (one port and two port) of synchronous resonators were fabricated on the same wafer. In order to calculate the distance between

the IDT and reflectors consider a standing wave pattern, as shown in **Figure 5.7**.

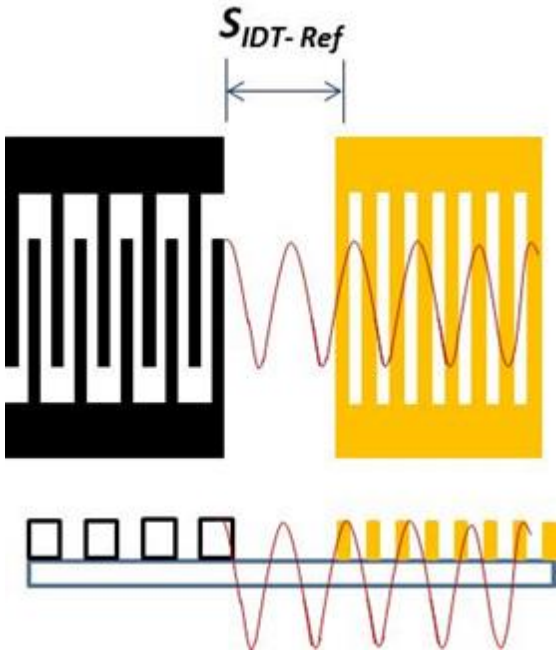

Figure 5.7: Standing wave pattern between the IDT and Reflectors

According to the condition previously, the minima of the travelling acoustic wave is assumed to be located at edge of the grating pattern, thus a minimum off-set distance needs to be set. This minimum separation distance between the IDT and reflector grating was set to λ/8. This minimum distance can further be increased by an integer half a wavelength to give an appropriate distance between the IDT and the reflectors, according to **Eq. 5.3**

$$S_{IDT\text{-}Grating} = \lambda/8 + y\,\lambda/2 \text{ (with } y = 0, 1, 2, 3, 4 \ldots..) \qquad \text{Eq.5.3}$$

5.5 SAW Resonator Design

A dual device configuration of the SH-SAW resonator has been realised, as shown in **Figure 5.8**. This particular layout configuration helps in eliminating common-mode effects such as temperature, pressure, flow rate etc. [142] [143]. The vertical separation between the individual sensors was set to 500µm.

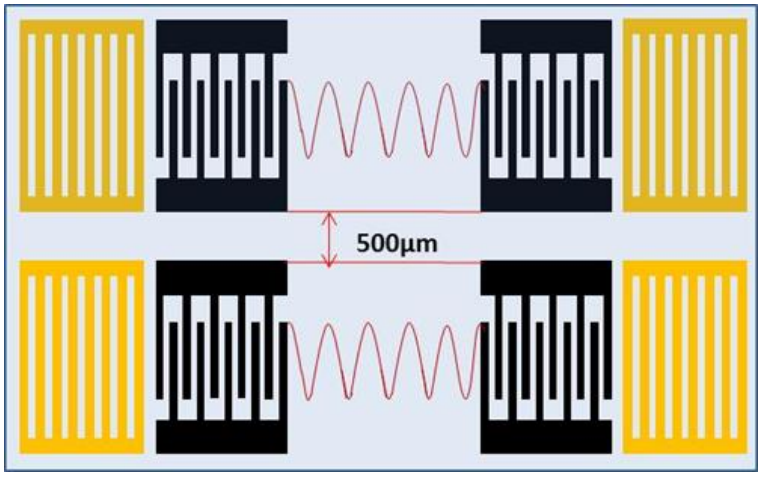

Figure 5.8: A dual synchronous SH-SAW resonator

The realisation of an efficient SAW layout is an important and necessary consideration for any bio-sensing applications as this has a direct impact on the ease of integrating the sensor with any peripheral microfluidics or circuitry. In most bio-sensing/liquid phase applications access to the sensing area is required for the immobilization of a biosensitive coating which may include protein, DNA or whole cells [63].

It is due to these conditions that an optimised sensor layout plays

a crucial role in determining the degree of flexibility available to the user during sensitive biological experiments. The layout of the sensor should also account for the interferences which will be caused by physical parameters, such as wire bonds, such that a balanced design can be achieved [64]. Typical SAW sensor designs employed previously have used thicker IDT supply rails. One of the major advantages of this particular approach was that the sensor could be bonded directly to the supply rails. The potential downside for this approach was the fact that after a few rounds of bonding, one starts getting quite close to the sensing area and IDT's, thus proving practically unsustainable. Also as the connection are on opposite sides of the sensor (one side for the input while the other for the output IDT) a relatively large PCB area is required for the sensor i.e. the sensor needs to be placed on a PCB board which has coax connection on both sides [9] [140]. Other factors which need to be accounted for are e.g. integrating the sensor with microfluidics, housing units for the bio-sensitive coating.

For the layout of the dual SH-SAW resonators presented in this thesis, separate bond pads (500µm X 500µm) have been employed for the input and output transducer with a common ground pad, as shown in **Figure 5.9**. With all the bonding pads located to one corner of the sensor chip, entire area of the sensors can be used for integrating microfluidics channels or carrying out IDT passivation processes without any

interruptions from wire bonds. In addition, large bond pads provide the ability to ultrasonically wire bond the sensor more often (if required) without interfering with its active components.

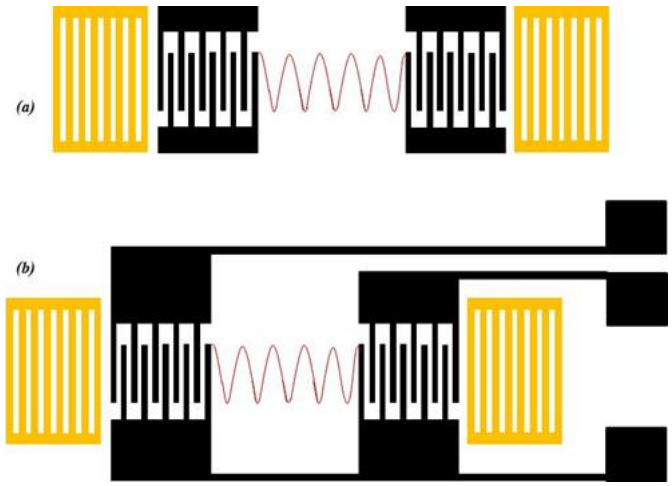

Figure 5.9: Schematic representation of the layouts used for a synchronous SH-SAW Resonator showing the traditionally used layout (a) and the layout designed and employed for the current work (b)

The layout editor used for the design of the SH-SAW synchronous resonator sensors was L-Edit v13 (Tanner Tools). Two different types of dual SH-SAW synchronous resonators were designed for the work presented in this thesis viz. one port and two port resonators.

5.5.1 Liquid Phase: SH-SAW microsensors

As specified previously, a one port resonator consists of only a set of IDTs, which act as the emitter as well as the receiver of the generated acoustic wave. The numbers of finger pairs were limited to 5.5 fingers

(split finger). The acoustic aperture of the IDT's was set to 3400μm or 50λ for SRL 321 and 1440 or 80λ for SRL 325. Each acoustic grating consists of 100 reflector strips with the separation between the reflector and the IDT set to 42.5μm for SRL321 and 11.25μm for SRL325 respectively. The supply rails width was set to 100μm with each bond pad having dimensions of 500μm x 500 μm respectively. The vertical separation distance between the individual sensors was set to 500μm.

For the two port resonator configuration, three different operating configurations were designed viz. free, metallized, heater. In the free design type, the sensing area of the resonator was left bare, with the intension of coating the device with a polymer waveguide layer. On the free surface both the SSBW and Leaky SH-SAW propagate on a 36° rotated Y-cut X propagating lithium tantalate crystal [144]. In this particular crystal direction, both the modes have very close phase velocities i.e. 4160m/s (SSBW) and 4212m/s (leaky SH-SAW). The leaky SH-SAW mode converts to the SSBW mode when the propagation area is free, thus a polymer waveguide has is coated onto the device sensing area in order to trap the energy of the wave on the device surface [145].

For the shorted design, the sensing area was covered with a gold layer which was grounded and in another design the sensing area consisted of meandering heater structures, as shown in Appendix 2. For the sensor devices SRL 322, 323, 324, the values for the IDT, acoustic

aperture, the number of reflector strips and the distance between the IDT and reflectors was kept exactly the same as the ones used for SRL 321. The delay path distance between the IDTs, for SRL 3222, 323, 324, was set to 5015.26µm or 73.75λ. For the sensor devices SRL 326, 327, 328, the values for the IDT, acoustic aperture, the number of reflector strips and the distance between the IDT and reflectors was kept exactly the same as the ones used for SRL 325. The delay path distance between the IDTs, for SRL 326, 327, 328, was set to 2002.53µm or 111.25λ.

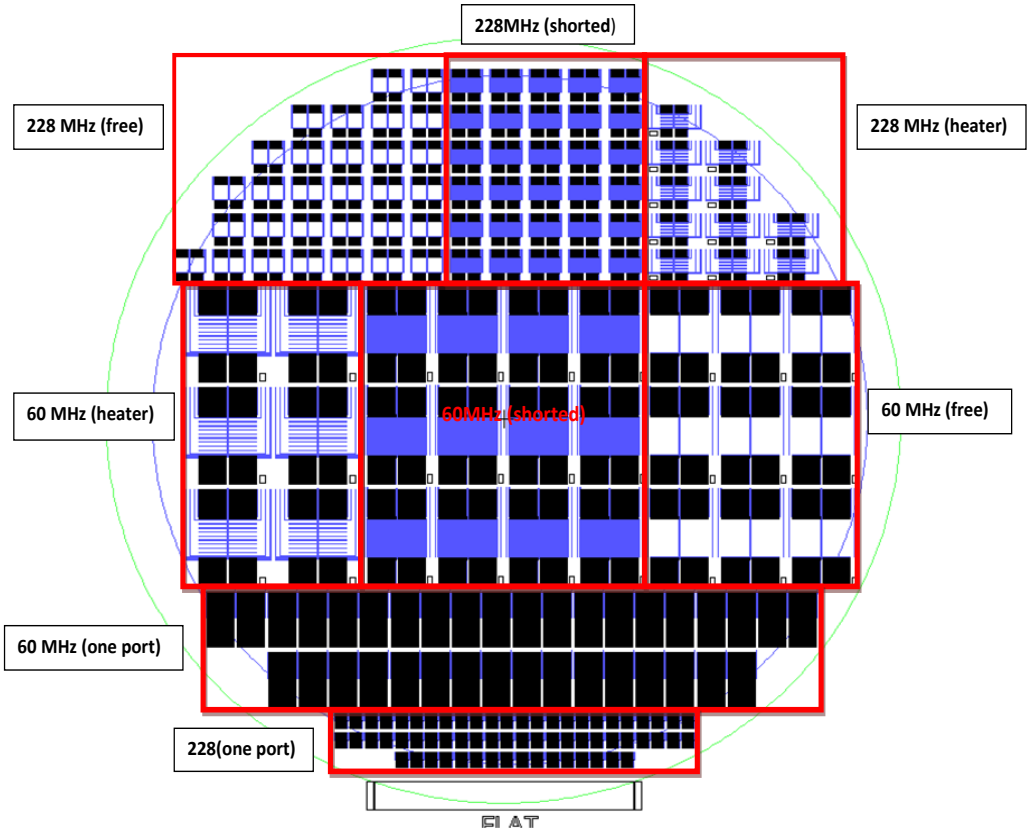

Figure 5.10: Extracted layout of the populated 4" wafer 36° YX $LiTaO_3$ wafer

5.6 Conclusion

In this chapter, basics of acoustic wave sensor design have been introduced. SAW microsensors have been designed for both the liquid and vapour phase. Two different configurations have been considered which include one port and a two port and three different designs have been considered for the two port resonators which include the free, shorted and the heater. The following chapter includes the fabrication details of the designed dual SH-SAW microsensors.

Chapter 6
Characterisation of SH-SAW microsensors and Measurement setup

6.1 Introduction

Post fabrication, the microsensors were packaged and mounted on a PCB board with coax connectors and characterised using different measurement setups. This chapter introduces the various measurements systems employed to characterize and the associated results of SAW microsensor characterisation. Here we also show the design and fabrication of various microfluidic components which facilitate in the realisation of an automated system integrated with the SAW microsensors along with its associated circuitry.

6.2 Wafer Dicing and Packaging

As shown in the earlier different frequencies each having 3 different designs, 2 operational configurations were present on the 4”

wafer. As the micro-device features are a function of λ, the 60.56 MHz devices were 13 x 13mm while the 226.89 MHz device had dimensions of 2 x 2mm. Due to this variety of designs the wafer could not be diced in a single run. Instead it was diced in 8 runs. **Figure 6.1** shows the picture of a section of the processed and diced wafer.

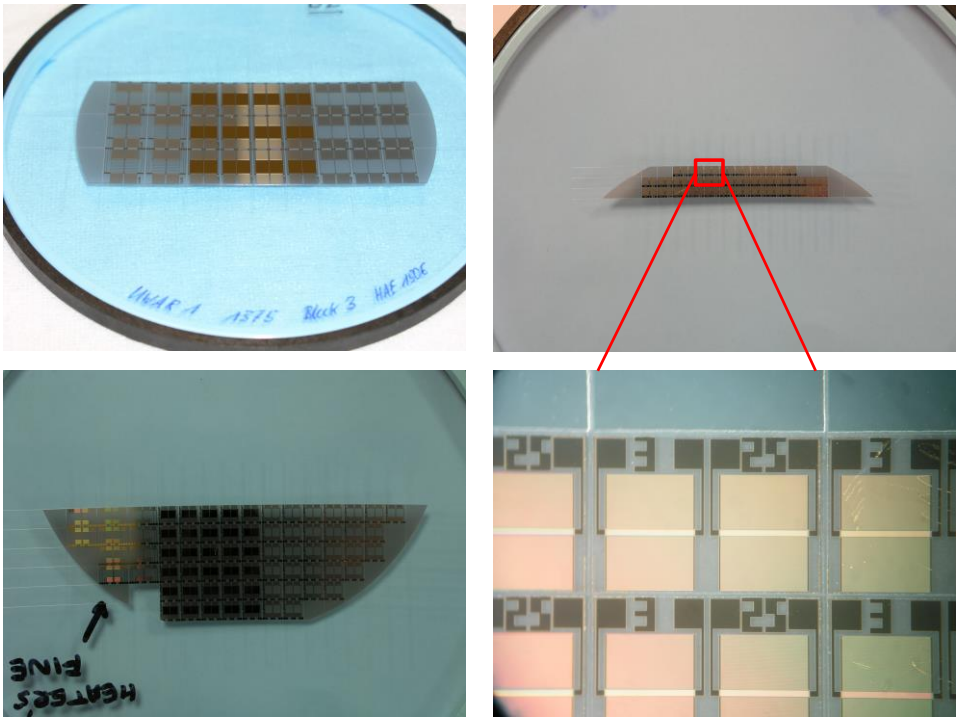

Figure 6.1: Fabricated and diced SH-SAW micro-sensors (resonators)

In order to protect the patterned IDT's, the photoresist was not removed while cutting. The wafer was diced using a Sola Basic Tempress saw (model 602) which has a diamond-coated blade which when live cuts at a high speed of ~30,000 rpm. In order to provide enough clearance (500μm) was left between individual designs the configurations. A 150μm thermocarbon blade was chosen. During the dicing the diamond coated

blade is impragnated with a stream of cooling deionised water and is designed to rinse out any dirt which arises when the saw cuts the wafer, as shown in **Figure 6.2, 6.3.**

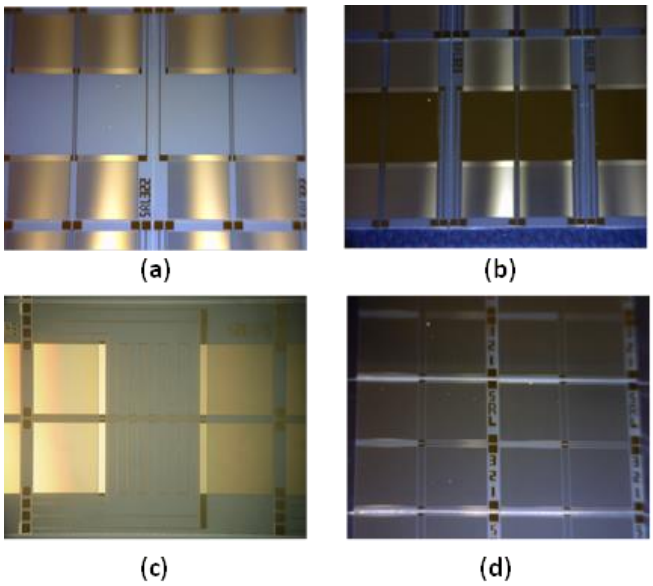

Figure 6.2: Fabricated 60 MHz SH-SAW micro-device (a) two port free device; (b) two port shorted device; (c) two port heater device; b) one port resonator

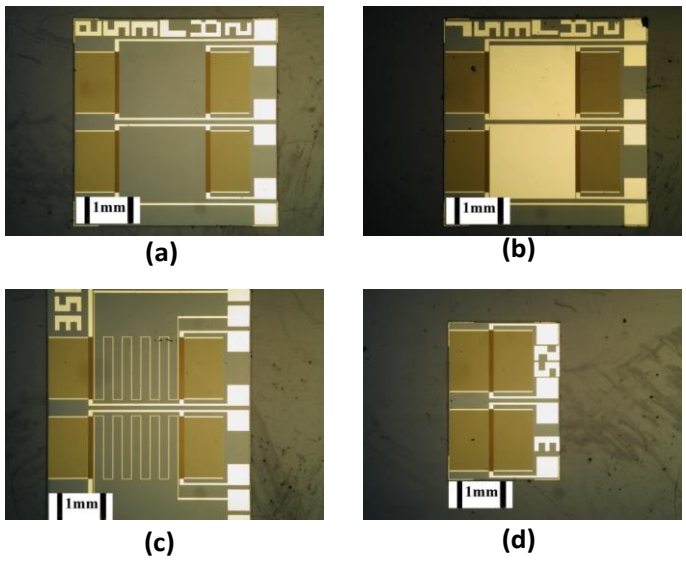

Figure 6.3: Fabricated 228 MHz SH-SAW micro-device (a) two port free device; (b) two port shorted device; (c) two port heater device; b) one port resonator

The wafers were loaded onto the appropriate side of a double sided chuck plate which is present to define the wafer sizes (2", 3", 4"). Being a brittle the piezoelectric wafer an initial test cut is always performed in order to define the steps or thickness through which the wafer will be diced. After the wafer has been diced, the individual devices can easily be peeled off the blue tape and can be mounted on a PCB, wire bonded and ready for use. The SH-SAW devices were then wire bonded using a wedge bonder.

6.3 Surface Acoustic Wave IDT Parameter Measurement

In order to obtain the frequency response of the SAW microsensor traditionally a network analyser is employed which measures acoustic wave's magnitude and phase as a function of frequency. As shown in the previous chapter, the generated acoustic waves are sensitive to different mechanical and electrical perturbation with the wave magnitude and phase changing as a function to time. Both the characteristic are crucial as they provide the user with information with regards to the different properties of the sensitive layer being measured. The knowledge of magnitude and phase response of the microsensor provides valuable information with regards to the nature of the immobilized layer. The network analyser is the traditional measurement tool employed to

characterise the scattering parameters (S parameters), which essentially describes the signal flow in the system, of the microsensor.

It consists of two coaxial connections also known as ports (Port-1 and Port-2), as shown in **Figure 6.4 (a)**. The test device is connected to the two ports. As the SH-SAW microsensors have a symmetrical design, the port did not matter as around as long as correct parameter was being measured. The S parameters are represented as ratios i.e. S_{in}/ S_{out} of the input and output signal levels, shown in **Figure 6.4 (b).**

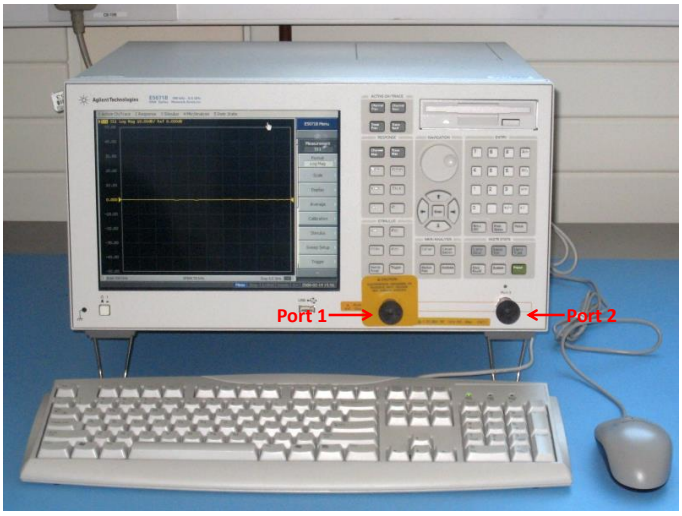

(a)

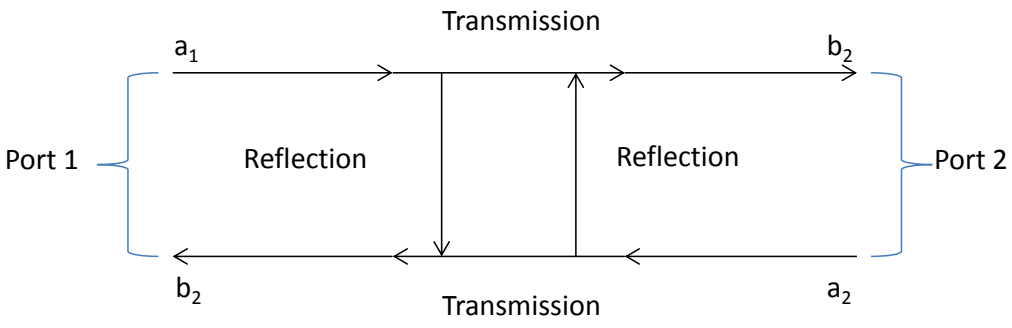

(b)

Figure 6.4: The Network Analyser with the different ports (a) and a schematic representation of the power between the ports (b)

The SAW microsensors are connected between the ports, also known as the reference plane, of the analyser and the energy flow, or signal flow, between the test ports can then be represented by a set of equations:

$$b_1 = a_1 S_{11} + a_2 S_{12} \quad \text{Eq. 6.1}$$

$$b_2 = a_1 S_{21} + a_2 S_{22} \quad \text{Eq. 6.2}$$

with the reflection (S_{11}, S_{22}) and transmission (S_{12}, S_{21}) coefficients represented as:

$$S_{11} = b_1/a_1 \quad \text{Eq. 6.3}$$

$$S_{22} = b_2/a_2 \quad \text{Eq. 6.4}$$

$$S_{12} = b_1/a_2 \quad \text{Eq. 6.5}$$

$$S_{21} = b_2/a_1 \quad \text{Eq. 6.6}$$

Modern network analysers are self-contained instruments which can store, manipulate and display data. After setting-up the device at the reference plane the reflection coefficient of the one port and two port SAW microsensors was measured.

6.3.1 RF characterization of one-port SH-SAW microsensors

As one port SAW microsensors have only a single electrical connection, which acts as both the input and the output port, the only output which can be measured is the reflected signal or the reflection coefficient i.e. the S_{11} or the S_{22}. The magnitude and phase response of

the SH-SAW microsensors was carried out. The measurements were performed under normal room temperature and without any over-layer or a surface film on the microsensors i.e. air.

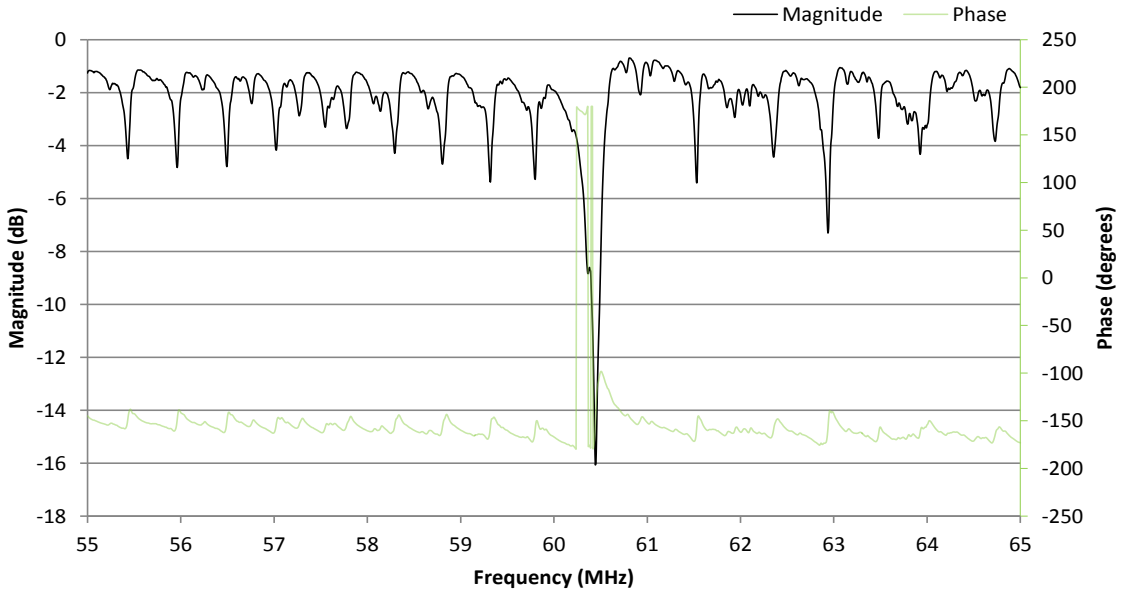

(a)

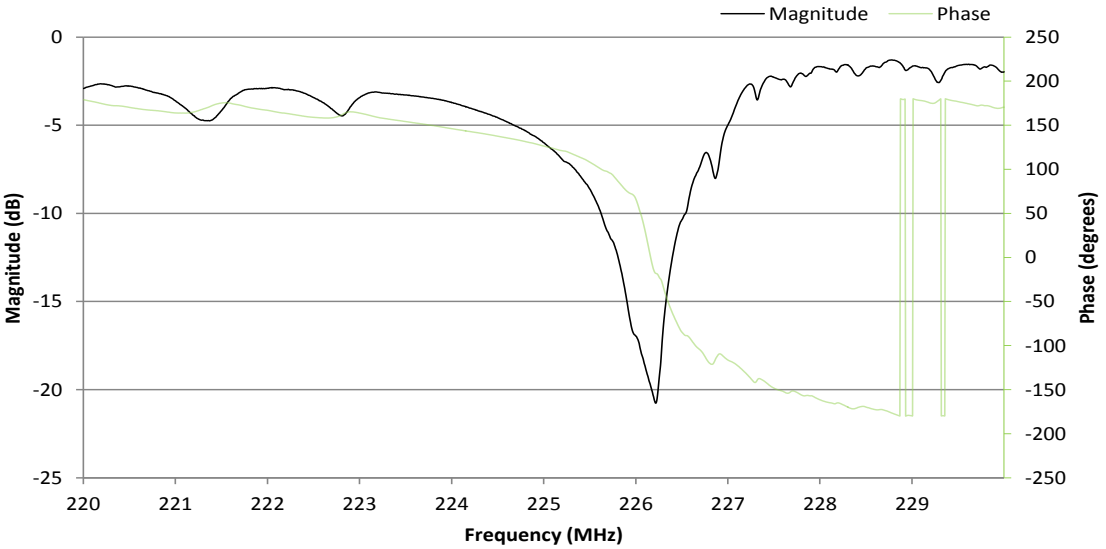

(b)

Figure 6.5: S_{11} parameter of the SH-SAW microsensors (a) 60.56MHz, (b) 228.79MHz

Figure 6.5 shows the reflection coefficients of the SH-SAW microsensors. It can be seen from the plots that a sharp resonance can be seen at the designed frequency for the 60.56MHz although the resonance peak is shifted by approximately 2 MHz for the 228.79MHz designed SH-SAW microsensors.

6.3.2 RF characterization of two-port SH-SAW microsensors

In contrast to the one port SAW microsensor, for which only the reflection coefficients can be measured, for the two-port resonator both the reflection and transmission coefficients can be measured. Although, in this case it is only the transmission coefficients (S_{12} or S_{21}) is of interest to the user as these devices consist of both an input port and an output port. The reflection co-efficient's are mainly measured to confirm the proper functioning of the IDT's if the user suspects that either of them are damaged. Thus, only the transmission characteristics ($S_{12,}$ $S_{21,}$) were measured for both the frequencies.

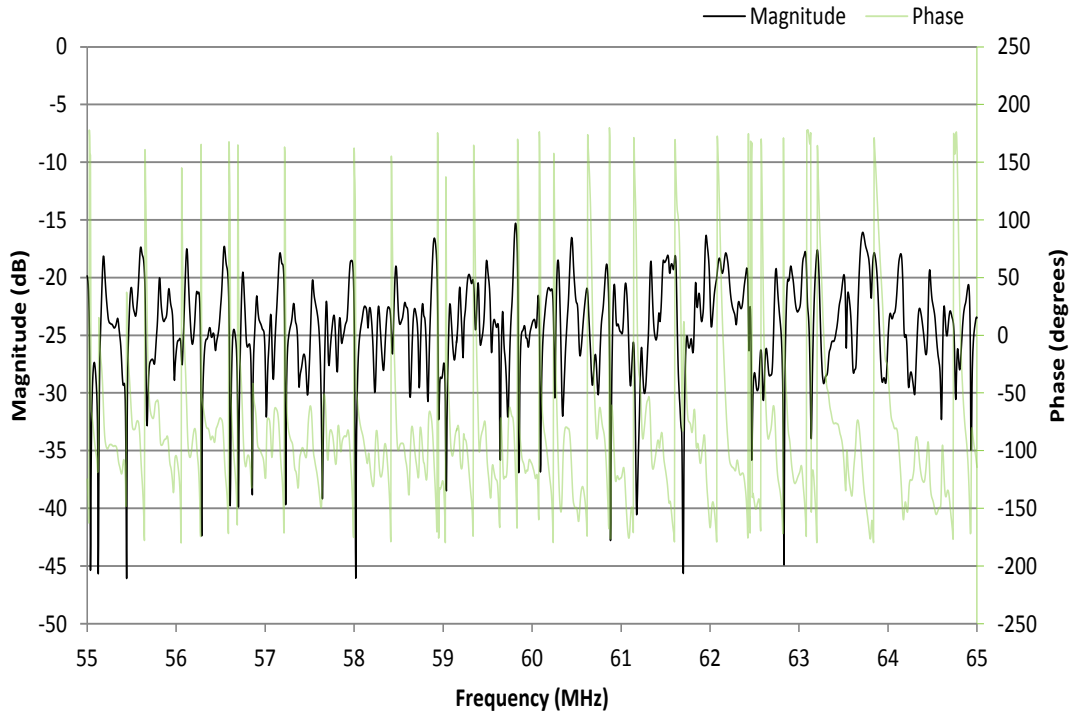
Magnitude
Phase
0
-5
-10
-15
-20
-25
-30
-35
-40
-45
-50
250
200
150
100
50
0
-50
-100
-150
-200
-250
55
56
57
58
59
60
61
62
63
64
65
Magnitude (dB)
Phase (degrees)
Frequency (MHz)

(a)

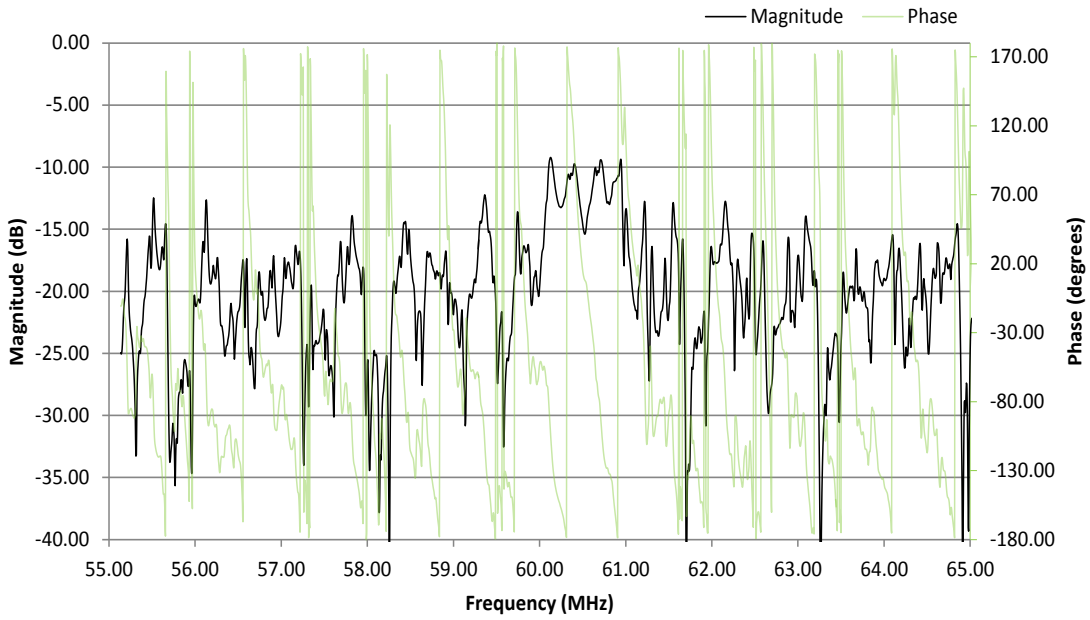
Magnitude
Phase
0.00
-5.00
-10.00
-15.00
-20.00
-25.00
-30.00
-35.00
-40.00
170.00
120.00
70.00
20.00
-30.00
-80.00
-130.00
-180.00
55.00
56.00
57.00
58.00
59.00
60.00
61.00
62.00
63.00
64.00
65.00
Magnitude (dB)
Phase (degrees)
Frequency (MHz)

(b)

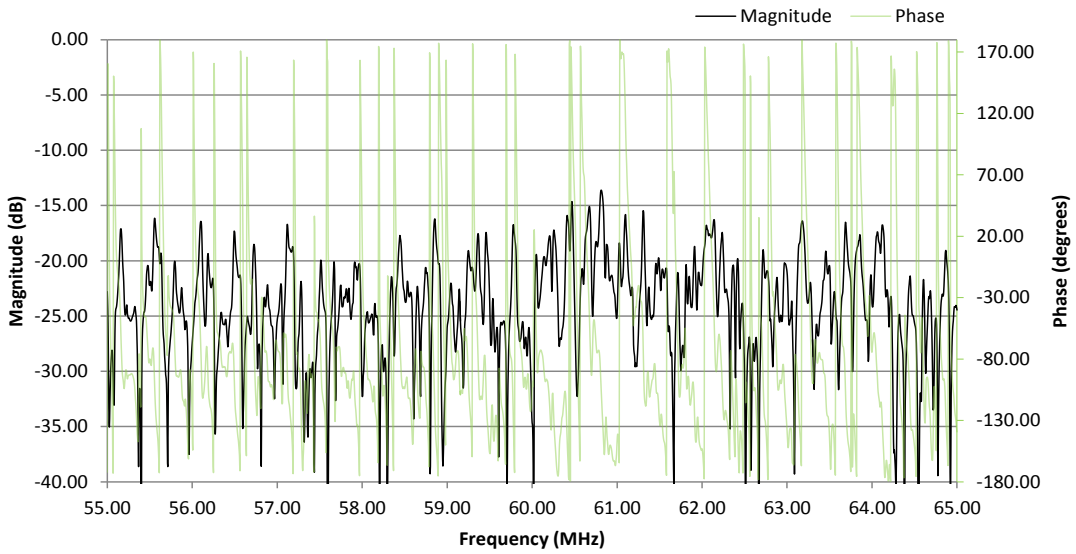

(c)

Figure 6.6 : S_{12} parameter of the 60.56 MHz SH-SAW microsensors (a) free, (b) shorted, (c) heater

Figure 6.6 shows the transmission coefficients of the SH-SAW microsensors. It can be seen from the plots that the acoustic wave suffers severe loss at the resonance frequency and thus a clear sharp peak is not available. Although for the SH-SAW microsensor with the shorted path **Figure 6.6 (b)** resonance can be observed around the design frequency of 60.56MHz.

In the similar fashion to the 60.56MHz SH-SAW microsensors, the 228.79 MHz SH-SAW microsensors were also connected to the network analyser and the transmission coefficients of the microsensor was measured under the same experimental conditions.

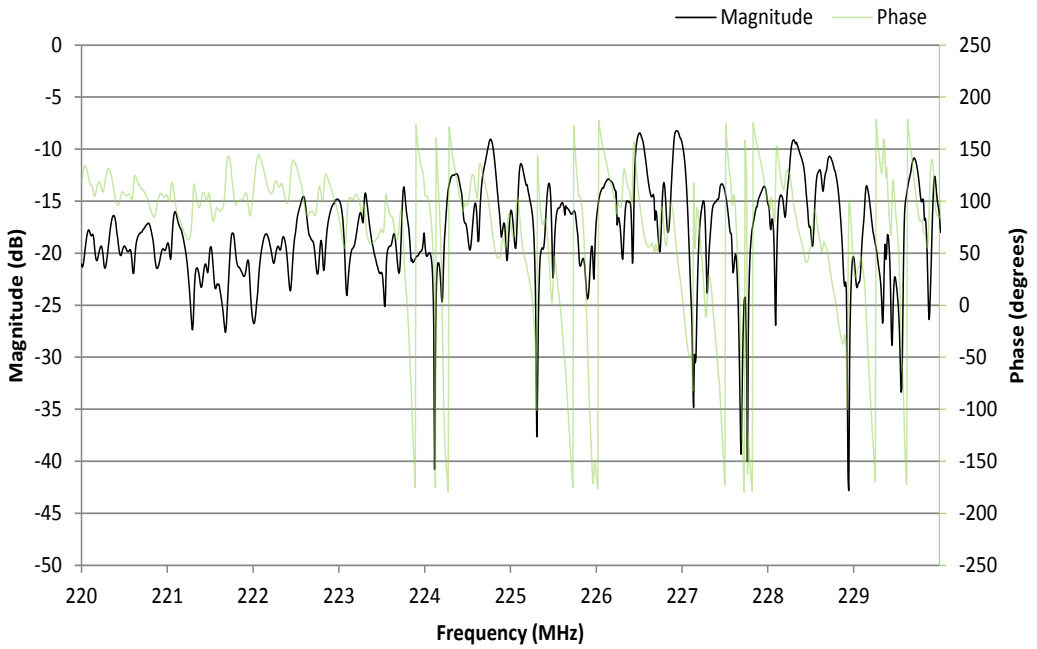
Magnitude
Phase
0
-5
-10
-15
-20
-25
-30
-35
-40
-45
-50
250
200
150
100
50
0
-50
-100
-150
-200
-250
220
221
222
223
224
225
226
227
228
229
Magnitude (dB)
Phase (degrees)
Frequency (MHz)

(a)

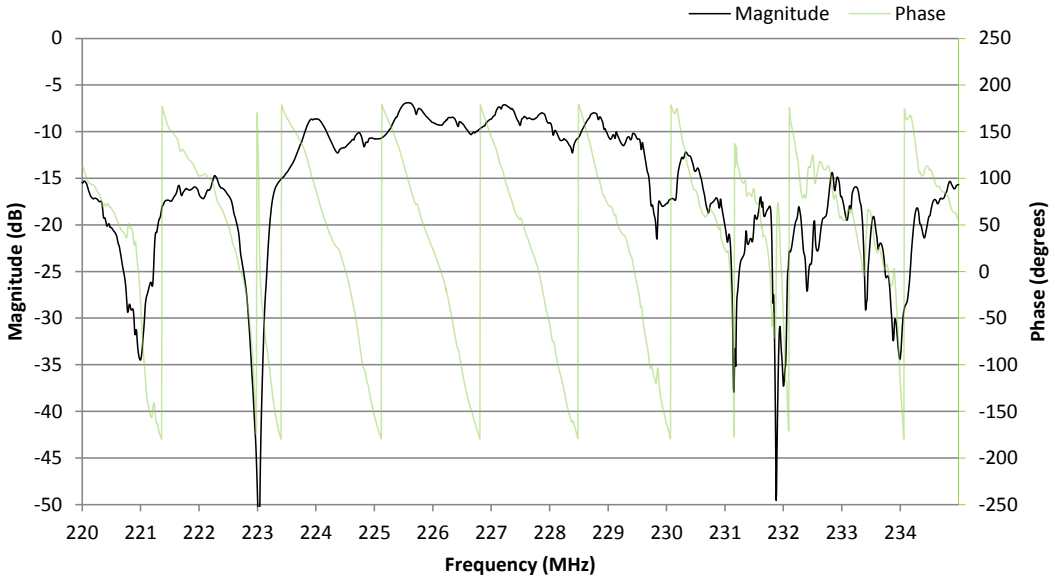
Magnitude
Phase
0
-5
-10
-15
-20
-25
-30
-35
-40
-45
-50
250
200
150
100
50
0
-50
-100
-150
-200
-250
220
221
222
223
224
225
226
227
228
229
230
231
232
233
234
Magnitude (dB)
Phase (degrees)
Frequency (MHz)

(b)

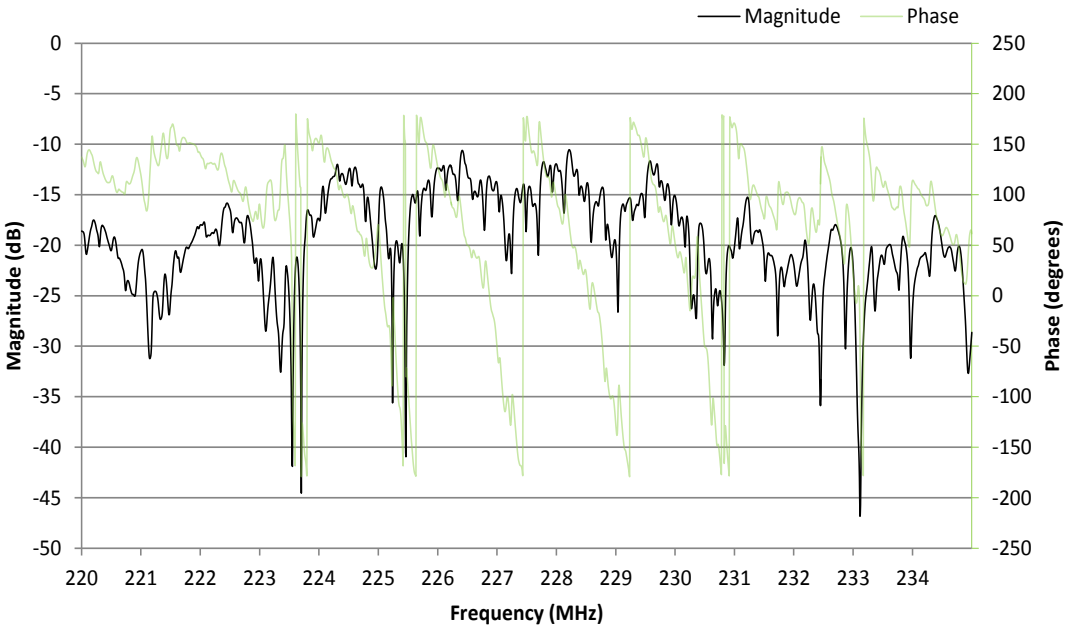

(c)

Figure 6.7: S_{12} parameter of the 228.69 MHz SH-SAW microsensors (a) free, (b) shorted, (c) heater

The loss profile measured for the 228.79Mz SH-SAW microsensors was found to be similar to the 60.56MHz microsensors i.e. the acoustic loss was greater for the free microsensors than for shorted microsensors. The most likely reason for such a characteristic is the presence of a SSBW (Bulk Wave). Hashimoto et al. in 2000 discovered that on a 36° rotated Y-cut X propagating lithium tantalate crystal, 2 different waves i.e. the SSBW and leaky SH-SAW are generated. As both the modes have very close phase velocities i.e. 4160ms-1(SSBW) and 4212ms-1(leaky SH-SAW) the leaky SH-SAW mode convert's to a SSBW mode when the propagation area is free [2]. The only way in which a pure leaky-SH-

SAW can be generated is in the presence of a waveguide which is usually in the form of a polymer coating or a metal deposition. Thus the shorted SH-SAW microsensors have a relatively better loss profile than the free of the heater design.

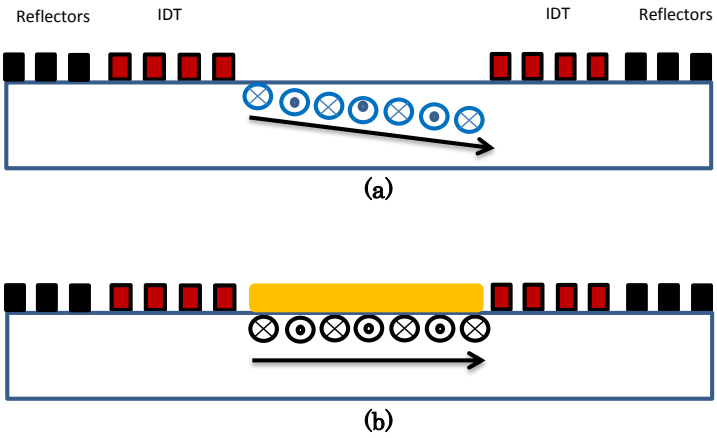

Figure 6.8: The presence of both types of waves in the crustal substrate (a) Bulk or SSBW and (b) Leaky

Despite the fact that a network analyzer is a stable setup that delivers very precise information with regards to the acoustic loss profiles of the microsensors, its potential downsides, in the current age of miniaturization and multi-channels measurements, outstrip its gains. The main downsides include the setup being time consuming with measurements restricted to only one sensor at one time and with no information provided with regards to the dynamic profile of the device in question. Some authors have presented work in which the amplitude and phase data from the microsensors has been recorded over an extended period of time but nearly all had to integrate their setup with a

LABVIEW generated program which was responsible for data collection [146] [101]. This, although being a practical solution to the bulkiness of the setup, still does not account for providing the user with the flexibility in order to test an array of microsensors. Thus another main focus of the work presented in this thesis was to miniaturize the measurement setup with the option of running multiple sensors in real-time.

6.34 Measurement Systems

There are, in essence, three types of measurement systems which are used for measuring the response of the acoustic wave microsensor as described by Wohltjen and Dessy in 1979. They are:

(a) amplitude measurement

(b) phase measurement

(c) frequency measurement system.

In an amplitude measurement the common mode RF output signals are split with a zero phase shift and are used to SAW sensor and the RF step attenuator. The diodes rectify the signal to produce a negative DC from the SAW sensor and a positive DC from attenuator. The signal from the unperturbed resonator is set to zero by the help of a potentiometer and a low-pass filter is then used to limit the bandwidth of the output signal.

A phase measurement system is similar to an amplitude measurement system with the only caveat being that the diodes are replaced by a double-balanced mixer. The common mode RF signal feeds into the mixer with a potential difference appearing at the mixer interface as a difference in IF frequency corresponding to the corresponding phase. The output signal is then fed to an amplifier through a RC filter circuit. **(Figure 6.9)** Although both the amplitude and phase measurement system unlike the network analyser method are portable and cost effective they have their associated advantages and disadvantages. Although amplitude heavy damping condition can be compensated by adjusting the external voltage amplitude, the method has a poor dynamic range 10,000:1 and 1000:1. This when compared to the frequency or time measurement systems which have a dynamic range of 10^7:1 is hardly precise or accurate. Furthermore the use of potentiometers complicates the setup and the system is prone to erroneous baseline readings.

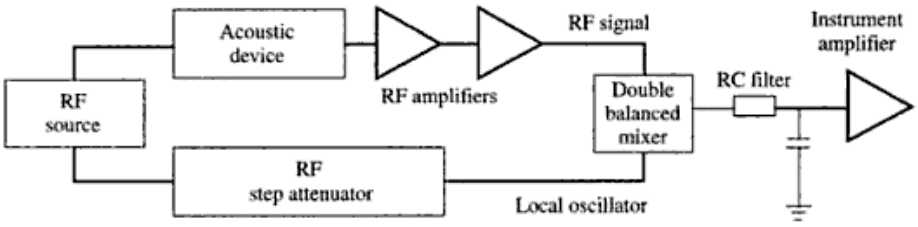

Figure 6.9: A phase measurement system

In a frequency measurement system, the acoustic wave resonators are employed as a feedback element in an oscillator circuit. **(Figure 6.9)** In an oscillator loop acoustic wave microsensor provides a feedback path for the amplifier, thus in order to obtain a stable oscillation the signal should add constructively to itself after having travelled through the loop. Therefore at the return point the signal should have:

- Equal amplitude
- Shifted in phase by 2π radians

Both of these conditions are met at the frequency point where the gain of the amplifier is greater than the insertion loss of the microsensors i.e. the resonant or harmonic frequencies. Although such a measurement technique provides no information with regards to the signal amplitude, it does provide valuable information such as information with regards to the frequency and the quality factor of the microsensor due to a mechanical loading.

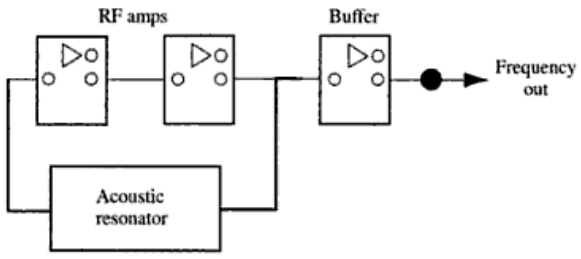

Figure 6.10: A frequency measurement setup

Therefore in view of the above information, besides measuring the attenuation magnitude and phase, with the help of the network

analyser, of the microsensors frequency based measurements approach was also adopted to monitor changes in the resonant frequency with respect to time- thus providing real-time information of the processes.

6.4.1 Oscillator Setup

In order to build stable oscillator circuit different topologies were review which included a Schmitt, Colpitts and Pierce circuits. The choice of an optimal circuit layout is driven by the frequency/phase characteristics of the acoustic wave microsensor which works as a part of the feedback element in the circuit. Ultimately the Schmitt oscillator topology was chosen for the current work, as shown in **Figure 6.10**.

In order to obtain a stable oscillation, two condition needed to be satisfied i.e. the acoustic wave magnitude, after amplification, should be greater than zero and the phase must shift by 2π radians.

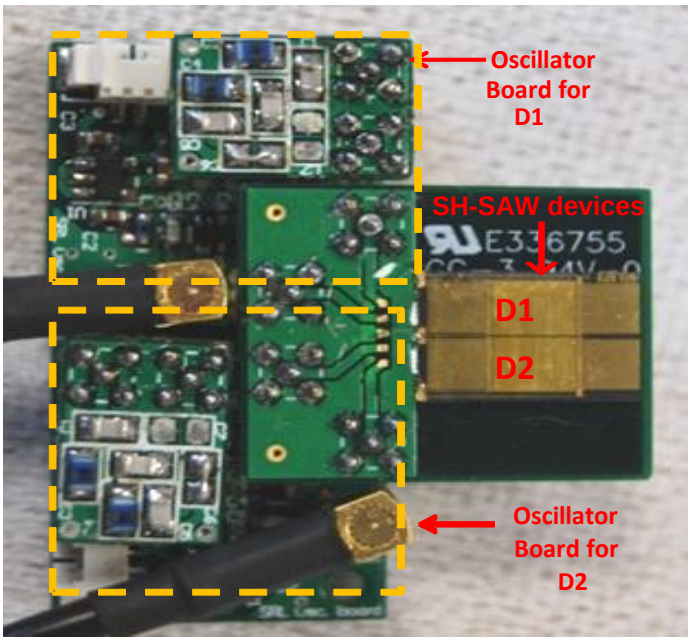

Figure 6.11: The fabricated oscillator board along with the mounted SH-SAW microsensor.

The SH-SAW oscillator circuitry was powered by a 4-channel variable power supply with the supply voltage limited to 4V AC. In order to acquire the data monitored by the oscillator board, the sensor outputs were connected to the JLM FQ4 interface data acquisition board (JLM Innovation GmbH, Germany) through SMA cables. Both the SH-SAW microsensors were mounted on the daughter boards was connected and baseline measurements were recorded.

6.5 Microfluidic Chamber Design

6.5.1 PDMS based central Housing Unit

In order to perform experiments in the liquid phase the first and foremost requirement is to confine the liquid and to do that a microfluidic chamber was designed and fabricated using a biocompatible polymer polydimithylsiloxane (PDMS) which has been employed in a large number of biological applications. The PDMS based microfluidic chamber was designed based on two key objectives:

- Limit the sensing area employed during experimentation for efficient use of the microsensor properties
- Provide the ability to use the system for measurement using biological coatings such as cells.

PDMS has become popular choice of material used extensively for fabricating microfluidic devices with different authors reporting their integration with acoustic wave microsensor [147]. It is a transparent elastomeric polymer which is highly flexible, optically transparent and demonstrates good biocompatibility. In addition to this, PDMS based microfluidic device provide a high surface area/volume ratio provides an efficient path for permeable to oxygen and CO_2 thus providing an ideal platform which can act as a compartmentalised microfluidic system for cull culture [148]. Also, cell culture chambers and devices, fabricated using PDMS, have been successfully demonstrated to be compatible with hepatocytes and with other insect cells although long term cell culture

growth has still been an issue [149] [150] [151]. Fabrication of PDMS based microfluidic channels, chambers can be carried out under normal laboratory conditions as opposed to cleanroom facilities, although in order to fabricate finer structures e.g. sub-µm channels, cleanroom facilities are employed [152] [153].

The PDMS chamber design was kept simple and straightforward, although the chambers were designed to be fabricated with hypodermal syringes. Additionally as dual devices were being employed, the pre-requisite of the design was to have a presence of a thin wall between the chambers which would separate the control sensor from the experimental sensor. Additionally, an inlet and an outlet were required for the chambers such that it could be integrated with an automated system and experiments could be run with different biological solutions. Two different types of PDMS chamber were realised in this study. One design was for the 60.56MHz SH-SAW micro-devices with the other design being for the 228.78MHz micro-devices.

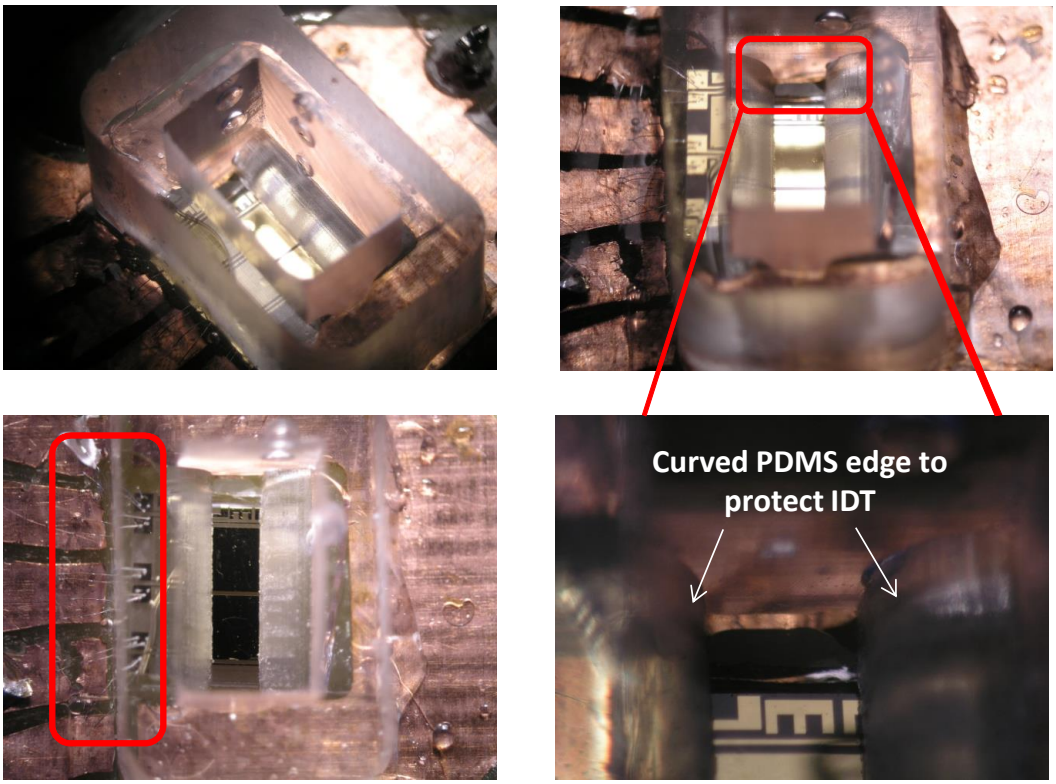

Figure 6.12: PDMS base microfluidic chambers

The oscillator setup including the SH-SAW microsensor and the central housing unit were integrated with a fully automated system which consisted of a six manifold mounted solenoid valves, a diaphragm metering pump connected by C-Flex® tubing, a NI-6009 multifunction data acquisition board (National Instruments, USA), and a custom high-current interface circuit. A Dino-Lite digital microscope (Dino-Lite Europe, The Netherlands) enables the real-time visual monitoring of the Sf9 cells on the sensor surface. A bio-compatible incubator is used to ensure temperature stability. The complete set-up is shown in **Figure 6.12**.

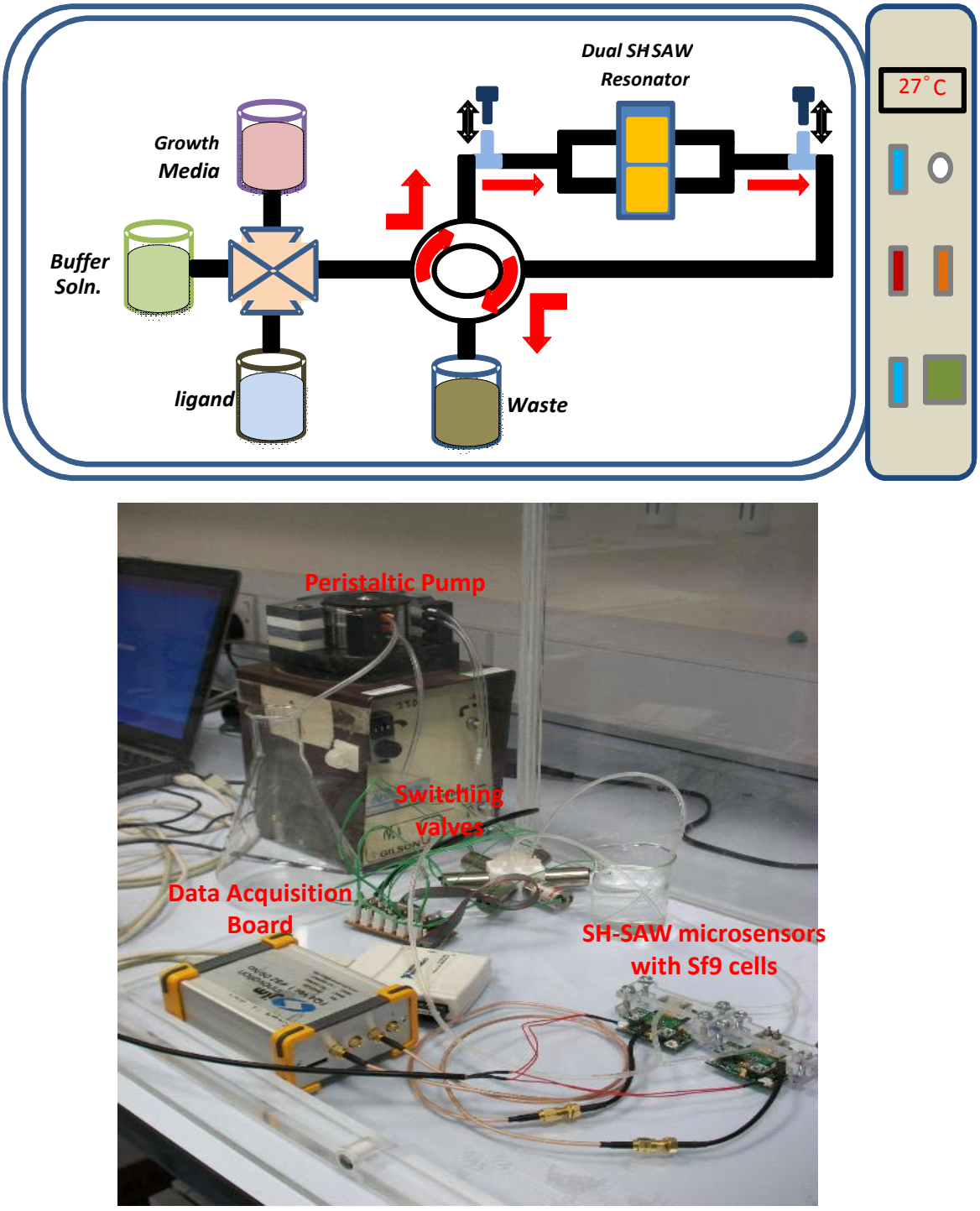

Figure 6.13: The Automated system along with the associated circuitry

6.6 Conclusion

In this chapter the characterization of the fabricated SH-SAW microsensors was carried out using a network analyzer. Additionally the SH-SAW microsensors, both the 60.56MHz and 228.79MHz have been integrated with an oscillator board and associated microfluidic chambers have been built and integrated with an automated system consisting of different valves, manifolds and tubing's. In the next chapter, the system developed here has been employed to monitor the adherence activity and GPCR–ligand interaction of Sf9 insect cell.

Chapter 7
Experimental results using Sf9 whole-cell coated SH-SAW microsensors

7.1 Introduction

The previous chapters have concentrated on the development of SAW microsensors which were capable of operating in the liquid phase. Subsequent chapters also demonstrated the development of an automated system along with peripheral microfluidic which included a central housing unit, fabricated out of a biocompatible polymer – PDMS. In this chapter, Sf9 cells were immobilized on the SH-SAW microsensor surface. After adhering to the gold surface, the concept of ligand-receptor interaction was examined by exposing the Sf9 insect cells to an insect neurotransmitter – octopamine hydrochloride. Octopamine acts as a ligand to the endogenously expressed octopamine receptors – a class of

GPCR receptors present in the Sf9 cell membrane. In addition to presenting the experimental methodology and results, the chapter also presents an empirical model that has been constructed which co-relates the experimental results to the background theory, presented in Chapter 4. A case study based approach has then been adopted which examines and debates the different possible scenarios and attempts have been made to explain the results.

7.2 Experimental Methodology

Insect cell line, Sf9, derived from parental colony *Spodoptera frugiperda*, was adopted as the functional sensing layer (the primary transducer) for the 60.56 and 228.79 MHz SH-SAW (shorted) microsensors. This particular cell line was adopted as their growth conditions were found to be less stringent than other cell lines e.g. HEK 293, and experiments could also be performed under normal room conditions i.e. 28°C or lower with no extra requirement of carbon dioxide or oxygen [148]. In addition to these properties, Sf9 cells were found to demonstrate good adherence characteristics on different substrate materials e.g. gold, lithium tantalate. This was confirmed by experiments performed by the iCHEM project partner – Department of Pharmacology and Physiology, University of Leicester. The iCHEM team at the Department of Pharmacology and Physiology, University of Leicester optically examined the adherence profile of Sf9 cells over a

period of 3 days and on four different surfaces - gold, lithium tantalate, quartz and zinc oxide, **Figure 7.1.**

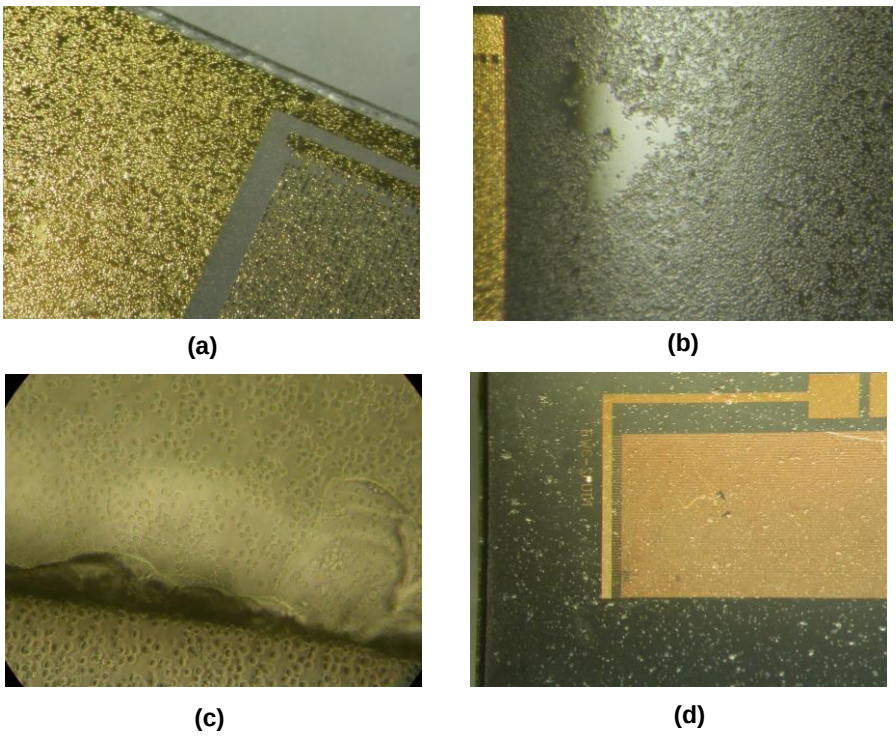

Figure 7.1: Sf9 cell adherence on (a) gold; (b) lithium tantalate (c) quartz (d) zinc oxide

The cells were viewed using a table-top optical microscope. Cell substrate interactions have been one to the major areas of research with different methods available to study the degree of cell adhesion to the substrate surface [91]. Cell counting revealed that the adherence preference was more towards gold and bare lithium tantalate surfaces than quartz and zinc based substrates.

Another property of Sf9 cell-line that made it attractive was their endogenously expressed octopamine receptors, a class of GPCR's, located in their cell membrane [154]. This meant that experiments demonstrating the concept of GPCR mediate ligand-receptor interactions could be performed on this cell-line. The naturally occurring ligand of the endogenously expressed receptors was octopamine hydrochloride – an invertebrate neurotransmitter [155].

The 60.56 and 228.79 MHz SH-SAW devices were employed for the experimental purposes with only one of the sensors of the dual setup immobilised with the Sf9 cell-line with the non-functionalised part of the chip acting as the experimental control, as shown in **Figure 7.2**

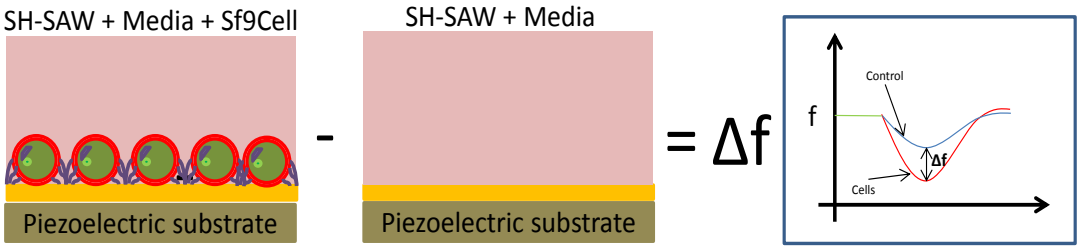

Figure 7.2: The dual SH-SAW sensor with the experimental and the control sensor and their differential signal.

The immobilizing area for Sf9 whole cells was limited to the delay path of the SH-SAW microsensors. This was based on the study performed by Lee et al. who examined the positional dependency of SAW resonator structures [94]. Their study focussed on identifying the "appropriate immobilisation points" on a SAW microsensor surface [94].

This was done by loading different regions of the microsensor surface and measuring the frequency characteristics of the device before and after immobilization [94]. Although, theoretically, the physical reflections occurred from the edges of the first grating, the standing wave pattern extended well beyond the edges of the grating with the wave energy found to be decaying exponentially for the regions beyond thus concluding that the area between the IDT's the acoustic resonator had a relatively flat energy distribution [94]. They concluded that there was non-uniform acoustic energy distribution on the SAW resonator surface and closely match the one represented by **Figure 7.3** [94].

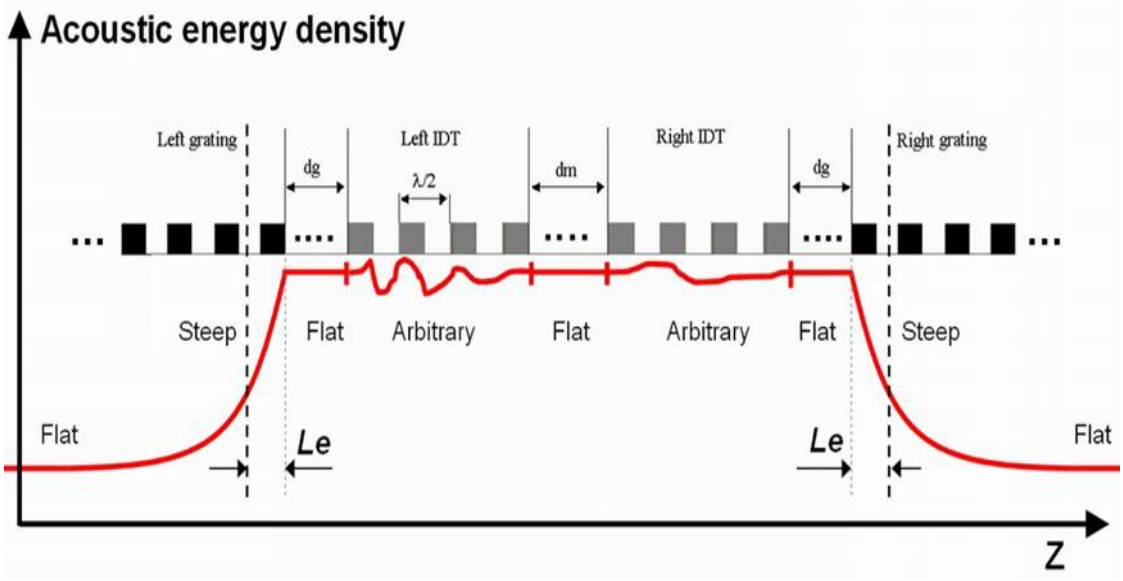

Figure 7.3: Acoustic energy distribution of the acoustic (surface) wave

In addition to the above outlined factor limiting the immobilization area on the SH-SAW microsensors, it would be convenient to control the number of cells that could be injected onto the sensor surface adding precision to the experimental procedure.

For the 60.56 MHz SH-SAW devices large PDMS based central housing units could be built on the delay path as the devices has larger dimensions. Extra care was taken while building PDMS chamber for the 228.79MHz SH-SAW devices as the delay path i.e. the growth area was very narrow and limited.

Additional care was also taken to protect the IDT's from the ionic cell growth medium. This was achieved by spray coating the IDT's with a 5% v/v PMMA polymer solution. The PDMS chamber was fabricated with curved edges and thick support side wall, as shown in **Figure 7.4**. This property helped in protecting the IDT from the ionic property of cell media by acting as an air tight sealant. **Figure 7.4** outlines the steps.

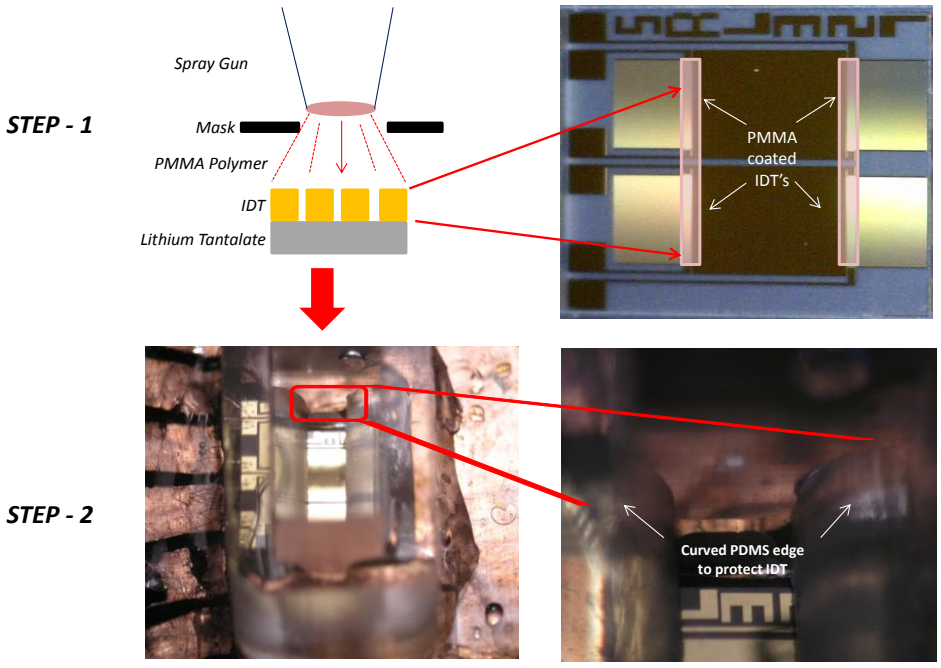

Figure 7.4: A two-step process adopted to protect the IDT's and ensure limited growth area.

After spray coating the IDT's the PDMS chambers were glued down using UV cured adhesive glue. Before starting each experiment, the entire setup – oscillator board, PDMS chamber + SH-SAW device was maintained inside an incubator at 28°C.

The next few sections outline the experimental results and observations made during the process. The sections have been divided into different experiments.

7.3 Experimental Results

7.3.1 Acoustically Monitoring Sf9 Cell adherence characteristics using 228.79MHz SH-SAW devices.

Initially, the test setup was maintained for half an hour in the incubator @ 28°C. After obtaining a stable baseline in air, cell growth media was added to the PDMS chamber on the 228.79 MHz SH-SAW (Shorted) devices. Due to the change in phase i.e. air to liquid, the loading effect of the growth media on the sensor surface caused an initial shift in the resonant frequency of ~12,000 Hz.

The setup was then left inside the incubator for a time period of 30 minutes in order for the temperature to re-stabilise. Thereafter 40,000 Sf9 cells were pipetted (t = 1460sec) into the PDMS chamber (experimental sensor) containing the growth medium. At this time a spike in signal level was seen, signifying a system disturbance. At t = 2600 sec, the top 10µl of the media in the PDMS chamber was replaced with fresh media, **Figure 7.5**. The same procedure was performed on the control sensor but instead of suspending cells at t = 1560 sec, an equal amount of growth media was suspended onto the microsensor. The adherence profile of the Sf9 cells along with the differential signal

(experimental– control) plots have been shown in **Figure 7.6.** The plot also show the background system noise. After removing the signal drift the cell adhesion process demonstrated a shift in resonant frequency of approximately 2500Hz.

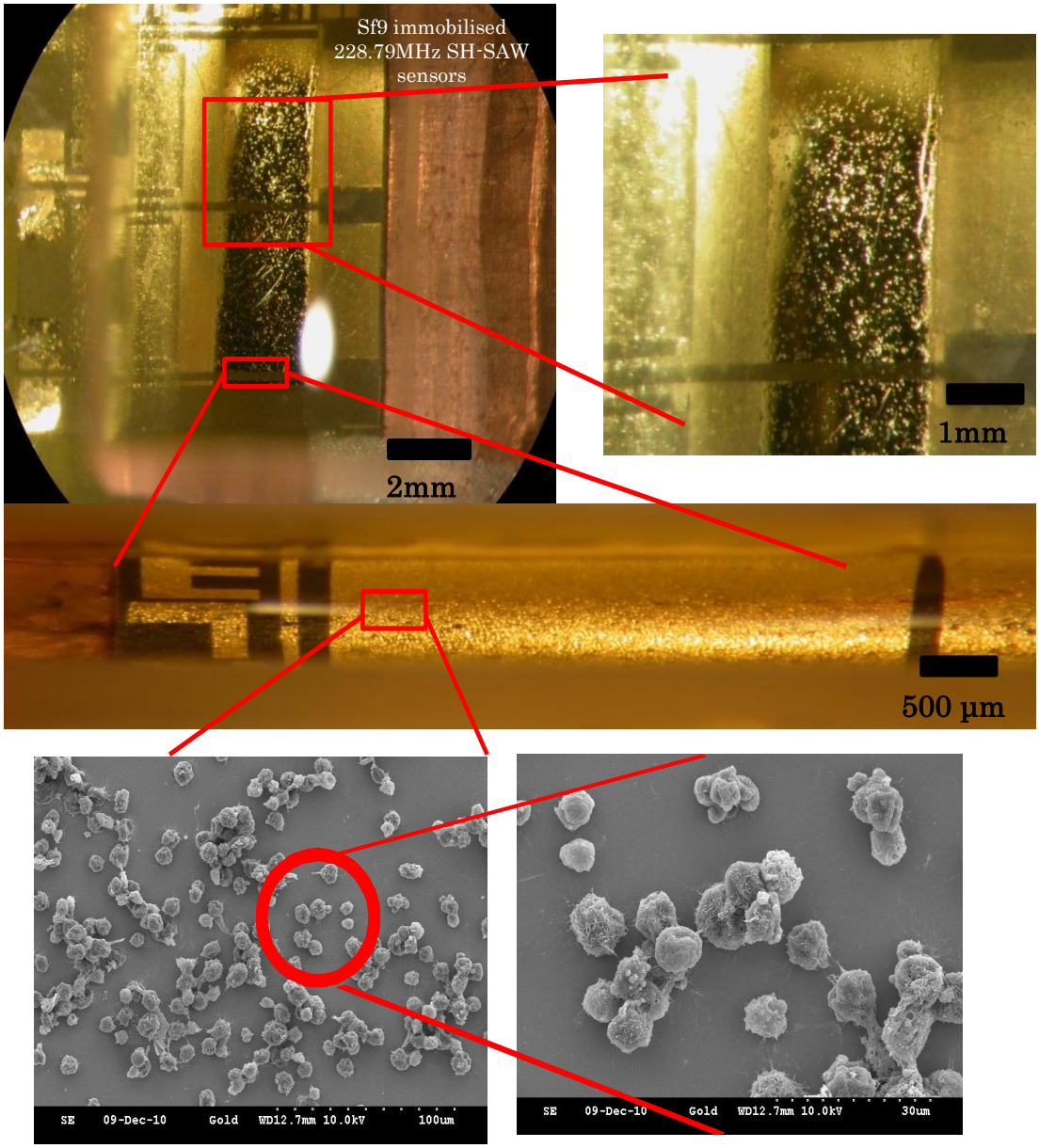

Figure 7.5: Immobilized Sf9 cells on the 228.79MHz SH-SAW microsensors along with SEM view of the adhered cells.

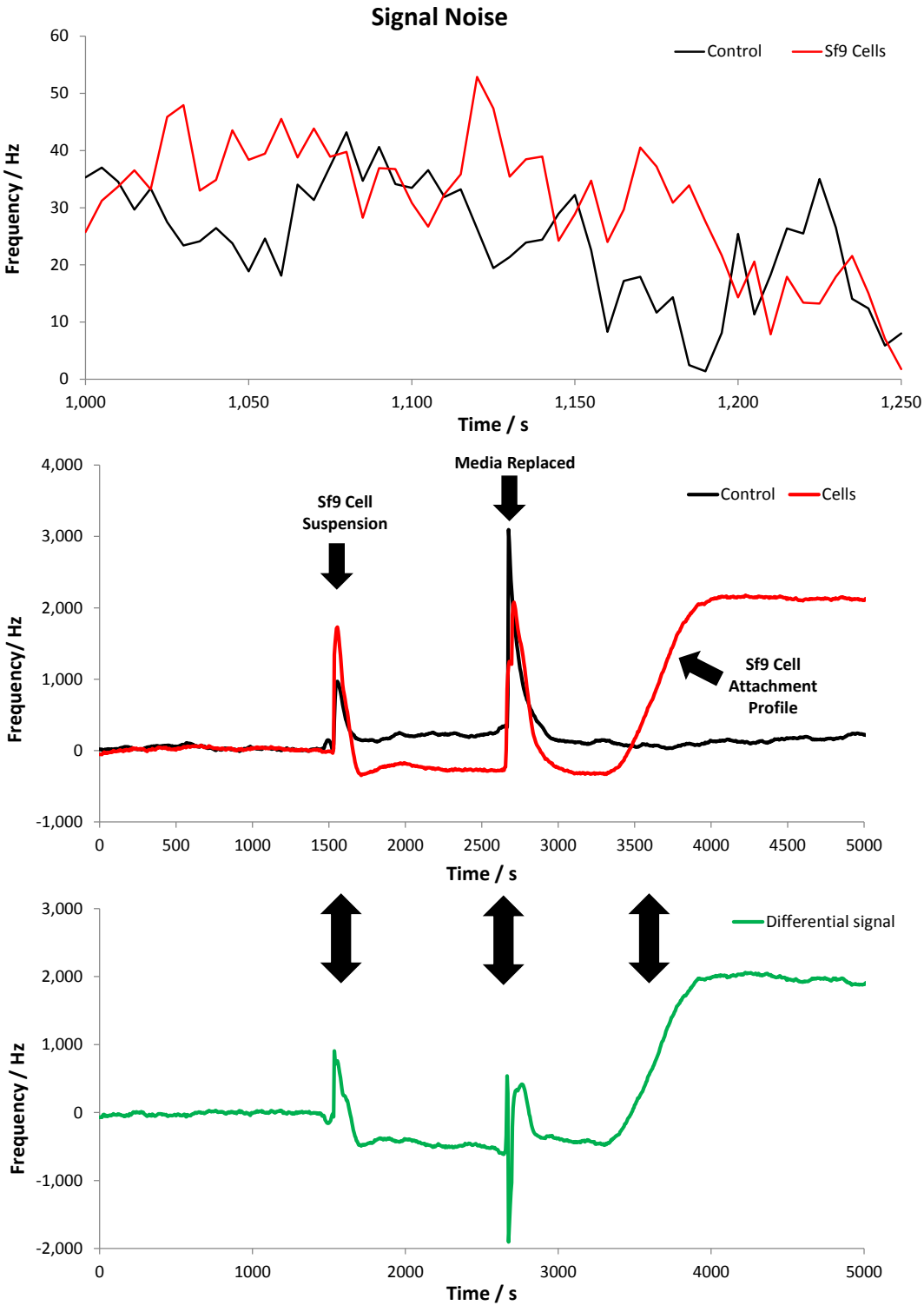

Figure 7.6: Sf9 cell attachment profile (a) signal background noise, (b) depicting the Sf9 cell suspension time and (c) showing the differential signal level

7.3.2 Acoustically monitoring receptor- ligand interactions by 228.79MHz SH-SAW devices.

After acoustically characterising the adherence profile of Sf9 cells on the gold surface the concept of GPCR mediated receptor-ligand interaction was examined by the help of octopamine hydrochloride - an invertebrate neurotransmitter. As specified earlier octopamine acts as the ligand for the endogenously expressed GPCR octopamine receptors present in the cell membrane of the Sf9 cells. Octopamine has been known for triggering intracellular responses e.g. opening of the ion channel, change the Ca^{2+} levels within the cells to name a few . The aim of this experiment was to acoustically monitor the downstream reactions triggered by the ligand-receptor interaction as shown in **Figure 7.7.**

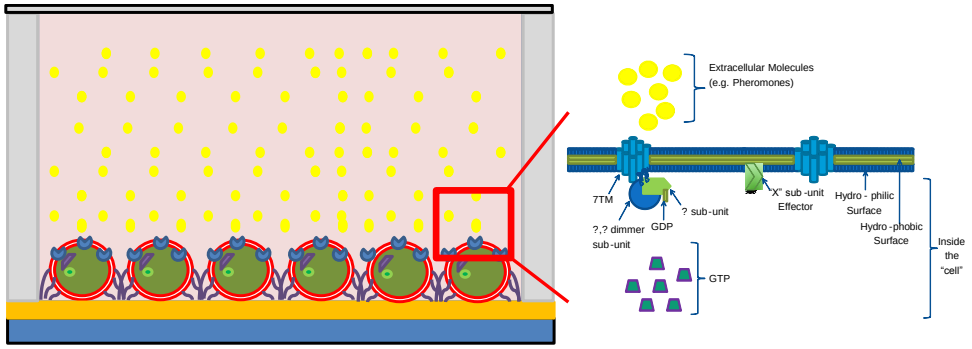

Figure 7.7: Sf9 cell response to ligand octopamine.

After the cells had completely adhered to the gold surface of the microsensor, the setup was allowed to stand for approximately one hour

@ 28°C. Thereafter octopamine hydrochloride of 100µM (final concentration – prepared in DI water) was manually pipetted onto the sensor surface – control and experimental sensors. **Figure 7.8** shows the octopamine mediate behaviour recorded by the 228.79MHz SH-SAW microsensors.

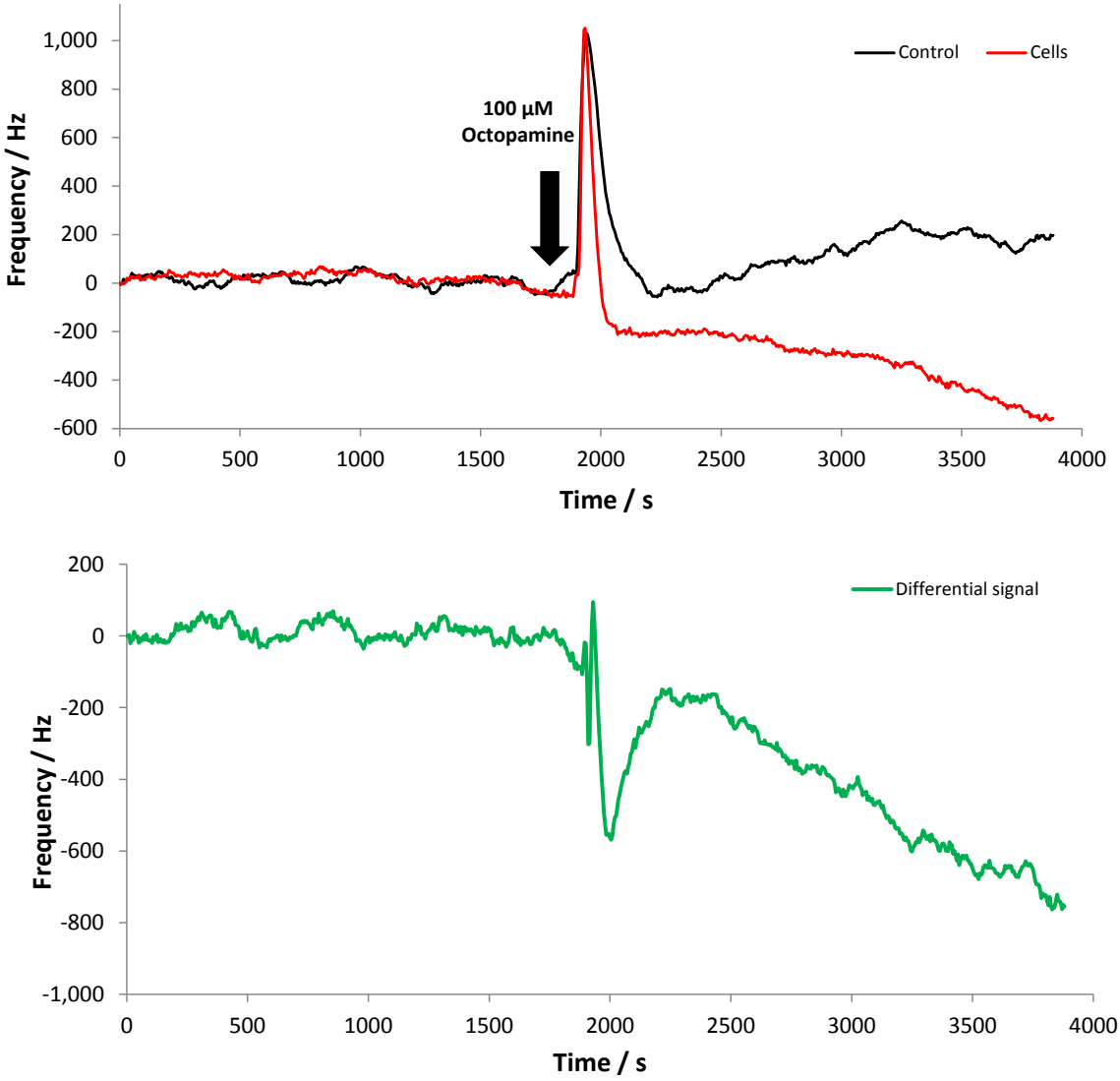

Figure 7.8: Sf9 cell response to 100µM Octopamine Hydrochloride.

The acoustic signal of the experimental sensor (with cells) showed a negative slop while the control signal was seen to have a slope trending positive. Both the acoustic signals were seen not to recover. The differential signal can be seen in **Figure 7.8**.

Experiments I and II demonstrated successful that a measurable response could be generated using the SH-SAW microsensors. Thus the cells to varying concentrations of the ligand (octopamine).

In order to successfully attempt this, the automated fluid delivery system, shown in Chapter 7 was employed using the 60.56MHz SH-SAW (shorted) devices. The key reasons why these devices were employed were

- higher acoustic penetration depth (72nm) when compared to the 228.79 MHz SH-SAW devices (37.4nm).
- large sensing area (5mm compared to 2mm) thus providing higher flexibility with regards to the PDMS chamber design.

As an automated system was being adopted, the PDM chambers were integrated and fabricated with a hypodermal syringe which would act as the input port through which Sf9 cells could be introduced onto the experimental sensor surface. The PDMS chamber was mounted onto the SH-SAW sensors chip by the help of Perspex strips, **Figure 7.9.**

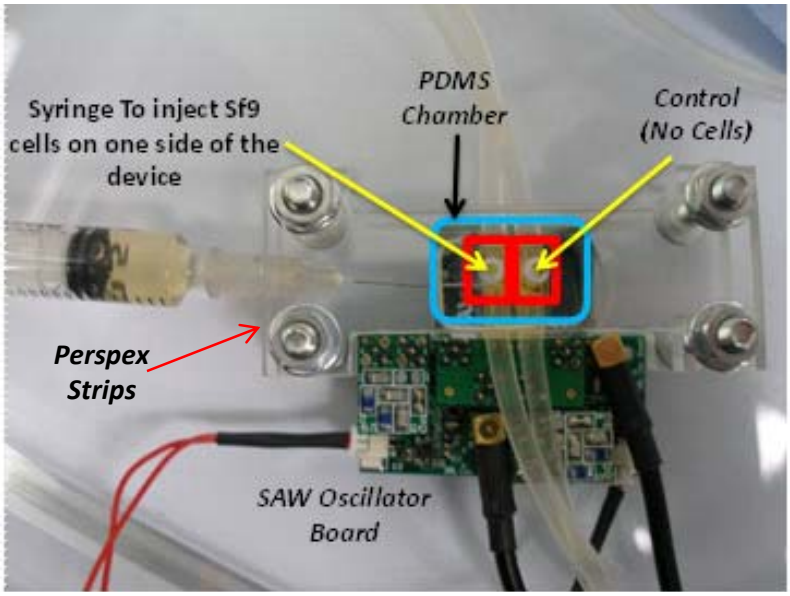

Figure 7.9: Experimental setup for 60.56MHz SH-SAW

7.3.3 Acoustically monitoring the adherence profile of Sf9 insect cells by 60MHz SH-SAW devices integrated with an automated system.

After allowing the automated system to stabilise for half an hour in the incubator @ 28°C a baseline in the cell growth media was obtained. The media was delivered using a laboratory based peristaltic pump and when the entire system was purged with growth media the pump was switch-off. The setup was then allowed to stand for approximately 30 minutes and thereafter 40,000 Sf9 cells @ t = 1460sec, were injected into the PDMS chamber (experimental sensor) using the hypodermal syringe. The entire process can be seen in **Figure 7.10**.

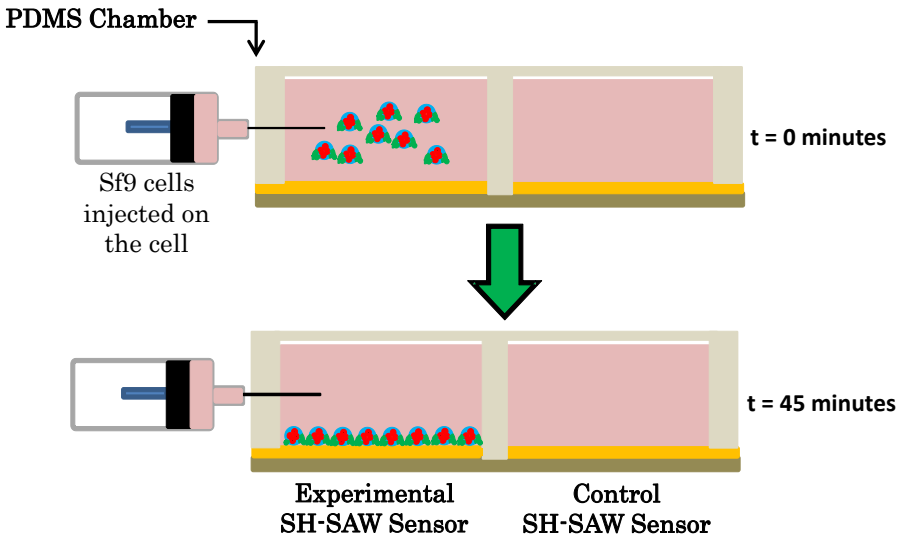

Figure 7.10: Process of Sf9 cell injection

As the system was disturbed during injection, a sharp spike, similar to the one observed in Experiment I and II was observed. **Figure 7.12** shows the cell adherence characteristics of the Sf9 cells on 60.56MHz SH-SAW (shorted) microsensor along with the differential signal, **Figure 7.11.**

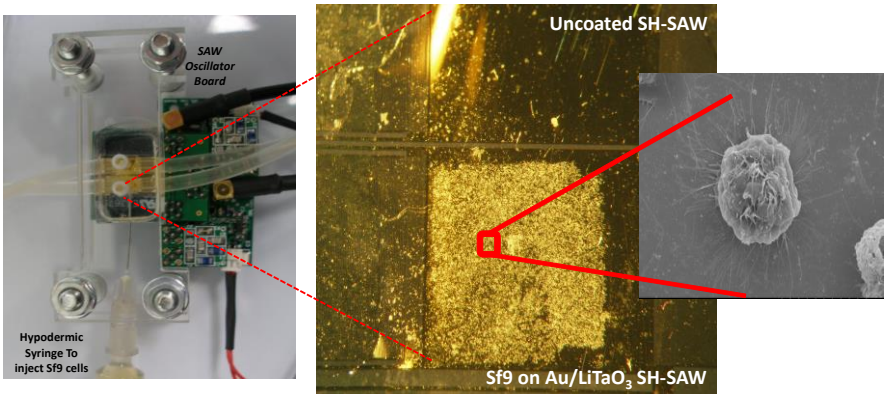

Figure 7.11 60.56 MHz SH-SAW microsensors with immobilized Sf9 cells

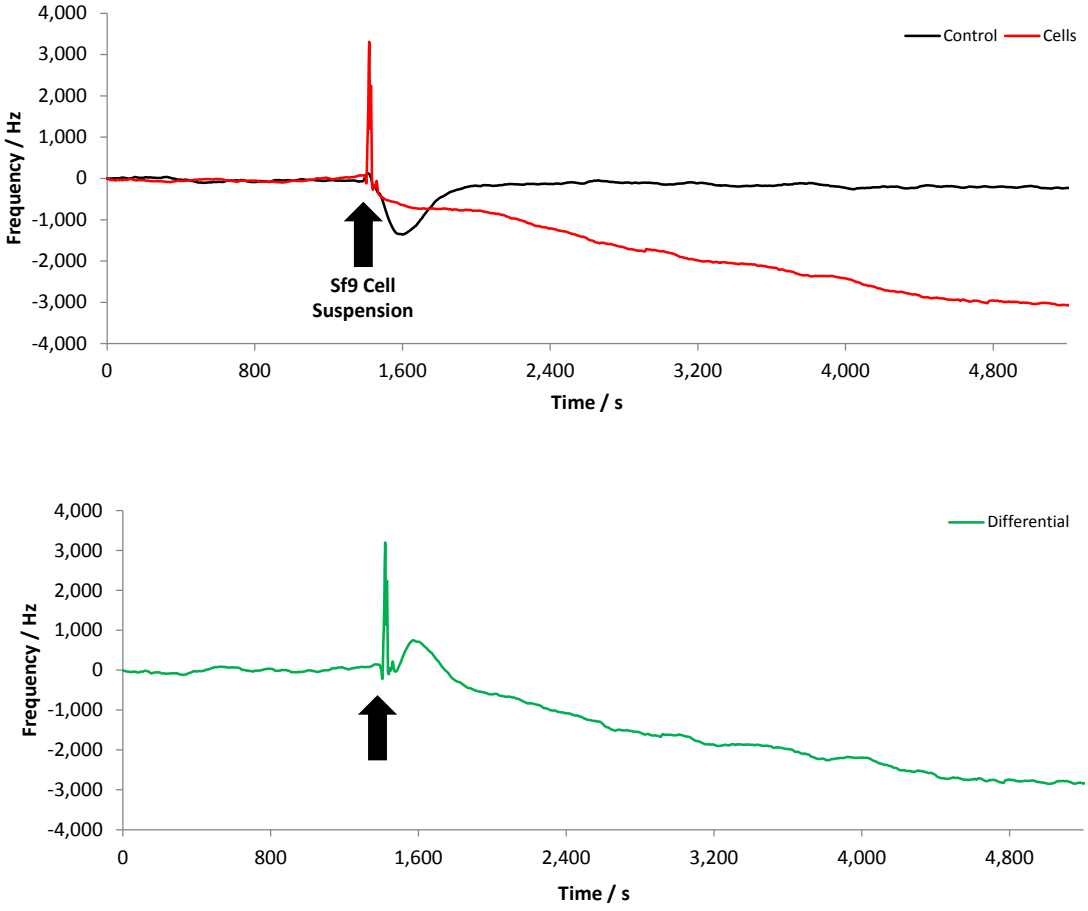

Figure 7.12: Sf9 cell attachment profile using 60MHz SH-SAW sensor.

The entire process of Sf9 cell adhesion was observed to last for approximately 45 minutes and the shift in the resonant frequency of the functionalised sensor with respect to the reference sensor was found to be ~2.8 kHz.

7.3.4 Acoustically measuring cellular reaction in Sf9 (W) type cells and Octopamine Hydrochloride using 60.56 MHz SH-SAW micro-sensors.

After examining the adherence characteristics of Sf9 cells on the SH-SAW microsensors octopamine concentration experiment were carried out using the automated system. Different concentrations (12.5, 25 and 50μM) of ligand were prepared in cell growth medium and exposed to the immobilised cells with each exposure lasting for 2 minutes. A switching valve, described in chapter 7, was employed to switch between octopamine and growth medium i.e. 2 minute octopamine exposure followed by 10 minute growth media exposure. Each experiment was repeated 3 times but for higher concentration i.e. 50μm the repeat measurements were kept low in order to prevent the cells from being poisoned by the ligand and thus eliminating any spurious frequency shifts. The plots along with their respective differentials are also shown in **Figure 7.13**. Labelled on the plots are the times when ligand first reaches and interacts with the experimental and the control sensor and when growth media hits the Sf9 cells.

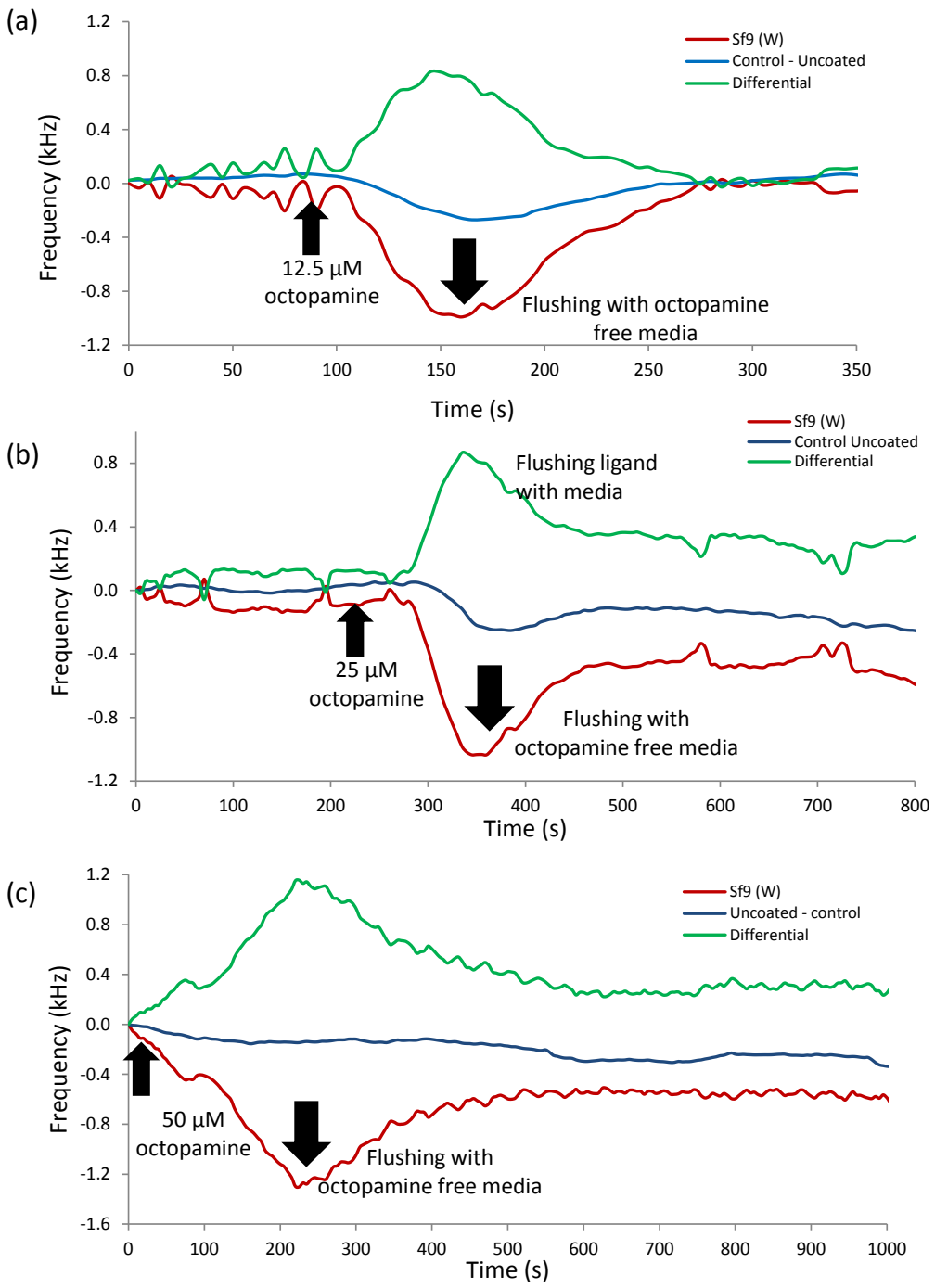

Figure 7.13: 60MHz Shorted SH-SAW resonator biosensor response to [a] 12.5µM Octopamine, [b] 25µM Octopamine and [c] 50µM Octopamine, along with their respective differential signal with the orange arrow indicting the time when octopamine flows over both the Sf9 (W) cells and the control and the purple arrow denoting the time when ligand free media flows over the control and cells.

Figure 7.13 provides the different resonant frequency shifts which are caused due to the interaction of octopamine with its associated receptor present on the cell membrane. Although the frequency shifts observed on the plots differ with regards to the low and high concentrations of the ligand octopamine.

7.4 Result Discussion

7.4.1 Sf9 Cell Attachment

In Experiments I and III, the process of cell adhesion to the gold surface of SH-SAW (60.56MHz and 228.79MHz) microsensors was acoustically monitored. It was found to take place in three distinct stages:

- A loading phase, Phase A, that depicts the disturbance to the frequency of the dual SH-SAW device when the Sf9 cells are injected onto the gold surface using the hypodermal syringe.
- An adherence phase, Phase B, which depicts the time when the Sf9 cells have settled on the surface of the microsensor and have begun to express their extracellular matrix, **Figure 7.14.**

- A saturation phase, Phase C, which depicts the time when the Sf9 cells have finished forming their extracellular matrixes and have adhered successfully to the sensor surface. The flattening of the acoustic wave signal signifies that the process of cell adhesion is complete with the final recorded value being ~2.5kHz and ~2.8kHz, **Figure 7.14 (a) and (b).**

This shift in the resonant frequency can then be co-related to the acoustic penetration depth of the designed SH-SAW devices which was approximately **72nm and 37.4nm** for the 60.56 and 228.79MHz SH-SAW (shorted) devices. The resonant frequency of the shorted sensor is perturbed by changes to the viscosity and density of the surrounding medium (within the penetration depth). Although, the resonant frequency is not seen to change when the cells are introduced in the chamber and thus any initial changes can be said to be due to the growth media being disturbed on the sensor surface or a disturbance to the system [156]. After the Sf9 cells make contact with the gold surface the acoustic wave is perturbed causing an initial measurable signal to be generated (Phase A). Shift in the resonant frequency seen during Phase B can be because of a contribution from many different events some of the many have been described below. Firstly it can be because of the interactions between the extracellular matrix (produced by the cell) and the gold surface.

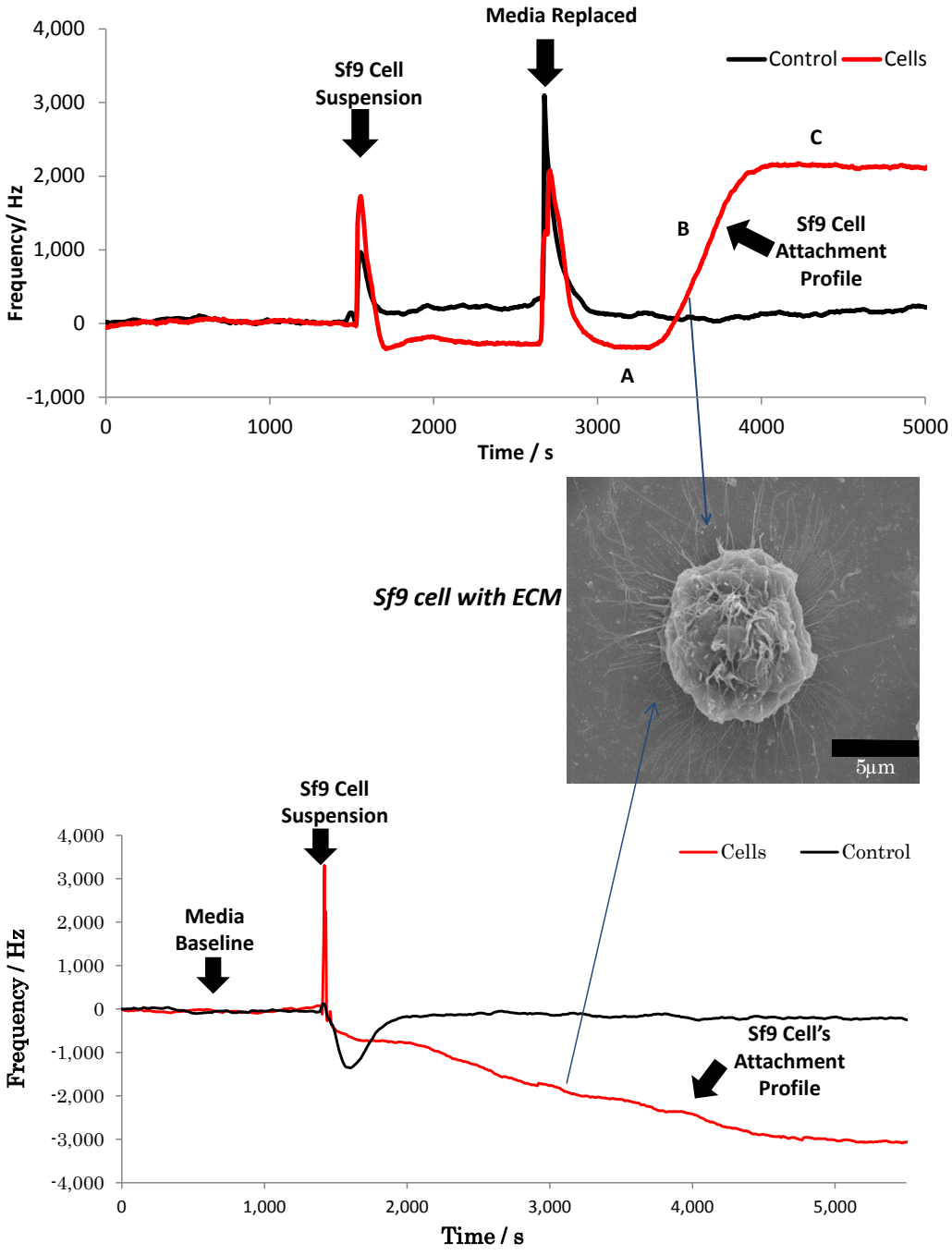

Figure 7.14: Sf9 cell attachment showing the different growth phases for 228.79MHz and 60.56MHz SH-SAW microsensors [9]

Guhr et al. in 2009 reported that changes to the resonant frequency during the adhesion process could arise because of the shear elasticity of the extracellular matrix produced by the cells [157]. Secondly, the change in frequency could be because attributed to the variations in the surface roughness of the bound Sf9 cell although such variations are process dependant and could also be contributing to the frequency shift. The same author employed love wave acoustic microsensors with LG2 cells and found that in addition to contributions from the interaction area between the cell and substrate i.e. ECM, contributions were also present from the main cell body. It should be noted that the acoustic penetration depth for their setup was 54nm [89]. Thirdly, the attachment of a cell to the surface can also cause changes to the cell tissue stiffness thus in-turn changing the resonant frequency of the surface. This was reported by Braet et al. in 1998 (employing endothelial cells) and Hutter et al. in 2005 [158] [159]. These reports confirmed Fox et al.'s initial finding, in 1985, which reported that cells lost volume and shrank in size (~3%) when they came in contact with surface [160]. Other reasons which could also contribute to the shift in the resonant frequency could be unaccounted energy dissipations from the cell during the attachment process.

Therefore it becomes clear that there might be more than a single factor contributing towards the shift in the resonant frequency during

the process of cell attachment. Although it can be inferred that changes to the sensor frequency are a contribution of the changes to the membrane, ECM, internal cell interactions and volume.

In order to now explain results obtained from the octopamine experiments, the generalised model resented in chapter 4 has been further developed and is presented in the following section.

7.4.2 Octopamine Concentration Result

7.4.2.1 Modified Generalised Model

The SH-SAW microsensors being used are in the shorted configuration and thus the resonant frequency is only affected by changed in the density and viscosity of the over-layer and can be represented by:

$$\left(\frac{\Delta V}{V}\right)_{Shorted} = \psi(\rho, \eta, T) \qquad \text{Eq. 7.1}$$

or,

$$\Delta f_s \cong \left\{\frac{\partial f}{\partial \rho}\Delta\rho + \frac{\partial f}{\partial \eta}\Delta\eta\right\} \qquad \text{Eq. 7.2}$$

where ρ and ρ are the density and permittivity of the sensing layer (in the present case). As the Sf9 cells were found to be spherical, although variations batch-to-batch size and shape needs to be accounted for

Also assuming an absence of a monolayer of Sf9 cells and the cells only cover a fraction (f_c) of the surface area which is within the volume of the acoustic wave we can modify to: **Eq. 7.1 and 7.2**

$$\Delta f_{s\,c\,l} \cong f_c\left\{\frac{\partial \Delta f_{cell}}{\partial \rho_{cell}}\Delta\rho_{cell} + \frac{\partial \Delta f_{cell}}{\partial \eta_{cell}}\Delta\eta_{cell}\right\} + (1-f_c)\left\{\frac{\partial \Delta f_{liquid}}{\partial \rho_{liquid}}\Delta\rho_{liuid} + \frac{\partial \Delta f_{liquid}}{\partial \eta_{liquid}}\Delta\eta_{liquid}\right\}$$

Eq.7.3

Refining the above equation to accommodate for fractional coverage area the contributions from non-immobilized sensor can be eliminated to give:

$$\Delta f_{s\,c\,l} - (1-f_c)\Delta f_{s\,l} \cong f_c\left\{\frac{\partial f_{cell}}{\partial \rho_{cell}}\Delta\rho_{cell} + \frac{\partial f_{cell}}{\partial \eta_{cell}}\Delta\eta_{cell}\right\} \quad \text{Eq. 7.4}$$

It is also know that the central frequencies of the SH-SAW microsensors have an associated penetration depth and that any changes to the viscosity and density that can be related to the acoustic penetration depth by

$$f = \frac{1}{\pi\,\delta^2}\cdot\ \frac{\eta}{\rho} \quad \text{Eq. 7.5}$$

From **Eq.7.5** another parameter can be extracted which is the rate of change of frequency with respect to the rate of change of density and

viscosity. Thus by partially differentiating **Eq. 7.5** w.r.t to η and ρ provides **Eq.7.6, 7.7:**

$$\frac{\partial(\Delta f)}{\partial(\eta_c)} = \frac{x}{\pi\,\delta^2}\left(\frac{1}{\rho_c}\right) \qquad \text{Eq. 7.6}$$

$$\frac{\partial(\Delta f)}{\partial(\rho_c)} = -\frac{x}{\pi\,\delta^2}\left(\frac{\eta_c}{{\rho_c}^2}\right) \qquad \text{Eq. 7.7}$$

Eq. 7.6 and 7.7 also provide directional information with regards to the changes in the resonant frequency of the SH-SAW microsensor. The resonant frequency increases due to a decrease in viscosity and an increase in density. **Eq. 7.6 and 7.7** can then be substituted into equations **Eq. 7.4** to get:

$$\Delta F \cong \Delta f_{s\,c\,l} - (1 - f_c)\Delta f_{s\,l} \cong f_c\left\{-\frac{1}{\pi\,\delta^2}\left(\frac{\eta_c}{{\rho_c}^2}\right)\Delta\rho_{cell} + \frac{1}{\pi\,\delta^2}\left(\frac{1}{\rho_c}\right)\Delta\eta_{cell}\right\} \qquad \text{Eq. 7.8}$$

$$\Delta F \cong \Delta f_{s\,c\,l} - (1 - f_c)\Delta f_{s\,l} \cong f_c\frac{1}{\pi\,\delta^2}\left\{\left(\frac{1}{\rho_c}\right)\Delta\eta_{cell} - \left(\frac{\eta_c}{{\rho_c}^2}\right)\Delta\rho_{cell}\right\} \qquad \text{Eq. 7.9}$$

$$\frac{1}{\pi\delta^2} = K(\text{a constant}) \qquad \text{Eq. 7.10}$$

$$\Delta F \cong K\,f_c\left\{\left(\frac{1}{\rho_c}\right)\Delta\eta_{cell} - \left(\frac{\eta_c}{{\rho_c}^2}\right)\Delta\rho_{cell}\right\} \qquad \text{Eq 7.11}$$

From Eq. 7.11 it becomes clear that the shift in the resonant frequency (ΔF) is primarily affected due to changes in the cell viscosity(η_{cell}), density (ρ_{cell}) and the volume of the cell or the fractional coverage area(f_c). The volume fraction depends not only on the number of Sf9 cell immobilized on the surface but also on the morphological and physiological properties of the biological cells e.g. any changes in cell volumes can have an effect on the volume fraction of the sensor area. Any changes to the volume of the cell through external liquid environment, due to ligand receptor activity or internal environment can alterf_c, η_{cell} and ρ_{cell}. Therefore in order to examine the effects on the Sf9 cells due to the liquid environment it is beneficial if the various properties of the liquid are defined. There are three different types of liquids based on their individual tonicity. They are (when compared to the internal environment of the cell):

- Hypotonic solution – external environment is less concentrated
- Hypertonic solution – external environment is more concentrated
- Isotonic solution – external environment similar to the internal

In addition to the environment the condition of the cell membrane can also influence the SH-SAW resonant frequency because it lies within the penetration depth of the microsensor.

The cellular organelles are enclosed within a "biological membrane". In 1972, Singer and Nicholson proposed the "fluid mosaic model" which is the traditionally accepted model to understand the structure of the cell or plasma membranes[161]. The cell membrane is semi-permeable membrane i.e. the biological cell dimension can change if the concentration of the external environment varying, thereby modifying the density and viscosity of the both the cell as well as the membrane itself. Thus, based on this information one can consider a simplistic model of the Sf9 whole cell considering each layer to be with an associated density, viscosity, conductivity, permittivity parameter. [157]. Based on the different SH-SAW sensor configurations, variables in the model can be narrowed down, as shown in **Figure 7.15.**

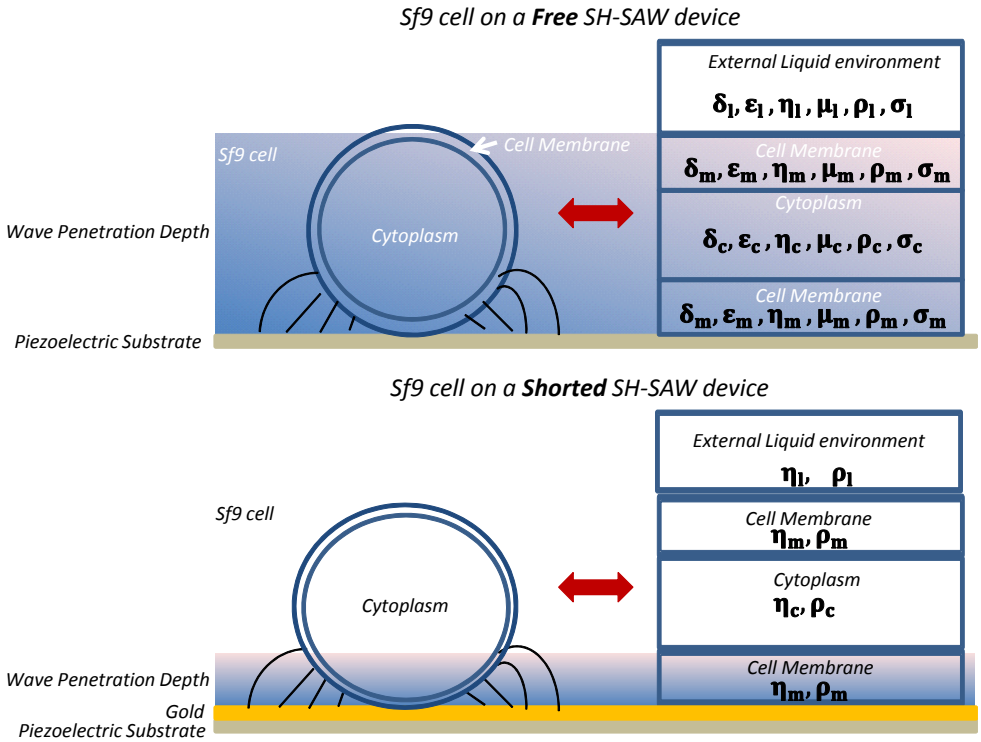

Figure 7.15: A simple model demonstrating the different layers of a biological cell immobilized on a SH-SAW with the colour gradient denoting the penetration depth of the acoustic wave device. (not to scale)

Based on the information with regards to the membrane properties, the external liquid environment, cell density and viscosity different scenarios can be constructed representing the different experimental conditions. Results obtained in Experiments II and IV can then be examined according to the different scenario's providing information with regards to the direction of the shift in resonant frequency.

Scenario No	External Environment Type	Cell Volume	Octopamine Response	Cytoplasm Properties		Membrane Properties		Membrane Stiffness
				ρ	η	ρ	η	Young's modulus
Scenario 1	Isotonic	No change	-	No Change	No Change	No Change	No Change	-
Scenario 2	Hypotonic	Increase	-	Decrease	Increases	Decrease	Increase	-
Scenario 3	Hypertonic	Decrease	-	Increase	Decrease	Increase	Decrease	-
Scenario 4	Isotonic + Ligand*	No change	YES	Increase	Decrease	Increase	Decrease	Increase
Scenario 5	Hypotonic + Ligand*	Increase	YES	Decrease	Increases	Decrease	Increase	Increase
Scenario 6	Hypertonic + Ligand*	Decrease	YES	Increase	Decrease	Increase	Decrease	Increase
Scenario 7	Isotonic + Ligand†	No change	YES	Increase	Decrease	Increase	Decrease	High
Scenario 8	Hypotonic + Ligand†	Increase	YES	Decrease	Increases	Decrease	Increase	High
Scenario 9	Hypertonic + Ligand†	Decrease	YES	Increase	Decrease	Increase	Decrease	High

* - Low ligand concentration

† - Higher ligand concentration

Figure 7.16: Different experimental scenarios with associated changes in cell properties

Scenario's 1-3 can be considered as the baseline because that represents the before octopamine interacts with the Sf9 cell's. It can be seen from **Figure 7.16** that two different ligand concentrations have been accounted. We can now apply the different experiment performed to the named scenarios.

7.4.2.2 Octopamine Hydrochloride concentration dependence

For Experiment II, 100μM concentration of octopamine hydrochloride solution was prepared in DI water. Thereafter the Sf9 cell immobilized sensor and the control sensor were both exposed to the 100μM solution. The resonant frequency of the control sensor was observed to rise. In contrast the experimental sensor frequency was seen to fall.

As water is considered a hypotonic solution i.e. less concentrated with respect to the internal concentration of the cell, scenario 5 and 8 can be applied to this particular case i.e. Hypotonic + ligand (high concentration). Thus there could be three possible contributing to the generated frequency shift. Firstly, due to the presence of a hypotonic solution, the cell volume can be expected to rise, as the concentration gradient will force the cell to accept more water molecules, thus in-turn changing the fractional area, cell viscosity and density. Secondly, when octopamine flows over the immobilised Sf9 cells, intra-cellular responses, mediated by GPCR's, are triggered as result of the receptor-ligand interaction. This triggers further downstream biological processes ultimately causing a small transient increase in the intracellular Ca^{2+} level (in the nM region) thus contributing to the change in cell conductivity, density, viscosity [5]. Thirdly, a high concentration of octopamine is used for this experiment and that the media was not refreshed therefore leaving a possibility for the receptor to be saturated by the ligand and not recovered to their normalised state thus also altering the rigidity and roughness of the Sf9 cell membrane.

As 228.79MHz shorted SH-SAW microsensors (wave penetration depth: 37nm) were employed for this experiment, it is highly unlikely that any area of the cytoplasm would be contributing towards the shift in the resonant frequency.

For the concentration related experiments, instead of preparing octopamine in DI water, different molar concentration were prepared in cell growth media – an isotonic solution. This was done in order to mitigate any changes to the cell volume as a result of external environments. Again by referring back to **Figure 7.16**, two possible scenarios can be applied to this particular experiment. They are scenario 4 and 7. Experiments were performed with the automated system and a 2 minutes exposure of octopamine was followed by a 10 minutes exposure of growth media thus also minimising receptor poisoning effects. Although these effects were minimised there can be other possible contributors to the shift in the resonant frequency. First, as 60.56MHz shorted SH-SAW microsensors were being used, a section of the cell cytoplasm could be contributing towards the resonant frequency shift. This is because the penetration depth of the 60.56MHz shorted SH-SAW microsensors was 73nm. Schröder et al. in 2010 published their findings which suggested that molecules within a cell changed their locations when membrane GPCR's were stimulated thus altering the viscosity of the Sf9 cells. Secondly the opening of the ion channels, as explained in the previous discussion section would alter the cytoplasmic viscosity, density and conductivity (in nM levels). Thirdly, at low concentration and for the first few exposures the resonant frequency was seen to recover to the media baseline but for higher concentration

exposure's stable response could not be measured thus questioning the changes in the rigidity of the ECM and their interactions with octopamine that could very well contribute to the generated frequency response.

7.5 Conclusion

In this chapter, Sf9 whole-cells were functionalized on 60.56MHz and 228.79MHz SH-SAW (shorted) microsensors. In a dual device configuration only one of the sensors was functionalised with Sf9 cells with the non-functionalised part acting as the experimental control. The adherence characteristics of Sf9 cells were acoustically monitored by 60.56 MHz and 228.79MHz SH-SAW microsensors. In addition to this, the concept of ligand-GPCR interaction was also examined and thus in effect demonstrating the novel concept of infochemical communication in the liquid phase. This was achieved by stimulating the endogenously expressed GPCRs by octopamine hydrochloride - an invertebrate neurotransmitter. Concentration (12.5, 25 and 50μM) related experiments were also carried out using the automated system developed in chapter 7. The ligand (octopamine hydrochloride) was employed in three different concentrations i.e. and experimental results were demonstrated. These results were co-related to the perturbation theory introduced in Chapter 3 and an approximate hypothesis was constructed to explain the findings.

The next chapter summarised the achievements of the research carried out in this thesis and how it has contributed towards the overall objectives of this thesis and of the iCHEM project. The next chapter also provides a detailed further work section and provided recommendations for further developing the system shown in this thesis.

Chapter 8
Conclusion and Further Work

8.1 Introduction

Chemical information communication plays a key role in the mediating the behavioural characteristics of insect, as described in Chapter 1 and 2. This form of communication system which is based on information being exchanged via specifically oriented odours has formed the basis of a label-free technology that is yet to be exploited. This was also the underpinning concept of the iCHEM project whose central aim was to develop a new class of technology based on the knowledge gained (by different project partners) by studying the various biosynthesis pathways of the moth, *S. littoralis*. In essence, the central challenge of the project was to mimic nature onto a technological platform. This came with its own set of challenges which were, to a certain extent managed in the work presented in this thesis. For example, in Chapter 3 a

prototype infochemical communication system was assembled and characterised with different volatile organic compounds instead of real pheromones. Fruit volatiles were employed in the current study as they could be acquired in volume content, were cost effective and were the major components of the blends, Apple, Hawthorn, dogwood [115]. In order to detect the volatiles blends, polymer coated QCM microsensor – a class of acoustic microsensors operating on the concept of piezoelectricity, array was employed. This prototype system was then characterised by emitting binary and ratiometric blends of fruit blends [1]. Although the volatiles could be detected by the polymer coated QCM array, selectivity i.e. decoding the emitted ratio was found to be poor.

In order to increase selectivity, polymer coated QCM microsensors were replaced by whole-cell (SF9) immobilised SAW microsensors - a different class of acoustic microsensors also based on the principle of piezoelectricity. This class of microsensors offered superior sensitivity, when compared to QCM's, which when coupled with a GPCR based whole-cell biological coating provided the essential selectivity lacking in the previous system. The whole-cell based biological coating was employed because they were robust and provided an in-tact machinery which could be incorporated with different OR's, thus in essence making it ligand specific.

The SAW microsensors were designed at different frequencies and fabricated on two different substrates – lithium tantalate and Quartz. Experiment were then successfully carried out using the lithium tantalate based SAW microsensors in a liquid environment demonstrating ligand-specific activation of the receptor expressed by the whole cell coating.

8.2 Objectives of the Current Research

This section reviews the key objectives of the research carried out in this thesis, listing its key achievements:

- Polymer coated QCM microsensor array were employed as a part of a novel infochemical communication system for the detection nl level of volatile organic solvents.
- SH-SAW microsensors based a dual device resonator configuration were designed and fabricated at two (60.56MHz, and 226.89MHz) different resonant frequencies. More importantly the resonant frequencies of the microsensors were chosen based on an associated wave penetration depth. The main advantage of this design methodology was to tailor the microsensor design specifically for the research performed in this thesis.
- The designed SH-SAW microsensors were characterised by employing a network analyser and integrated with an

oscillator setup and their sensing area was modified by immobilizing Sf9 insect whole-cells expressing endogenous GPCR octopamine receptors.

- An automated microfluidic system was built, consisting of a central housing unit, constructed of a biocompatible polymer – PDMS, housing the Sf9 insect cells on the surface acoustic wave microsensors, tubing, a six way valve integrated and controlled by LabView software.
- Octopamine hydrochloride, an invertebrate neurotransmitter, was employed as a ligand for the naturally occurring receptors in the Sf9 cell membrane.
- A scenario based approach was adopted in order to characterise the shifts in the response of the microsensor the addition of ligand. By employing such a methodical study, the different contributing factors to the resonant frequency shift could then be macroscopically examined.
- Rayleigh based SAW (R-SAW) microsensors were also designed at four different resonant frequencies. The microsensors were fabricated with aluminium and gold electrodes. These particular types of SAW microsensors were designed in order for future experiments to be carried out in the vapour phase.

8.3 Future Work

With regards to the work performed in this thesis, the future work can be categorised into two aspects - first related to technological aspects (sensing system design, microsensor design) and second related to the biological aspect (transfection of whole cells with ORs).

Vapour phase experiments employing R-SAW microsensors coated with sensitive polymer coatings would need to be carried out in essence realising an electronic nose. Additionally, in order to achieve higher sensitivities, other forms of acoustic wave microsensor designed can be investigated. These could include flexural bulk acoustic wave resonators (FBAR's) which operate at higher frequencies > 1GHz. One advantage of employing FBAR sensors is the fact that their fabrication processes are compatible with standard CMOS technology. Thus, a fully functional Lab-on-Chip application can be realised. Finally, a time dependant model which examines the receptor-ligand interaction can developed and benchmarked against fluorescent imaging techniques such as FRET and SPR.

Other future work could also include designing a complete biophysics based model based on e.g. Monte Carlo simulators, examining receptor ligand interaction and taking into account the action potentials of the cell membrane in essence providing useful information with regards to the polarisation-depolarisation of the membrane.

Finally, it should be noted that recommending any future work on the biological aspect of the work i.e. OR, GPCR falls outside the purview of the work presented in this thesis.

References

[1] P. Acronym, P. F. Title, B. Infochemical, and C. Proposal, "Sixth Framework Programme Priority 2 Information Society Technologies Contract for : SPECIFIC TARGETED RESEARCH PROJECT," 2007.

[2] A. J. Taylor and D. D. Roberts, *Flavor Perception*. 2004.

[3] U. Klaschka, "Chemical communication by infochemicals.," *Environmental science and pollution research international*, vol. 16, no. 4, pp. 367-9, Jun. 2009.

[4] U. Klaschka, "The infochemical effect—a new chapter in ecotoxicology.," *Environ Sci Pollut Res*, vol. 15, pp. 452-462, 2008.

[5] M. Lof, L. Hemerik, and M. D. Gee, "Chemical communication : does odor plume shape matter ?," vol. 18, pp. 61-70, 2007.

[6] L. B. Buck and R. Axel, "A novel multigene family may encode odorant receptors – a molecular-basis for odor recognition.," *Cell*, vol. 65, pp. 175-187, 1991.

[7] M. Cole et al., "Biomimetic insect infochemical communication system.," in *Sensors, 2009 IEEE*, pp. 1358 - 1361.

[8] T. S. Ha and D. P. Smith, "Odorant and pheromone receptors in insects.," *Frontiers in cellular neuroscience*, vol. 3, no. September, p. 10, Jan. 2009.

[9] S. Pathak, M. D. Jordan, Z. Rácz, R. A. J. Challiss, J. W. Gardner, and M. Cole, "Detection of ligand-elicited cellular responses using Surface Acoustic Wave biosensors.," *Physiology*, vol. 1, pp. 1-2, 2011.

[10] M. Cole, J. W. Gardner, S. Pathak, T. C. Pearce, and Z. Rácz, "Procedia Chemistry Towards a biosynthetic infochemical communication system," *Sensors (Peterborough, NH)*, vol. 0, pp. 1-4, 2009.

[11] Z. Rácz, S. B. Olsson, J. W. Gardner, T. C. Pearce, B. S. Hansson, and M. Cole, "Challenges of Biomimetic Infochemical Communication," in *Proceedings of the 2nd European Future Technologies Conference and Exhibition 2011 (FET 11)*, pp. Volume 7, 2011, Pages 106–109.

[12] L. C., H. W.M., and M. S.B.J., "Sex pheromones and their potential role in the evolution of reproductive isolation in small ermine moths (Ypnomeutidae).," *Chemoecology*, vol. 2, pp. 28 - 30, 1991.

[13] T. JA, S. SJ, J. RA, and B. GJ., "Insect pheromones - an overview of biosynthesis and endocrine regulation.," *Insect Bio- chem. and Mol. Biol.*, vol. 29, no. 6, pp. 481-514, 1999.

[14] M. Cole, J. W. Gardner, S. Pathak, T. C. Pearce, and Z. Rácz, "Towards a biosynthetic infochemical communication system.," *Sensors (Peterborough, NH)*, pp. 1-4, 2009.

[15] G. C. Rains, J. K. Tomberlin, and D. Kulasiri, "Using insect sniffing devices for detection.," *Trends in biotechnology*, vol. 26, no. March, pp. 288 - 294, 2008.

[16] "Physiology or Medicine 1973 - Press Release." [Online]. Available: http://www.nobelprize.org/nobel_prizes/medicine/laureates/1973/press.html. [Accessed: 20-Sep-2012].

[17] K. Von Frisch, *Bees: Their Vision, Chemical Senses, and Language*. Cornell University Press, 1956.

[18] W. V. D. G. V. Naters and J. R. Carlson, "Insects as chemosensors of humans and crops.," *Nature*, vol. 444, no. November, 2006.

[19] K. Touhara and L. B. Vosshall, "Sensing Odorants and Pheromones with Chemosensory Receptors," *Annual Review of Physiology*.

[20] T. L. Carus, *Lucretius: Onthe Nature of Things*. Baltimore: Johns Hopkins Univ. Press, 1995.

[21] A. JE, "Stereochemical theory of olfaction.," *Nature*, vol. 198, no. 8, pp. 271 - 72, 1991.

[22] P. Xu, R. Atkinson, D. N. M. Jones, and D. P. Smith, "Drosophila OBP LUSH is required for activity of pheromone-sensitive neurons.," *Neuron*, vol. 45, no. 2, pp. 193-200, Jan. 2005.

[23] R. Axel, "The molecular logic of smell.," *Sci. Am.*, vol. 273, pp. 154–159, 1995.

[24] J. Riesgo-Escovar, D. Raha, and J. R. Carlson, "Requirement for a phospholipase C in odor response: overlap between olfaction and vision in

Drosophila.," *Proceedings of the National Academy of Sciences of the United States of America*, vol. 92, no. 7, pp. 2864-8, Mar. 1995.

[25] R. Glatz and K. Bailey-Hill, "Mimicking nature's noses: from receptor deorphaning to olfactory biosensing.," *Progress in neurobiology*, vol. 93, no. 2, pp. 270-96, Feb. 2011.

[26] M. D. Bruyne, K. Foster, J. R. Carlson, and N. Haven, "Odor Coding in the Drosophila Antenna," vol. 30, pp. 537-552, 2001.

[27] R. Vassar, R., Chao, S. K., Sitcheran, A. Nunez, J. M., Vosshall, L. B., and R. Axel, "Topographic organization of sensory projections to the olfactory bulb.," *Cell*, vol. 79, pp. 981–991, 1994.

[28] K. J. Sullivan, S. L, Bohm, S., Ressler and L. B. Horowitz, L. F., and Buck, "Target-independent pattern specification in the olfactory epithelium.," *Neuron*, vol. 15, pp. 779–789, 1995.

[29] "Graphics Hunt," *2007-2009*. .

[30] Y. Hu, L. Rajan, and W. P. Schilling, "Ca2+ signaling in Sf9 insect cells and the functional expression of a rat brain M5 muscarinic receptor.," *The American journal of physiology*, vol. 266, no. 6 Pt 1, pp. C1736-43, Jun. 1994.

[31] S. H. Lee and T. H. Park, "Recent advances in the deveopment of bioelectronic nose.," *Biotechnol. Bioprocess Eng.*, vol. 15, pp. 22-29, 2010.

[32] J. Vidic, "Bioelectronic Noses Based on Olfactory Receptors," no. January, 2010.

[33] L. Ding, D. Du, X. Zhang, and H. Ju, "Trends in cell-based electrochemical biosensors.," *Current medicinal chemistry*, vol. 15, no. 30, pp. 3160-70, Jan. 2008.

[34] H. Q. Zhao, L. Ivic, J. M. Otaki, M. Hashimoto, K. Mikoshiba, and S. Firestein, "Functional expression of amammalian odorant receptor.," *Science*, vol. 279, pp. 237-242, 1998.

[35] P. Banerjee and A. K. Bhunia, "Mammalian cell-based biosensors for pathogens and toxins," *Trends in biotechnology*, no. January, pp. 179-188, 2009.

[36] E. Kougianos, "Biosensors : A tutorial review," 2006.

[37] J. Castillo et al., “Biosensors for life quality Design , development and applications,” *Sensors And Actuators*, vol. 102, pp. 179-194, 2004.

[38] S. H. Lee and T. H. Park, “odo,” *Biotechnology and Bioprocess Engineering*, vol. 15, no. 1, pp. 22-29, Mar. 2010.

[39] D. Grieshabar, R. MacKensie, J. Voros, and E. Reimhault, “Electrochemical biosensors - sensor principles and architectures.,” *Sensors*, vol. 8, pp. 1400-1458, 2008.

[40] R. . Thevenot, K. Toth, R. A. Durst, and G. S. Wilson, “Electrochemical biosensors: recommended definitions and classification.,” *Biosens. Bioelectron.*, vol. 16, pp. 121-131, 2001.

[41] M. Nirschl, F. Reuter, and J. Vörös, “Review of Transducer Principles for Label-Free Biomolecular Interaction .,” *Biosensors*, vol. 1, no. 3, pp. 70-92, Jul. 2011.

[42] M. Schöning and A. Poghossian, “Bio FEDs (field-effect devices): State-of-the-art and new directions.,” *Electroanalysis*, vol. 18, pp. 1893 - 1900, 2006.

[43] P. Estrela et al., “Label-free sub-picomolar protein detection with field-effect transistors.,” *Analytical chemistry*, vol. 82, no. 9, pp. 3531-6, May 2010.

[44] A. H. D. Graham, J. Robbins, C. R. Bowen, and J. Taylor, “Commercialisation of CMOS Integrated Circuit Technology in Multi-Electrode Arrays for Neuroscience and Cell-Based Biosensors.,” *Sensors (Basel, Switzerland)*, vol. 11, no. 5, pp. 4943-71, Jan. 2011.

[45] R. Sethi, “Transducer aspects of biosensors.,” *Biosens. Bioelectron.*, vol. 9, pp. 243 - 264, 1994.

[46] J. Kimura and T. Kuriyama, “FET biosensors.,” *J. Biotechnol.*, vol. 15, pp. 239-254, 1990.

[47] H. Yoon et al., *Polypyrrole nanotubes conjugated with human olfactory receptors: High- performance transducers for FET-Type Bioelectronic nose.* 2009, pp. 2755-2758.

[48] E. M. Neuhaus, A. Mashukova, W. Zhang, J. Barbour, and H. Hatt, “A specific heat shock protein enhances the expression of mammalian olfactory receptor proteins.,” *Chem. Senses.*, vol. 31, pp. 445-452, 2006.

[49] E. Akyilmaz and E. Dinckaya, "An amperometric microbial biosensor development based on Candida tropicalis yeast cells for sensitive determination of ethanol.," *Biosens. Bioelectron.*, vol. 20, pp. 1263-9, 2005.

[50] T. Neufeld, D. Biran, R. Popovtzer, T. Erez, E. Z. Ron, and J. Rishpon, "Genetically engineered pfabA pfabR bacteria: an electrochemical whole cell biosensor for detection of water toxicity.," *Anal. Chem.*, no. 78, pp. 4952-6, 2006.

[51] H. F. Cui, J.-S. Ye, Y. Chen, S.-C. Chong, and F.-S. Sheu, "Microelectrode array biochip: tool for in vitro drug screening based on the detection of a drug effect on dopamine release from PC12 cells.," *Anal. Chem.*, vol. 78, pp. 6347-55, 2006.

[52] K. M. L. May, Y. Wang, L. G. Bachas, and K. W. Anderson, "Development of a whole-cell-based biosensor for detecting histamine as a model toxin.," *Anal. Chem.*, no. 76, pp. 4156-61, 2004.

[53] R. S. Marks, D. C. Cullen, I. Karube, C. R. Lowe, and H. H. Weethall, *Handbook of Biosensors and Biochips - 1*. 2007, p. 375.

[54] E. A. J. Erijman and T. M. Jovin, "FRET imaging.," *Nat. Biotechnol.*, vol. 21, pp. 1387-1395, 2003.

[55] H. J. Ko and T. H. Park, "Functional analysis of olfactory receptors expressed in HEK-293 cell system using cameleons.," *Biotechnol., J. Microbiol.*, vol. 17, pp. 928-933, 2007.

[56] J. Homola, S. S. Yee, and G. Gauglitz, "Surface plasmon resonance sensors: a review.," *Sens. Actuators B: Chem.*, vol. 54, pp. 3-15, 1999.

[57] P. J. Harding, T. C. Hadingham, J. M. McDonnell, and A. Watts, "Direct analysis of a GPCR-agonist interaction by surface plasmon resonance.," *Eur. Biophys. J.*, vol. 35, pp. 709-712, 2006.

[58] P. Stenlund, G. J. Babcock, J. Sodroski, and D. G. Myszka, "Capture and reconstitution of G protein-coupled receptors on a biosensor surface.," *Anal. Biochem.*, vol. 316, pp. 243-250, 2003.

[59] C. Bieri, O. P. Ernst, S. Heyse, K. P. Hofmann, and H. Vogelc, "Micropatterned immobilization of a G protein-coupled receptor and direct detection of G protein activation.," *Nat. Biotech.*, vol. 17, pp. 1105-1108, 1999.

[60] J. Y. Lee, H. J. Ko, S. H. Lee, and T. H. Park, "Cell-based measurement of odorant molecules using surface plasmon resonance.," *Enzy. Microb. Technol.*, vol. 39, pp. 375-380, 2006.

[61] S. H. Lee, H. J. Ko, and T. H. Park, "Real-time monitoring of odorant induced cellular reactions using surface plasmon resonance.," *Biosens. Bioelectron.*, vol. 25, pp. 55-60, 2009.

[62] Y. Fang, "Label-Free Biosensors for Cell Biology," *International Journal of Electrochemistry*, vol. 2011, pp. 1-16, 2011.

[63] K. Länge, B. E. Rapp, and M. Rapp, "Surface acoustic wave biosensors: a review.," *Analytical and bioanalytical chemistry*, vol. 391, no. 5, pp. 1509-19, Jul. 2008.

[64] K. Länge et al., "Packaging of Surface Acoustic Wave (SAW) based Biosensors : an Important Issue for Future Biomedical Applications," *Control*, vol. 0, no. c, pp. 321-325, 2004.

[65] J. F. Tressler, S. Alkoy, and R. E. Newnham, "Piezoelectric Sensors and Sensor Materials," *Journal of Electroceramics*, 1998.

[66] J. G. Gualtieri, J. A. Kosinski, and A. Ballato, "Piezoelectric materials for saw applications.," *IEEE Ultrasonics Symposium*, pp. 403-412, 1992.

[67] D. L. García-González and R. Aparicio, "Sensors: From biosensors to the electronic nose," *Grasas y Aceites*, vol. 53, no. 1, pp. 96-114, Oct. 2007.

[68] C. March-iborra, Á. Montoya-baides, and A. Arnau-vives, "Surface Generated Acoustic Wave Biosensors for the Detection of Pathogens: A Review," *Biosensors*, pp. 5740-5769, 2009.

[69] W. G. Hankel, "No Title," *Abh. Sächs*, vol. 12, p. 547, 1881.

[70] W. G. Hankel, "No Title," *Ber. Sachs*, vol. 33, p. 52, 1881.

[71] J. Curie and P. Curie, "No Title," *Bull, Soch. Fr. Mineral.*, vol. 3, no. 90, 1880.

[72] J. W. Gardner, V. K. Varadan, and O. O. Awadelkarim, *Microsensors, MEMS and Smart Devices : Technology, Applications and Devices*. 2001, p. 306.

[73] D. S. Ballantine et al., *Acoustic Wave Sensors: Theory, Design, and Physico-Chemical Applications*. Academic Press, 1997.

[74] J. F. Nye, *Physical Properties of Crystals*. 1957, p. 173.

[75] L. Rayleigh, "On Waves Propagates along the Plane Surface of an Elastic Solid.," *Proc. London Math. Soc.*, vol. 17, no. 1, pp. 4 - 11.

[76] D. P. Morgan, *Surface-Wave Devices for Signal Processing*. 1978.

[77] J. P. Black, "MEMS-Based System for Particle Exposure Assessment Using Thin-Film Bulk Acoustic Wave Resonators and IR / UV Optical Discrimination," 2006.

[78] J. W. Gardner, V. K. Varadan, and O. O. Awadelkarim, *Microsensors, MEMS and Smart Devices.* 2007, p. 347.

[79] B. A. Auld, *Acoustic Fields and Waves in Solids - Vol II*. 1973.

[80] D. S. Ballantine et al., *Acoustic Wave Sensors : Theory, Design, and Pysico-chemical Applications*. Academic Press, 1997.

[81] R. S. Marks, D. C. Cullen, I. Karube, C. R. Lowe, and H. H. Weethall, *Handbook of Biosensor and Biochips - 1*. 2007, p. 597.

[82] J. W. Gardner and P. N. Bartlett, *Electronic Noses: Principles and Applications*. 1999, p. 88.

[83] G. Sauerbrey, "Use of quartz vibrator forweighing thin layers and as a micro-balance.," *Zeitschrift fur Physik*, vol. 155, no. 2, pp. 206 - 222, 1959.

[84] Q. Ameer and S. B. Adeloju, "Polypyrrole based electronic noses for environmental and industrial analysis.," *Sens. Actuators. B.*, vol. 106, pp. 541-552, 2005.

[85] B. Wyszynski, P. Somboon, and T. Nakamoto, "Pegylated lipids as coatings for QCM odor-sensors.," *Sens. Actuators. B.*, vol. 121, pp. 538-544, 2007.

[86] B. Adhikari and S. Majumdar, "Polymers in sensor applications," *Progress in Polymer Science*, vol. 29, no. 7, pp. 699-766, Jul. 2004.

[87] T. Z. Wu, "A piezoelectric biosensor as an olfactory receptor for odour detection: electronic nose.," *Biosensors & Bioelectronics*, vol. 14, no. 1, pp. 9-18.

[88] C. Wu, L. Wang, J. Zhou, L. Zhao, and P. Wang, "The progress of olfactory transduction and biomimetic olfactory-based biosensors," *Chinese Science Bulletin*, vol. 52, no. 14, pp. 1886-1896, Jul. 2007.

[89] M. Saitakis, A. Tsortos, and E. Gizeli, "Biosensors and Bioelectronics Probing the interaction of a membrane receptor with a surface-attached ligand using whole cells on acoustic biosensors," *Biosensors and Bioelectronics*, vol. 25, no. 7, pp. 1688-1693, 2010.

[90] J. Wegener, J. Seebach, a Janshoff, and H. J. Galla, "Analysis of the composite response of shear wave resonators to the attachment of mammalian cells.," *Biophysical journal*, vol. 78, no. 6, pp. 2821-33, Jun. 2000.

[91] J. Wegener, a Janshoff, and H. J. Galla, "Cell adhesion monitoring using a quartz crystal microbalance: comparative analysis of different mammalian cell lines.," *European biophysics journal : EBJ*, vol. 28, no. 1, pp. 26-37, Jan. 1999.

[92] K. Nakamura, "Review Paper Shear-Horizontal Piezoelectric Surface Acoustic Waves," *Japanese Journal of Applied Physics*, vol. 46, no. 7, pp. 4421-4427, 2007.

[93] W. D. Hunt and D. D. Stubbs, "Time-dependent signatures of acoustic wave biosensors," *Proceedings of the IEEE*, vol. 91, no. 6, pp. 890-901, Jun. 2003.

[94] S. H. Lee, "Theoretical and Experimental Characterization of Time-Dependent Signatures of Acoustic Wave Based Biosensors .," 2006.

[95] Y. Kwon and Y. Roh, "Development of SH-SAW sensors for underwater measurement," vol. 42, pp. 409-411, 2004.

[96] T. Kogai and H. Yatsuda, "Liquid Sensor Using SAW and SH-SAW on Quartz," *Ultrasonics*, pp. 552-555, 2006.

[97] M. Tom-Moy, R. L. Baer, and T. P. D. Darlene Spira-Solomon, "Atrazine Measurements Using Surface Transverse Wave Device.," *Anal. Chem*, vol. 67, pp. 1510 - 1516, 1995.

[98] E. Berkenpas, S. Bitla, P. Millard, and M. P. da Cunha, "Pure Shear Horizontal SAW Biosensor on Langasite.," *IEEE Trans. Ultrason., Ferroelect,. Freq. Contr.*, vol. 51, pp. 1404 - 1411, 2004.

[99] T. Moriizumi, Y. Unno, and S. Shiokawa, "New sensor in liquid using Leaky SAW.," in *IEEE Freq. Cont. Symp.*, 1987, pp. 579 - 582.

[100] T. M. a Gronewold, "Surface acoustic wave sensors in the bioanalytical field: recent trends and challenges.," *Analytica chimica acta*, vol. 603, no. 2, pp. 119-28, Nov. 2007.

[101] M. Saitakis, a. Dellaporta, and E. Gizeli, "A surface acoustic wave sensor for the study of membrane-protein/ligand interactions using whole cells," *2008 IEEE International Frequency Control Symposium*, pp. 356-359, May 2008.

[102] M. B. Assouar, P. Kirsch, and P. Alnot, "New Love wave liquid sensor operating at 2 GHz using an integrated micro-flow channel," *Measurement Science and Technology*, vol. 20, no. 9, p. 095203, Sep. 2009.

[103] K. K. Zadeh, A. Trinchi, W. Wlodarski, and A. Holland, "A novel Love-mode device based on a ZnO/St-cut quartz crystal structure for sensing applications.," *Sensors Actuators A*, vol. 100, pp. 135 - 143, 2002.

[104] W. H. King, "No Title," *Jr., Anal. Chem.*, vol. 36, p. 1735, 1964.

[105] K. Yanoa et al., "Development of a chemical vapor sensor using piezoelectric quartz crystals with coated unusual lipids," *Analytica Chimica Acta*, vol. 340, 1997.

[106] W. H. King, "Piezoelectric Sorption Detecto," *Anal. Chem.*, vol. 36, pp. 1735-39, 1964.

[107] N. Kasai, I. Sugimoto, and M. Nakamura, "Discrimination of odorants of definite concentrations by using plasma-organic-film-coated QCR sensors," *Sensors And Actuators*, pp. 114-119, 2000.

[108] B. Adhikari and S. Majumdar, "Polymers in sensor applications.," *Materials Science*, vol. 29, pp. 699-766, 2004.

[109] W. Jay, R. A. Mcgill, and M. H. Abraham, "Chemically selective polymer coatings for Acousctic Vapor Sensors and Arrays," in *IEEE Ultrasonics SymposiumUltrasonics*, 1992, pp. 275-280.

[110] A. Hierlemann, E. T. Zellers, and A. J. Ricco, "Use of Linear Solvation Energy Relationships for Modeling Responses from Polymer-Coated Acoustic-Wave Vapor Sensors.," *Anal. Chem.*, vol. 73, no. 14, pp. 3458-3466, 2001.

[111] J. W. Grate and M. H. Abraham, "Solubility interactions and the design of chemically selective sorbent coatings for chemical sensors and arrays.," *Sensors and Actuators B*, vol. 3, pp. 85-111, 1991.

[112] J. W. Grate, "Hydrogen-bond acidic polymers for chemical vapor sensing.," *Chemical reviews*, vol. 108, no. 2, pp. 726-45, Feb. 2008.

[113] S. Sarkar, N. Levit, and G. Tepper, "Deposition of polymer coatings onto SAW resonators using AC electrospray.," *Sensors And Actuators*, vol. 114, pp. 756-761, 2006.

[114] M. V. Voinova, "On Mass Loading and Dissipation Measured with Acoustic Wave Sensors: A Review," *Journal of Sensors*, vol. 2009, pp. 1-13, 2009.

[115] C. E. L. Jr, H. Dambroski, S. Nojima, J. L. Feder, S. H, and W. L. Roelofs, "Variability in response specificity of apple , hawthorn , and flowering dogwood-infesting Rhagoletis flies to host fruit volatile blends : implications for sympatric host shifts," *Entomologia Experimentalis et Applicata*, pp. 55-64, 2005.

[116] M. Cole, "Biosynthetic Infochemical Communication - Second Periodic Activity Report," 2007.

[117] I. D. Avramov, "Design of Rayleigh SAW Resonators for Applications as Gas Sensors in Highly Reactive Chemical Environments," *Solid State Physics*, pp. 381-388, 2006.

[118] M. Nirschl, F. Reuter, and J. Vörös, "Review of Transducer Principles for Label-Free Biomolecular Interaction Analysis," *Biosensors*, vol. 1, no. 3, pp. 70-92, Jul. 2011.

[119] I. D. Avramov, K. L, S. Rupp, B. Rapp, and M. Rapp, "Polymer Coating Behavior of Rayleigh-SAW Resonators with Gold Electrode Structure for Gas Sensor Applications," vol. 54, no. 1, 2007.

[120] I. Avramov, "Design of Rayleigh SAW Resonators for Applications as Gas Sensors in Highly Reactive Chemical Environments," *2006 IEEE*

International Frequency Control Symposium and Exposition, pp. 381-388, Jun. 2006.

[121] G. S. Sehra, "Surface acoustic wave based flavour sensor system.," 2005.

[122] J. Kondoh and S. Shiokawa, "Shear-Horizontal Surface Acoustic Wave Sensors," *Sensors (Peterborough, NH)*.

[123] T. Moriizumi, Y. Unni, and S. Shiokawa, "New sensor in liquid using leaky SAW," *Ultrasonic Symp. Proc.*, vol. 1, pp. 579-582, 1987.

[124] A. Venema, E. Nieuwkoop, M. J. Vellekoop, M. S. Nieuwenhuizen, and A. W. Barendsz, "DESIGN ASPECTS OF SAW GAS SENSORS," *Sensors (Peterborough, NH)*, vol. 10, pp. 47 - 64, 1986.

[125] W. Soluch, "Design of SAW synchronous resonators on ST cut quartz.," *IEEE transactions on ultrasonics, ferroelectrics, and frequency control*, vol. 46, no. 5, pp. 1324-6, Jan. 1999.

[126] J. Kondoh, Y. Matsui, and S. Shiokawa, "New Biosensor Using Shear Horizontal Surface Acoustic Wave Device," *Japanese Journal of Applied Physics*, vol. 32, pp. 2376-2379, 1993.

[127] E. Gizeli, "Study of the sensitivity of the acoustic waveguide sensor.," *Analytical chemistry*, vol. 72, no. 24, pp. 5967-72, Dec. 2000.

[128] D. S. Ballantine, S. J. Martin, and A. J. Ricco, "Acoustic Wave Sensors," *Sensors (Peterborough, NH)*.

[129] F. Josse, F. Bender, and R. W. Cernosek, "Guided shear horizontal surface acoustic wave sensors for chemical and biochemical detection in liquids," *Anal. Chem.*, vol. 73, pp. 5937 - 5966, 2001.

[130] V. K. Varadan and J. W. Gardner, "Smart tongue and nose," *Proc. SPIE Conf. Smart Electronics and MEMS*, vol. 3673, pp. 67–75, 1999.

[131] M. Cole, G. Sehra, J. W. Gardner, and V. K. Varadan, "Development of Smart Tongue Devices for Measurement of Liquid Properties," *IEEE Sensors Journal*, vol. 4, no. 5, pp. 543-550, Oct. 2004.

[132] M. Hoummady, A. Campitelli, and W. Wlodarski, "Acoustic wave sensors: design, sensing mechanisms and applications," *Smart Materials and Structures*, vol. 6, no. 6, pp. 647-657, Dec. 1997.

[133] J. Caron, R. B. Haskell, J. C. Andle, and J. F. Vetelino, "Temperature stable piezoelectric substrates for SAW gas sensors," *Sensors And Actuators*, vol. 35, pp. 141-145, 1996.

[134] W. Soluch, "Design of SAW delay lines for sensors," *Sensors And Actuators*, vol. 67, no. 3, 1998.

[135] E. J. Staples and R. C. Smythe, "Surface Acoustic Wave Resonators on ST-Quartz," *1975 Ultrasonics Symposium*, no. 2, pp. 307-310, 1975.

[136] R. M. White and F. W. Voltmer, "No Title," *Appl. Phys. Lett.*, vol. 7, p. 314, 1965.

[137] R. M. White, "No Title," *Proc. IEEE*, vol. 58, pp. 1238-1276, 1970.

[138] W. Wang and S. He, "A Love Wave Reflective Delay Line with Polymer Guiding Layer for Wireless Sensor Application," *Sensors (Peterborough, NH)*, pp. 7917-7929, 2008.

[139] O. Tigli and M. E. Zaghloul, "A Novel Circular SAW (Surface Acoustic Wave) Device in CMOS," *2007 IEEE Sensors*, pp. 474-477, 2007.

[140] I. I. Leonte, "High Frequency Acousto-Electric Microsensors for Liquid Analysis.," 2008.

[141] V. P. Plessky and C. S. Hartmann, "Characteristics of leaky SAWs On 36-LiTaO3 in Periodic Structures of Heavy Electrodes," *Proceedings of IEEE Ultrasonics Symposium*, pp. 1239-1242, 1993.

[142] J.-P. Yang, C.-Y. Shen, Y.-J. Chen, H.-C. Huang, and R.-C. Hwang, "The estimations of ammonia concentration by using neural network SH-SAW sensors," *Expert Systems with Applications*, vol. 38, no. 5, pp. 4774-4779, May 2011.

[143] I. Leonte, M. Hunt, G. Sehra, M. Cole, and J. W. Gardner, "SAW Bioliquids Sensor with RF Interrogation," *Antenna*.

[144] K.-ya Hashimoto, H. Asano, T. Omori, and M. Yamaguchi, "Ultra-Wideband Surface Acoustic Wave Devices Using Cu-Grating/Rotated-YX-LiNbO 3 -Substrate Structure.," *Japanese Journal of Applied Physics*, vol. 43, no. 5, pp. 3063-3066, May 2004.

[145] F. Martin, M. I. Newton, G. Mchale, K. A. Melzak, and E. Gizeli, "Pulse mode shear horizontal-surface acoustic wave (SH-SAW) system for liquid based sensing applications," vol. 19, pp. 627-632, 2004.

[146] M. Saitakis, A. Dellaporta, and E. Gizeli, "Measurement of Two-Dimensional Binding Constants between Cell-Bound Major Histocompatibility Complex and Immobilized Antibodies with an Acoustic Biosensor," *Biophysical Journal*, vol. 95, no. 10, pp. 4963-4971, 2008.

[147] F. Li, J. H.-C. Wang, and Q.-M. Wang, "Monitoring cell adhesion by using thickness shear mode acoustic wave sensors.," *Biosensors & bioelectronics*, vol. 23, no. 1, pp. 42-50, Aug. 2007.

[148] H. Yu, I. Meyvantsson, I. a Shkel, and D. J. Beebe, "Diffusion dependent cell behavior in microenvironments.," *Lab on a chip*, vol. 5, no. 10, pp. 1089-95, Oct. 2005.

[149] P. J. Hung, P. J. Lee, P. Sabounchi, R. Lin, and L. P. Lee, "Continuous Perfusion Microfluidic Cell Culture Array for High-Throughput Cell-Based Assays," *Biotechnology*, 2004.

[150] E. Leclerc, Y. Sakai, and T. Fujii, "Cell Culture in 3-Dimensional Micro ¯ uidic Structure of PDMS," *Biomedical Microdevices*, vol. 1, pp. 109-114, 2003.

[151] G. M. Walker, M. S. Ozers, and D. J. Beebe, "Hybrid Bio / Arti ® cial Microdevices : Insect Cell Culture in Micro ¯ uidic Channels," *Methods*, pp. 161-166, 2002.

[152] H.-W. Wu, X.-Z. Lin, S.-M. Hwang, and G.-B. Lee, "The culture and differentiation of amniotic stem cells using a microfluidic system.," *Biomedical microdevices*, vol. 11, no. 4, pp. 869-81, Aug. 2009.

[153] A. Bange, H. B. Halsall, and W. R. Heineman, "Microfluidic immunosensor systems," *Integration The Vlsi Journal*, vol. 20, pp. 2488-2503, 2005.

[154] N. Orr, G. L. Orr, and R. M. Hollingworth, "The Sf9 cell line as a model for studying insect octopamine-receptors," *Insect Biochemistry and Molecular Biology*, vol. 22, no. 6, pp. 591-597, Sep. 1992.

[155] T. Roeder, "Tyramine and octopamine: ruling behavior and metabolism.," *Annual review of entomology*, vol. 50, no. 20, pp. 447-77, Jan. 2005.

[156] Z. Rácz, M. Cole, J. W. Gardner, S. Pathak, M. D. Jordan, and R. A. J. Challis, "CELL-BASED SURFACE ACOUSTIC WAVE RESONANT MICROSENSOR FOR BIOMOLECULAR AGENT DETECTION Sensors Research Laboratory , University of Warwick , Coventry , UK Department of Cell Physiology and Pharmacology , University of Leicester , Leicester , UK REFERENCES," *Sensors (Peterborough, NH)*, no. C, pp. 6-7.

[157] G. Guhr, H. Schmidt, and M. Weihnacht, "A new tool to assess mechanical and dielectric properties of tissues.," *Conference proceedings : ... Annual International Conference of the IEEE Engineering in Medicine and Biology Society. IEEE Engineering in Medicine and Biology Society. Conference*, vol. 2009, pp. 729-32, Jan. 2009.

[158] B. F, R. C, W. E, and R. M, "Comparison of fixed and living liver endothelial cells by atomic forcemicroscopy.," *Appl Phys A-Mater*, vol. 66, pp. 575–578, 1998.

[159] J. Hutter, "Atomic force microscopy investigation of the dependence of cellular elastic moduli on glutaraldehyde fixation.," *J Microsc-Oxford*, vol. 219, pp. 61–68, 2005.

[160] F. CH, J. FB, W. J, and R. PP, "Formaldehyde fixation.," *J Histochem Cytochem*, vol. 33, pp. 845–853, 1985.

[161] S. J. SINGER and G. L. NICOLSON, "The fluid mosaic model of the structure of cell membranes.," *Science*, pp. 720-731, 1972.

Appendix A

Polymer Selection

A-1 Polymer Selection Experimental Results

Batch – 1 Experiments 1: 100nl of Ethyl Acetate , 0 nl 3-methyl-but-1-ol

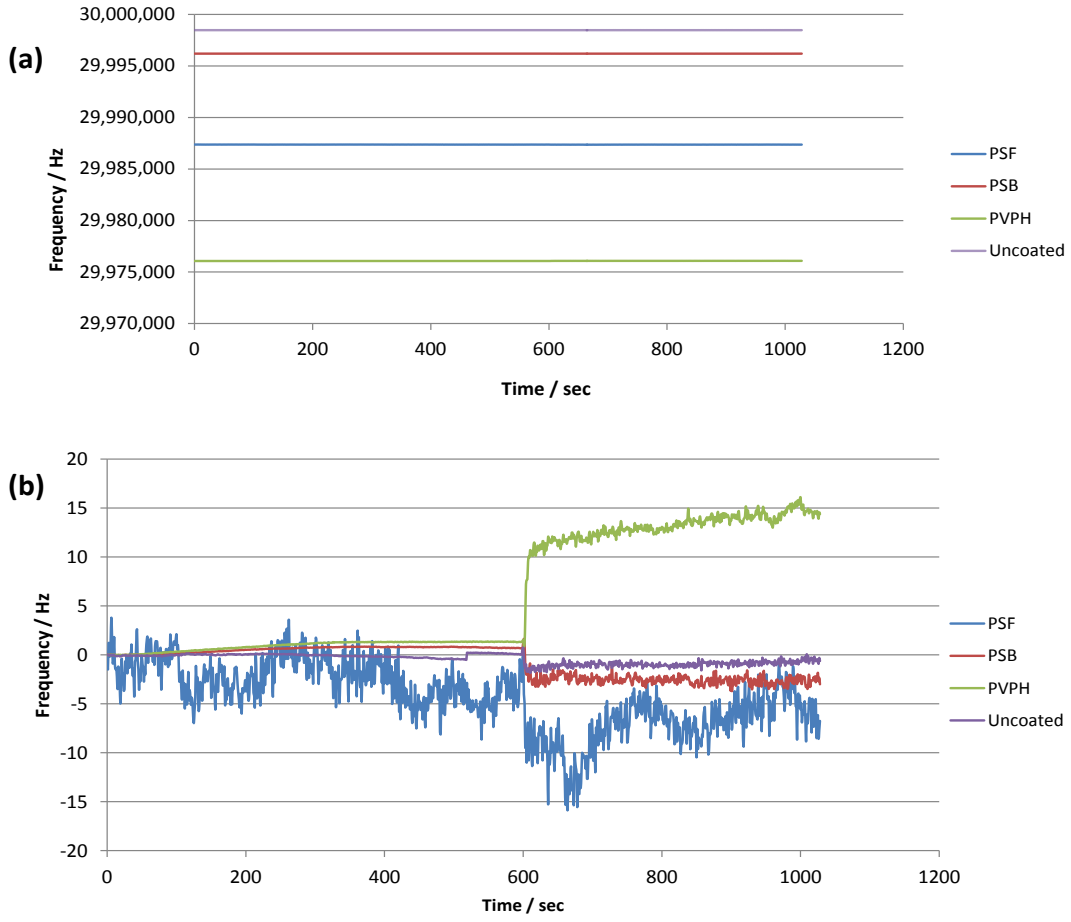

Figure A-1.1: Shown is the frequency response of the polymer coated QCM microsensors (a) the resonant frequency shown (b) the offset removed plot showing the response with better resolution

Batch – 1

Experiments 2: 0nl of Ethyl Acetate , 1000 nl 3-methyl-but-1-ol

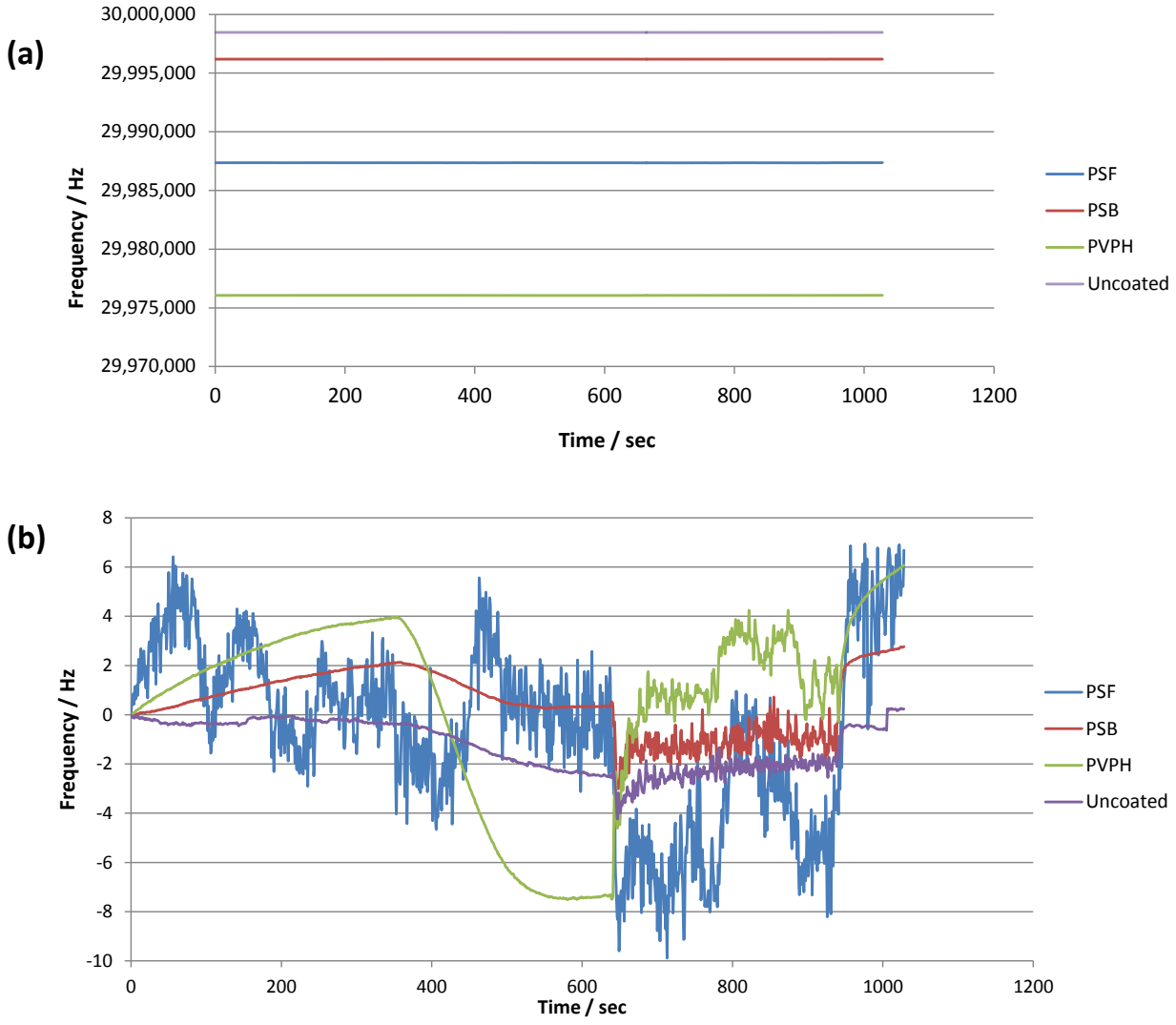

Figure A-1.2: Shown is the frequency response of the polymer coated QCM microsensors (a) the resonant frequency shown (b) the offset removed plot showing the response with better resolution

Batch – 2

Experiments 1: 100nl of Ethyl Acetate , 0 nl 3-methyl-but-1-ol

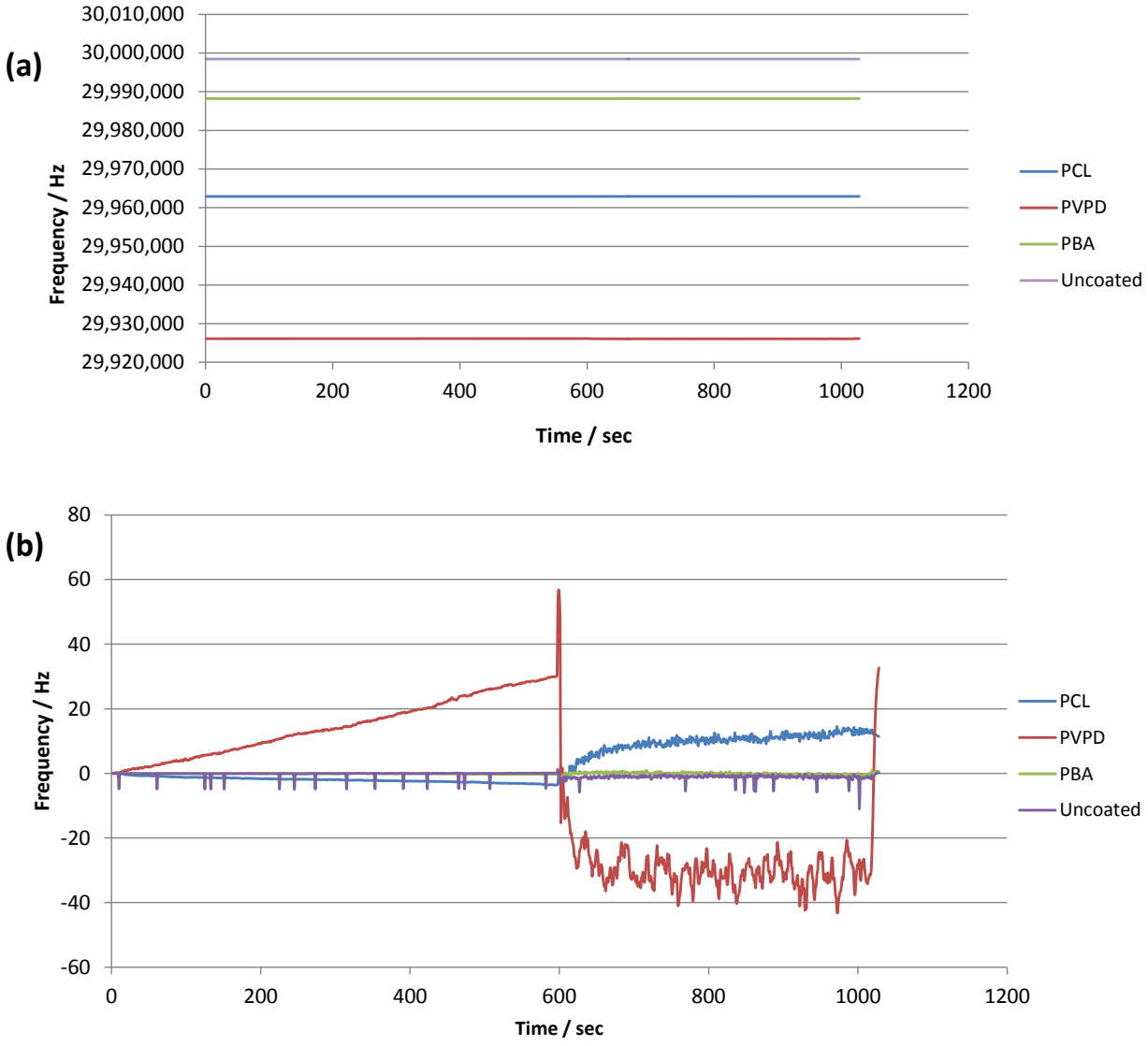

Figure A-1.3: Shown is the frequency response of the polymer coated QCM microsensors (a) the resonant frequency shown (b) the offset removed plot showing the response with better resolution

Batch – 2

Experiments 1: 0nl of Ethyl Acetate , 100 nl 3-methyl-but-1-ol

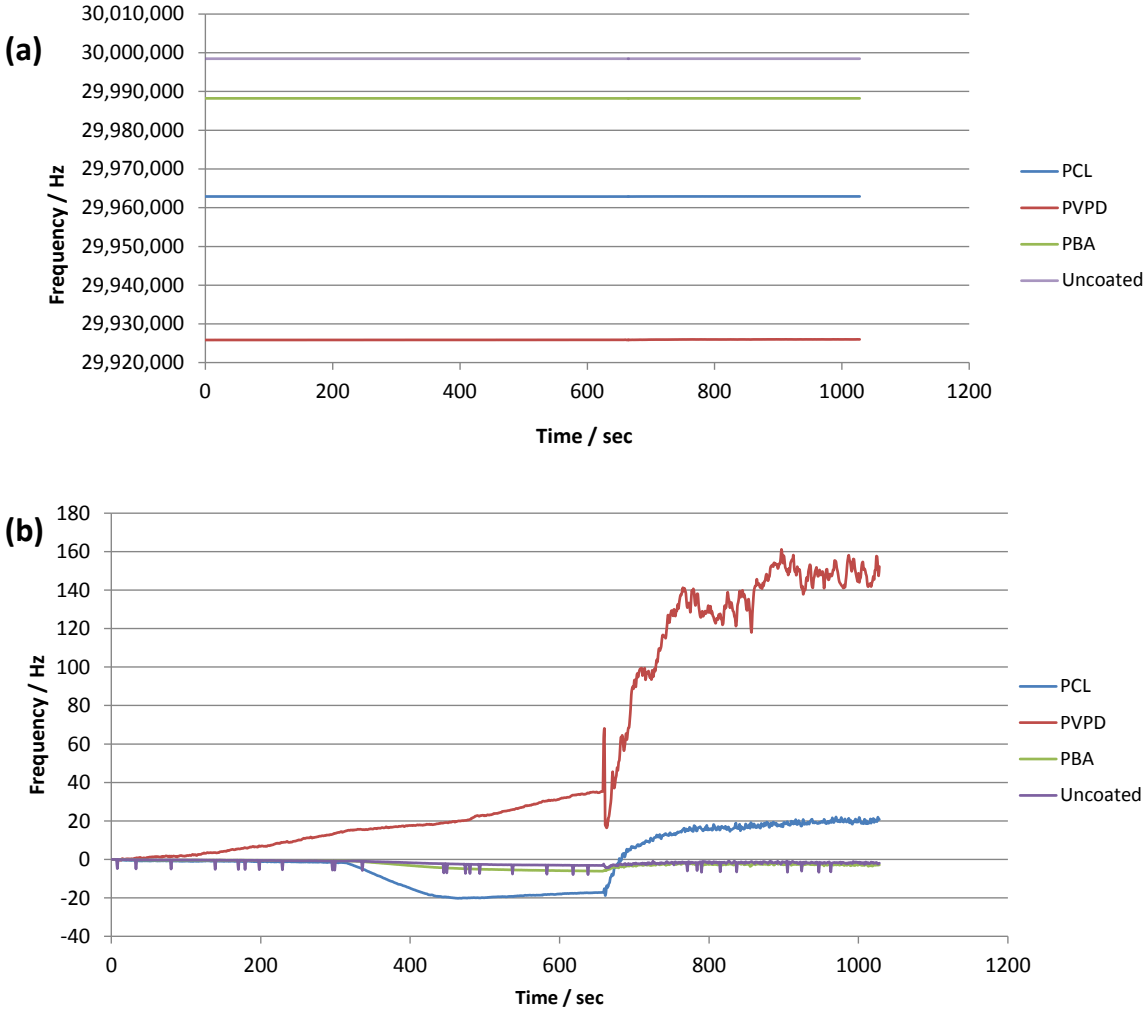

Figure A-1.4: Shown is the frequency response of the polymer coated QCM microsensors (a) the resonant frequency shown (b) the offset removed plot showing the response with better resolution

Batch – 3

Experiments 1: 100nl of Ethyl Acetate , 0 nl 3-methyl-but-1-ol

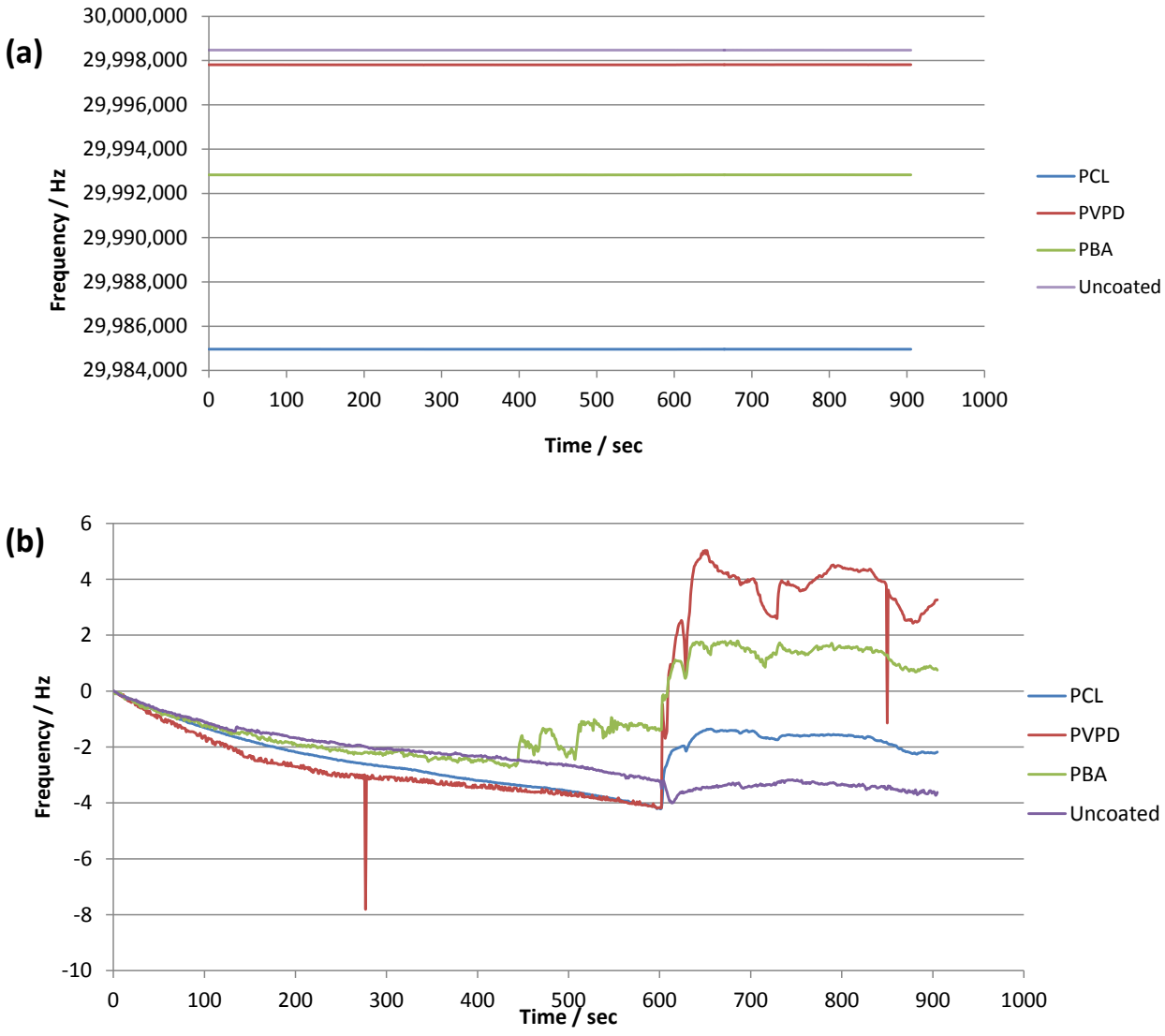

Figure A-1.5: Shown is the frequency response of the polymer coated QCM microsensors (a) the resonant frequency shown (b) the offset removed plot showing the response with better resolution

Batch – 3

Experiments 2: 0nl of Ethyl Acetate , 100 nl 3-methyl-but-1-ol

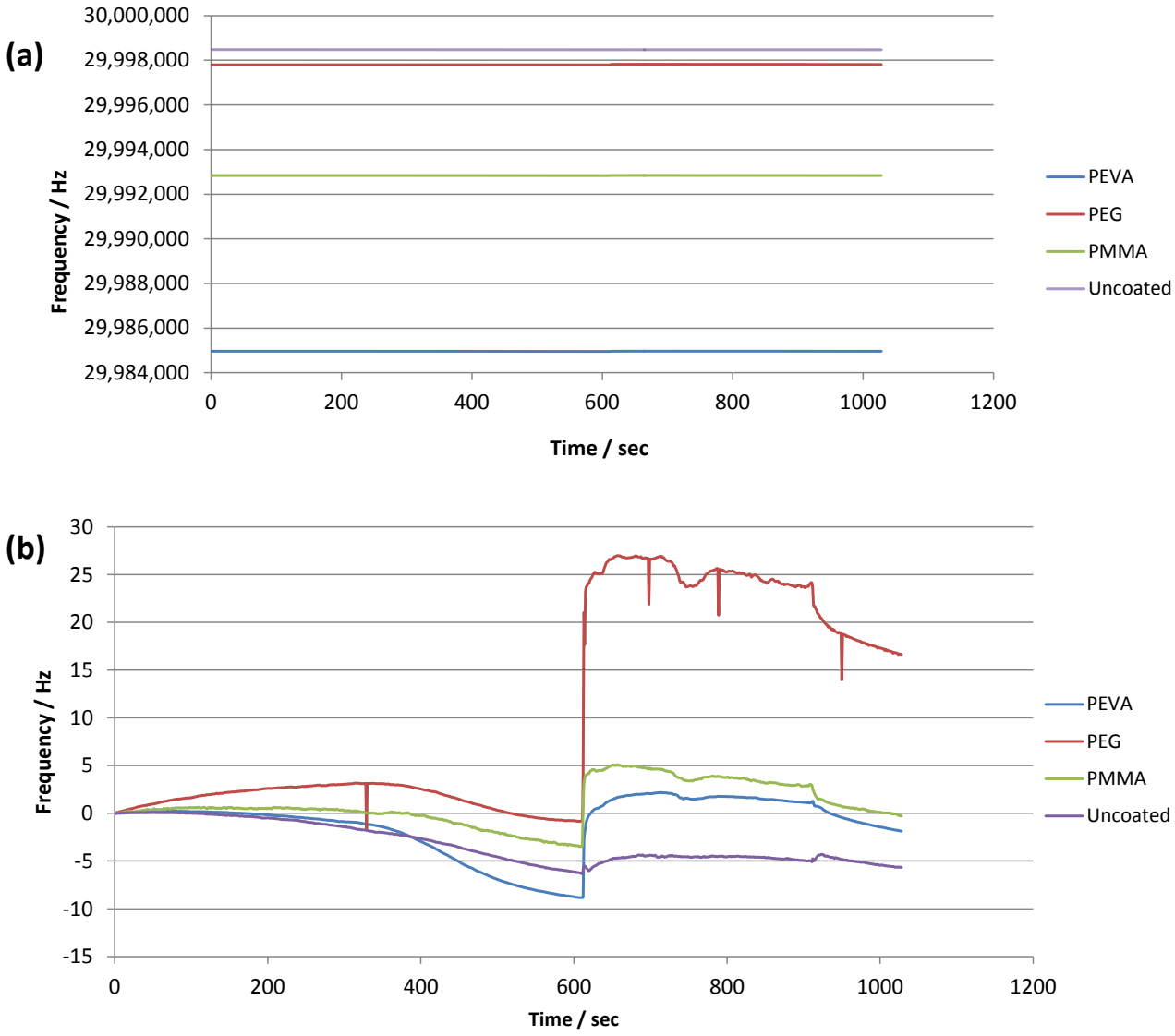

Figure A-1.6: Shown is the frequency response of the polymer coated QCM microsensors (a) the resonant frequency shown (b) the offset removed plot showing the response with better resolution

Appendix B

Ratiometric Experiments

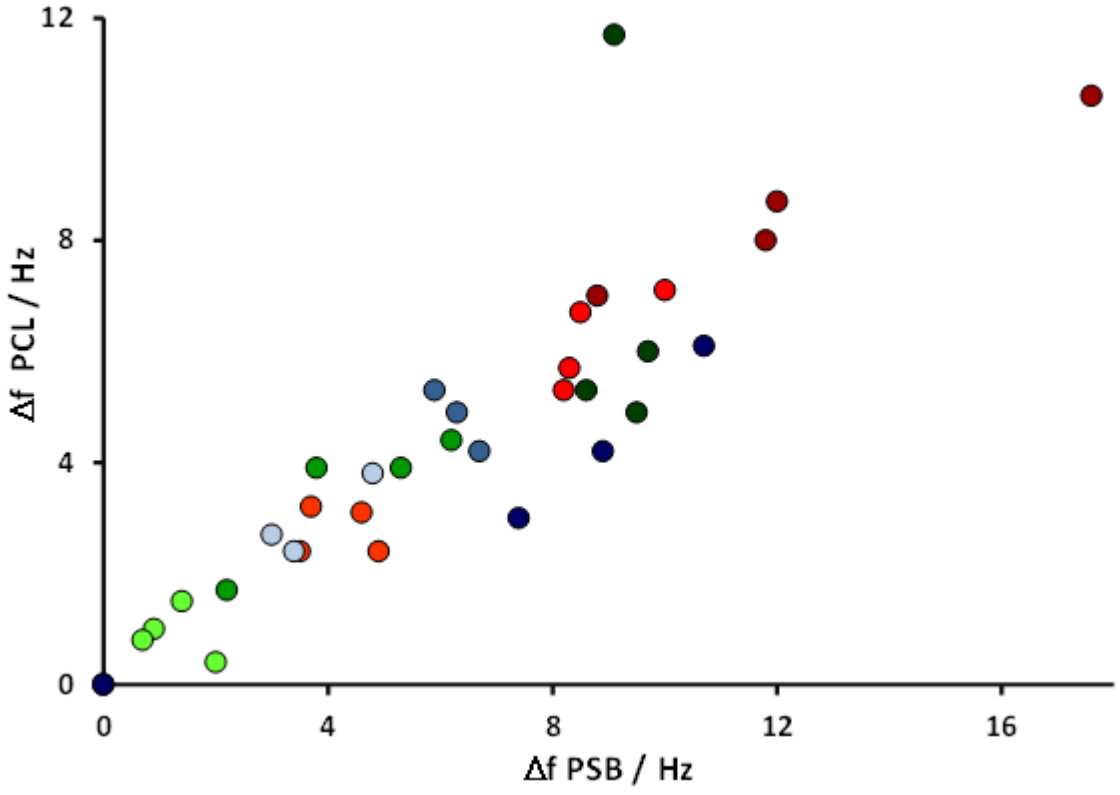

Figure AB -1 : Extracted data from the 36 measurements providing the frequency shift for each run

Ratio	Polymer coated QCM				Volatiles
1:3	PSB	PCL	PEG	Blank	3M: EA (nl)
Run 1	0.9	1	0	0	22 :335
Run 2	1.4	1.5	0	0	
Run 3	0.7	0.8	0	-0.4	
Run 4	2	0.4	0.3	0.1	
Run 1	3.8	3.9	5	1.7	44 :670
Run 2	2.2	1.7	1.7	0.6	
Run 3	6.2	4.4	1.4	1.6	
Run 4	5.3	3.9	1.4	1	
Run 1	9.1	11.7	2	1.6	67 :1006
Run 2	8.6	5.3	2.3	2.1	
Run 3	9.7	6	2.3	2.4	
Run 4	9.5	4.9	2.2	2	
3:1	PSB	PCL	PEG	Blank	
Run 1	4.6	3.1	0	0	67:110
Run 2	3.5	2.4	0	0	
Run 3	4.9	2.4	0	0	
Run 4	3.7	3.2	0	0	
Run 1	8.5	6.7	0	0	134 :222.5
Run 2	8.2	5.3	0	0	
Run 3	10	7.1	0	0	
Run 4	8.3	5.7	0	0	
Run 1	8.8	7	0	0	201:335
Run 2	12	8.7	0	0	
Run 3	17.6	10.6	0	0	
Run 4	11.8	8	0	0	
1:1	PSB	PCL	PEG	Blank	
Run 1	0	0	0	0	50 :250
Run 2	3.4	2.4	0	0	
Run 3	4.8	3.8	0	0	
Run 4	3	2.7	0	0	
Run 1	5.9	5.3	0	0	100 :500
Run 2	6.3	4.9	0	0	
Run 3	6.7	4.2	0	0	
Run 4	0	0	0	0	
Run 1	0	0	0	0	150:750
Run 2	8.9	4.2	0	0	
Run 3	7.4	3	0	0	
Run 4	10.7	6.1	0	0	

Figure AB - 2 : Extracted data for 36 measurements providing the frequency shift (Hz) for each run (3M: 3 methyl-butan-1-ol; EA: Ethyl Acetate)

Appendix - C

SH-SAW microsensors on $LiTaO_3$ (36° Y cut X propagating)

Frequency [MHz]	Type of device	λ [μm]	IDT Finger Width [λ/8] [μm]	Number of finger pairs per IDT	Acoustic Aperture [xλ's [μm]	Delay path length [μm]	Number of stripes per reflector pair	Distance between IDT -Reflectors [μm]	Heater Strip width [μm]	No of Devices/ wafer
60.56	One Port Resonator	68	8.5	5.5	3400 [50λ]	-	100	42.5	-	14
60.56	Two Port Resonator Free path	68	8.5	5.5	3400 [50λ]	5015.26	100	42.5	-	7
60.56	Two Port Resonator Shorted path	68	8.5	5.5	3400 [50λ]	5015.26	100	42.5	-	12
60.56	Two Port Resonator With Heater path	68	8.5	5.5	3400 [50λ]	5015.26	100	42.5	51	6
228.79	One Port Resonator	18	2.25	5.5	1440 [80λ]	-	100	11.25	-	18
228.79	Two Port Resonator With Free path	18	2.25	5.5	1440 [80λ]	2002.53	100	11.25	-	22
228.79	Two Port Resonator With Shorted path	18	2.25	5.5	1440 [80λ]	2002.53	100	11.25	-	25
228.79	Two Port Resonator With Heater path	18	2.25	5.5	1440 [80λ]	2002.53	100	11.25	13.5	9

Appendix - D

Rayleigh SAW on ST-Quartz

Frequency [MHz]	Type of device	λ [µm]	IDT Finger Width [λ/4] [µm]	Number of finger pairs per IDT	Acoustic Aperture [xλ's [µm]	Delay path length [µm]	Cavity Length [µm] Ref edge to edge	Number of stripes per reflector pair	Distance between IDT - Reflectors [µm]	Heater Strip width [µm]	No of Devices/ wafer
262.98	One Port Resonator	12	3	60.5	720[60λ]	-	738	550	7.5	-	26
262.98	Two Port Resonator Free path	12	3	60.5	720[60λ]	303	1764	550	7.5	-	18
262.98	Two Port Resonator Shorted path	12	3	60.5	720[60λ]	303	1764	550	7.5	-	18
262.98	Two Port Resonator Heated path	12	3	60.5	720[60λ]	303	1764	550	7.5	9	3
525.6	One Port Resonator	6	1.5	70.5	600[100λ]	-	429	700	3.75	-	23
525.6	Two Port Resonator Free path	6	1.5	70.5	600[100λ]	241.5	1092	700	3.75	-	24
525.6	Two Port Resonator Shorted path	6	1.5	70.5	600[100λ]	241.5	1092	700	3.75	-	24
525.6	Two Port Resonator Heated path	6	1.5	70.5	600[100λ]	241.5	1092	700	3.75	4.5	7
869	One Port Resonator	3.632	0.908	80.5	472[130]	-	223.368	700	2.27	-	29
869	Two Port Resonator Free path	3.632	0.908	80.5	472[130λ]	200.668	788.144	700	2.27	-	30
869	Two Port Resonator Shorted path	3.632	0.908	80.5	472[130λ]	200.668	788.144	700	2.27	-	30
869	Two Port Resonator Heated path	3.632	0.908	80.5	472[130λ]	200.668	788.144	700	2.27	2.724	7
1575	One Port Resonator	2	0.50	80.5	401[200λ]	-	163	700	1.25	-	40

Appendix - E

SH-SAW Microsensor Layout

2 port 60.56 MHz SH-SAW (Free)

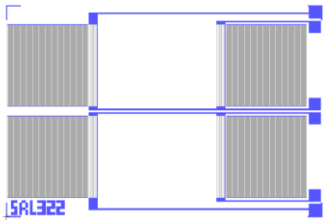

2 port 60.56 MHz SH-SAW (Shorted)

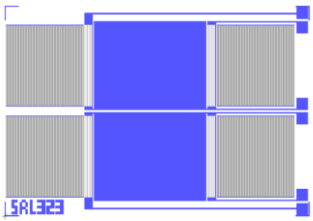

2 port 60.56 MHz SH-SAW (Free)

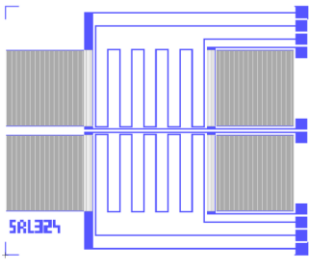

1 port 60.56 MHz SH-SAW

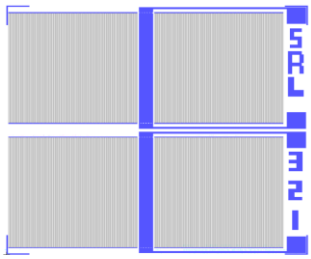

2 port 228.79 MHz SH-SAW (Free)

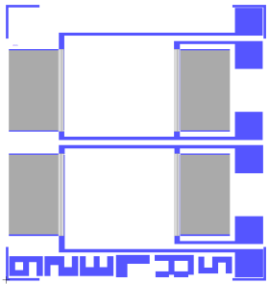

2 port 228.79 MHz SH-SAW (Shorted)

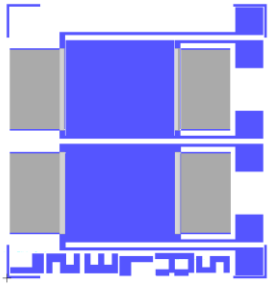

2 port 228.79 MHz SH-SAW (Free)

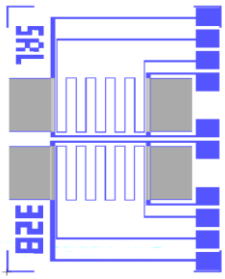

1 port 228.79 MHz SH-SAW

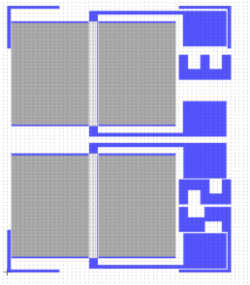

Appendix - F

SAW microsensor Fabrication Procedure

A-E.1 Masks Design

The steps, outlined in **Figure AE1** were employed.

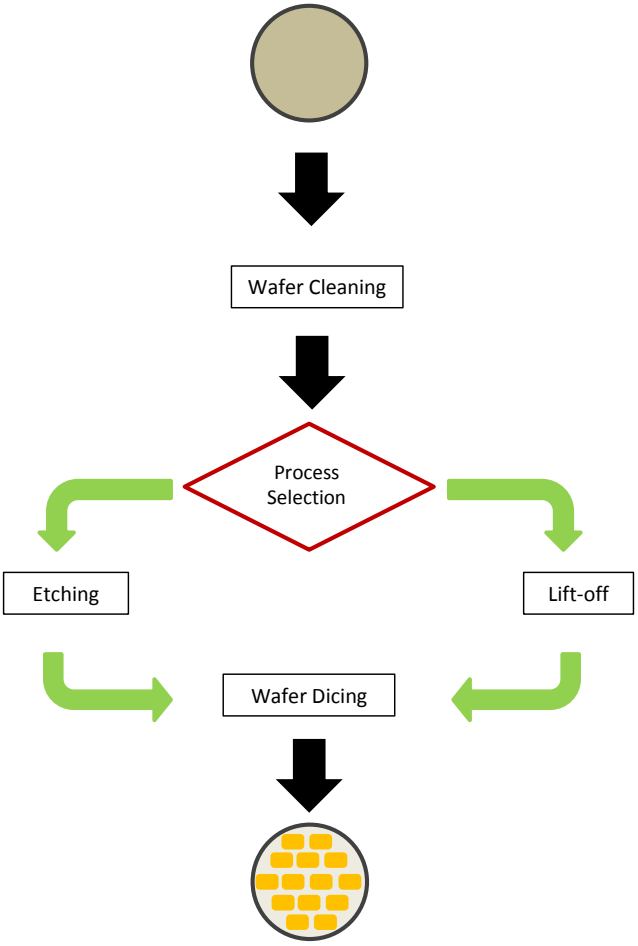

Figure AE1: Overview of the process employed for fabrication of IDT's

A-E.2 Masks Design

- The mask designs are first designed using CAD software package e.g. Tanner Tools and exported to GDS II format, an industry standard.
- This format is compatible with an e-beam writer which by the process of lithography writes the designs on a standard 5″ glass plates.
- A 1.5mm, 5" white chrome flint glass substrate with an anti-reflective chrome coating was manufactured by Delta Masks BV.
- The chrome side was written down with a positive field. The minimum feature size of SH-SAW micro-device was 2.25μm.

A-E.3 Wafer Preparation

- It is a mandatory requirement to clean/prepare the wafer surface as a contaminant free surface guarantees good adhesion and uniformity of the deposited metal layer. IT should be performed in a cleanroom environment.
- Surface contaminants e.g. dust and organic particles were removed by employing trichloroethylene and acetone (both at 60°C for 10 minutes) bath followed by a 30 minute bake in an oven at 60°C.
- Secondary or obstinate contaminants were removed by using a 3:1 solution of DI water and ammonium hydroxide and one part of 30% un-stabilised hydrogen peroxide (at 75°C for 10 minutes).
- The wafer was then be placed in a detergent solution (industrial) and ultrasonically agitated (at 60°C for 10 minutes) followed by DI rinse.
- The clean piezoelectric wafer was then dried using compressed filtered nitrogen.

A-E.4 Photolithography

- Two methods can be employed for optical exposure (i) shadow printing; (ii) projection printing.
- The shadow printing technique was employed to fabricate the SH-SAW microsensors while projection printing has been employed for the fabrication of Rayleigh SAW microsensors, , as shown in **Appendix F**
- In shadow printing the mask, with the pattern, was brought in contact (known as contact printing) or is kept in

close proximity (also known as proximity printing) with the photoresist coated wafer, as shown diagrammatically in **Figure AE2**.

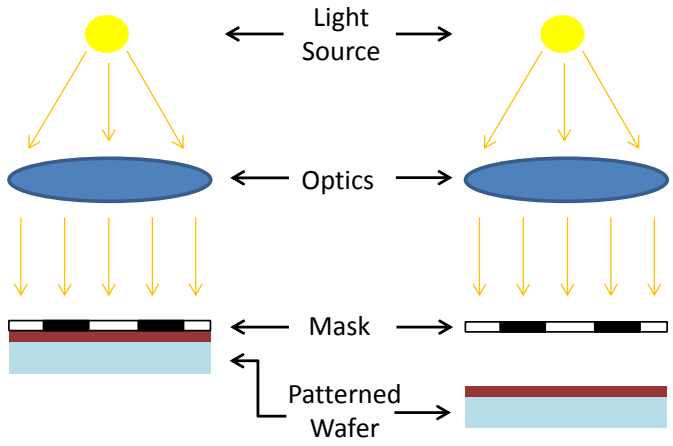

Figure AE2: Shadow Printing Technique

- In projection printing, the image of the pattern on the mask, placed at a distance (usually centimetres), was projected onto the resist coated wafer. Only a small area of the mask was stepped (scanned) at a given time which was then populated over the entire area of the wafer thus providing increased resolution. This pattern on the mask remains stationary while the projected image is stepped or populated by translating the wafer in 2D e.g. projecting and image of the sensor chip and then moving the wafer to the next site to repeat the process, as shown in **Figure AE3**.

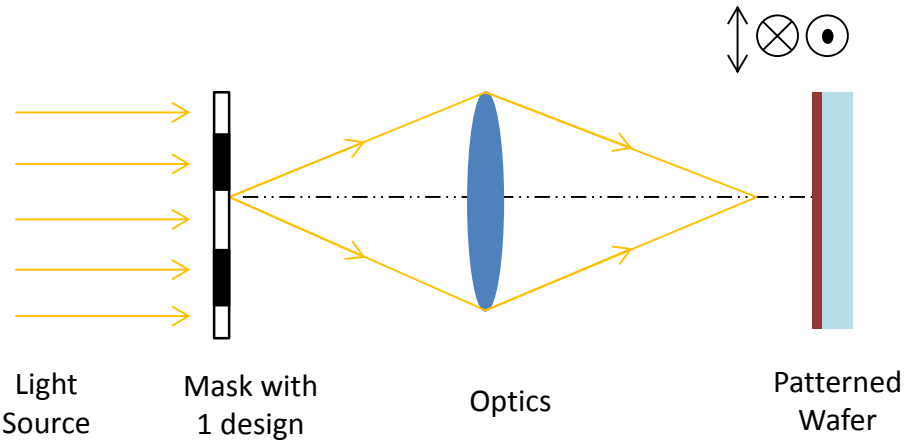

Figure AE3 Projection printing or step and repeat Lithography

- It is also known as the "step-and-repeat-projection" with a demagnification ratio of M : 1 (M denotes the number of reduction on the wafer). One of the many advantages of projection printing technique is the fact that larger areas wafer can be printed without modifying the lens. If one wants to fabricate sensors with smaller dimensions approaching nm range then this is employed as it is more convenient.
- Various regions of the sensor were defined by the patterns which are projected from the mask onto the resist on the substrate but this patterned layer needs to be transferred once more to the underlying layer. This is usually achieved by etching or lift-off techniques.

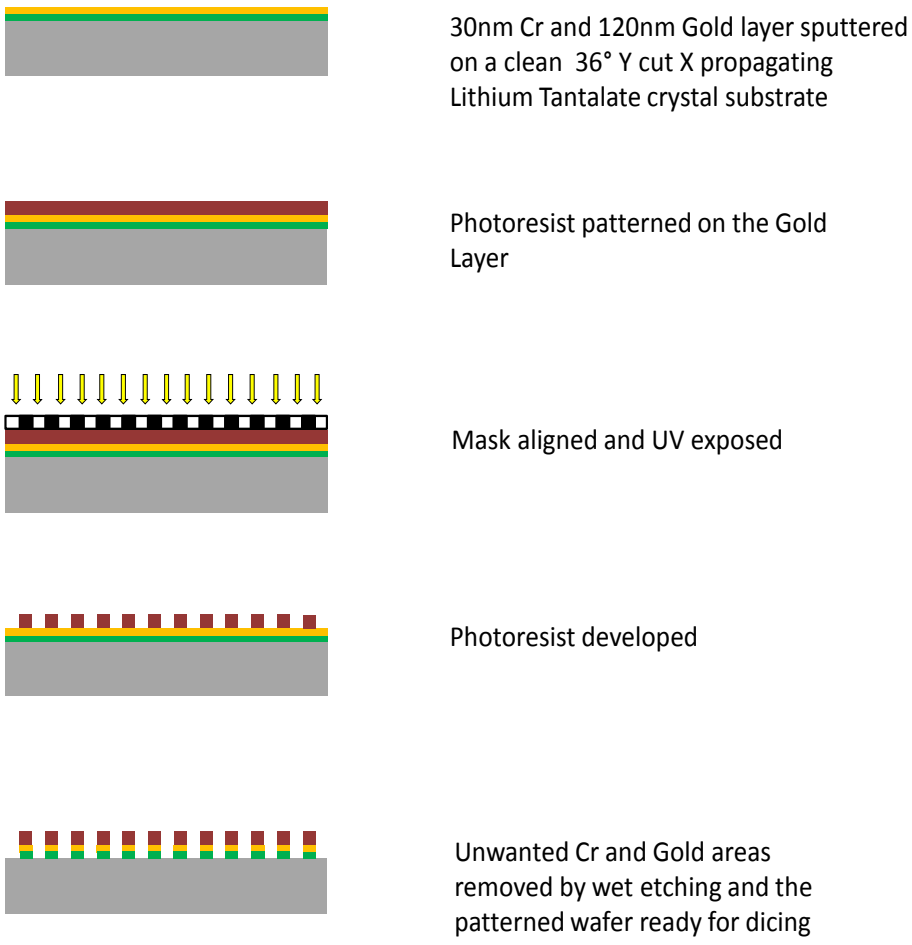

Figure AE4: Process of fabrication of the SAW micro-devices

- As shown, the two different processes can be employed in order to pattern the IDT's are Lift-off and Etching, **Figure AE5**.

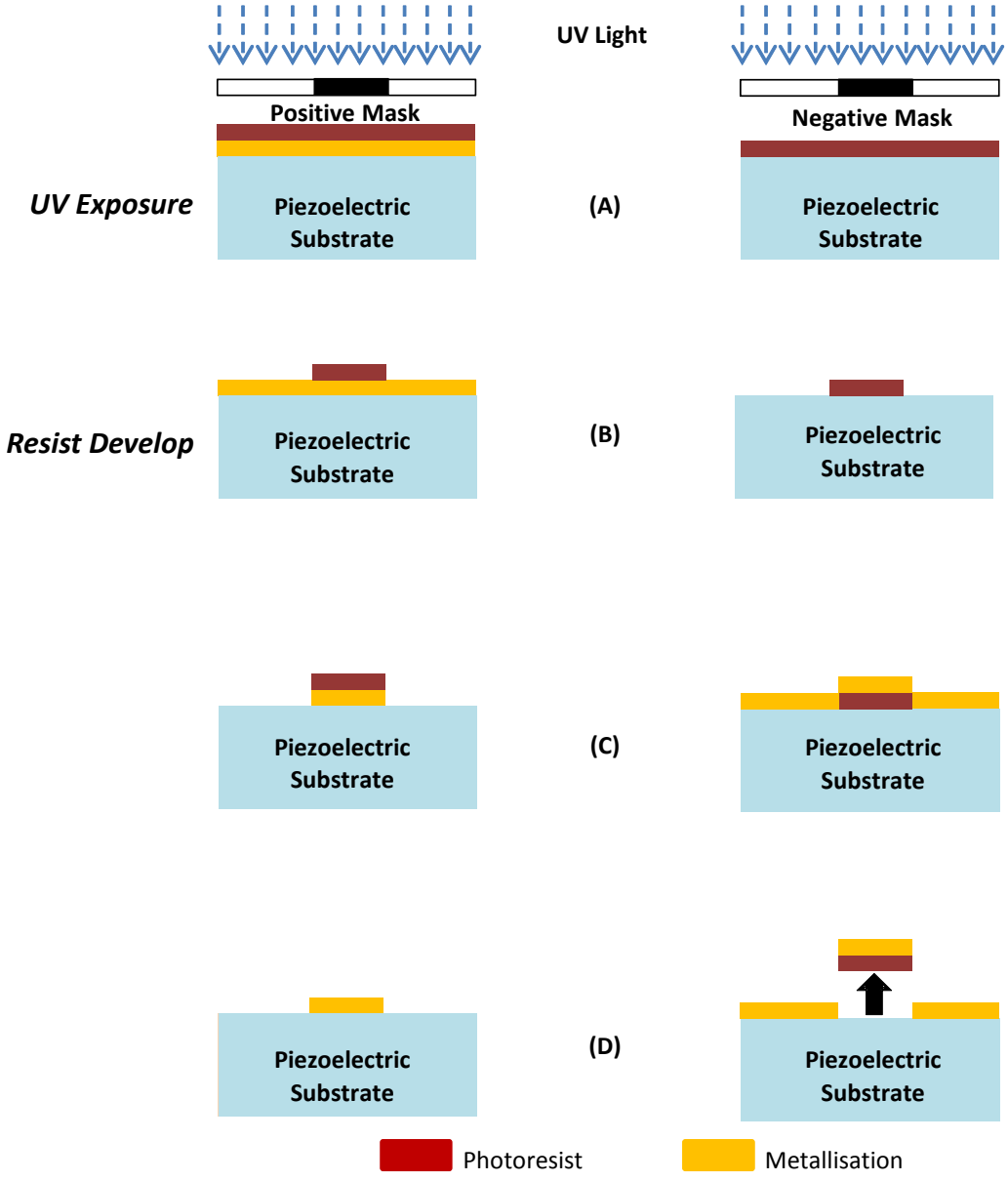

Figure AE5: Basic lithographic processes used to pattern the IDT on a piezoelectric substrate: presented on left is etching and on right is lift-off

Appendix - G

Fabricated Rayleigh SAW microsensor on 4" wafer

AG.1: Gold Metallisation

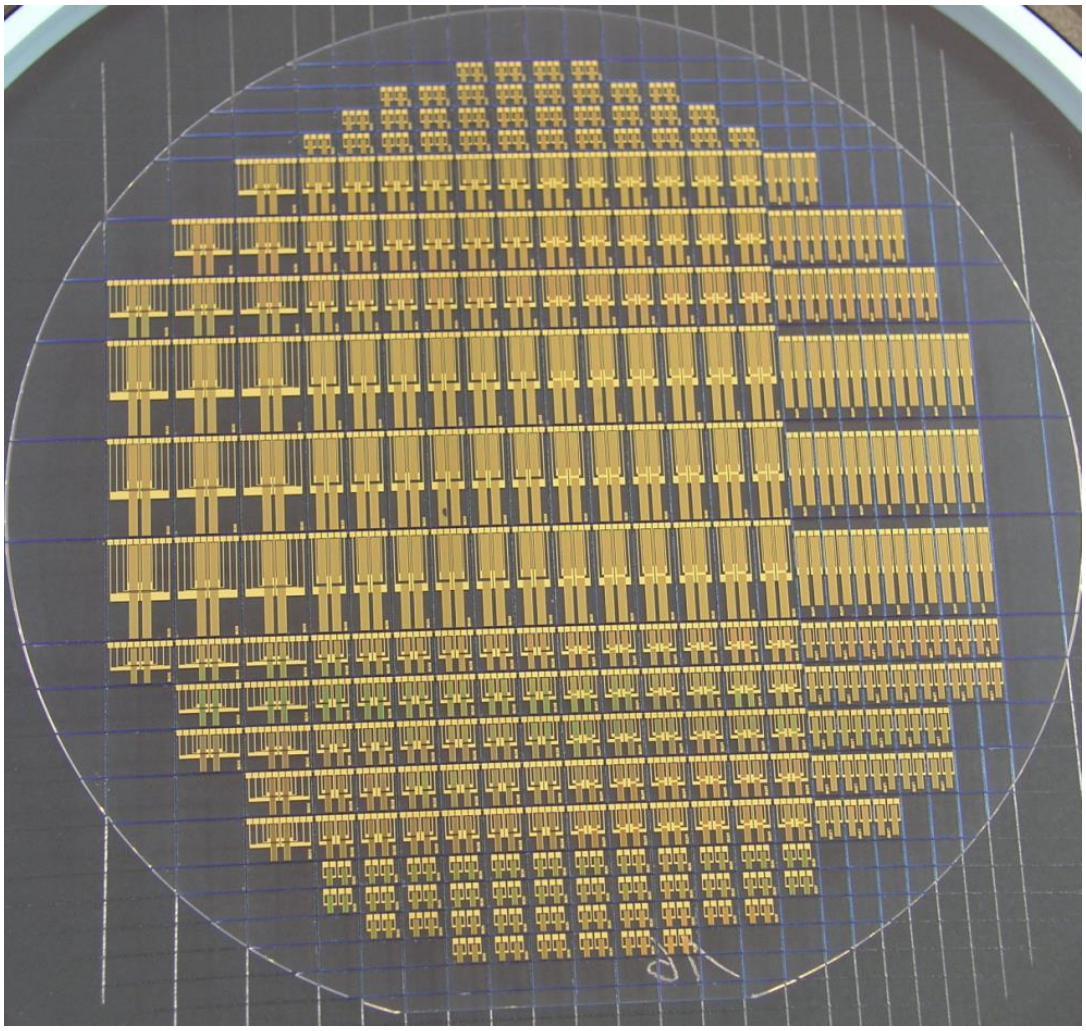

Figure AG1: Fabricated Rayleigh SAW microsensors on a 4" ST- Quartz wafer with Gold metallisation

AF.2: Aluminum Metallisation

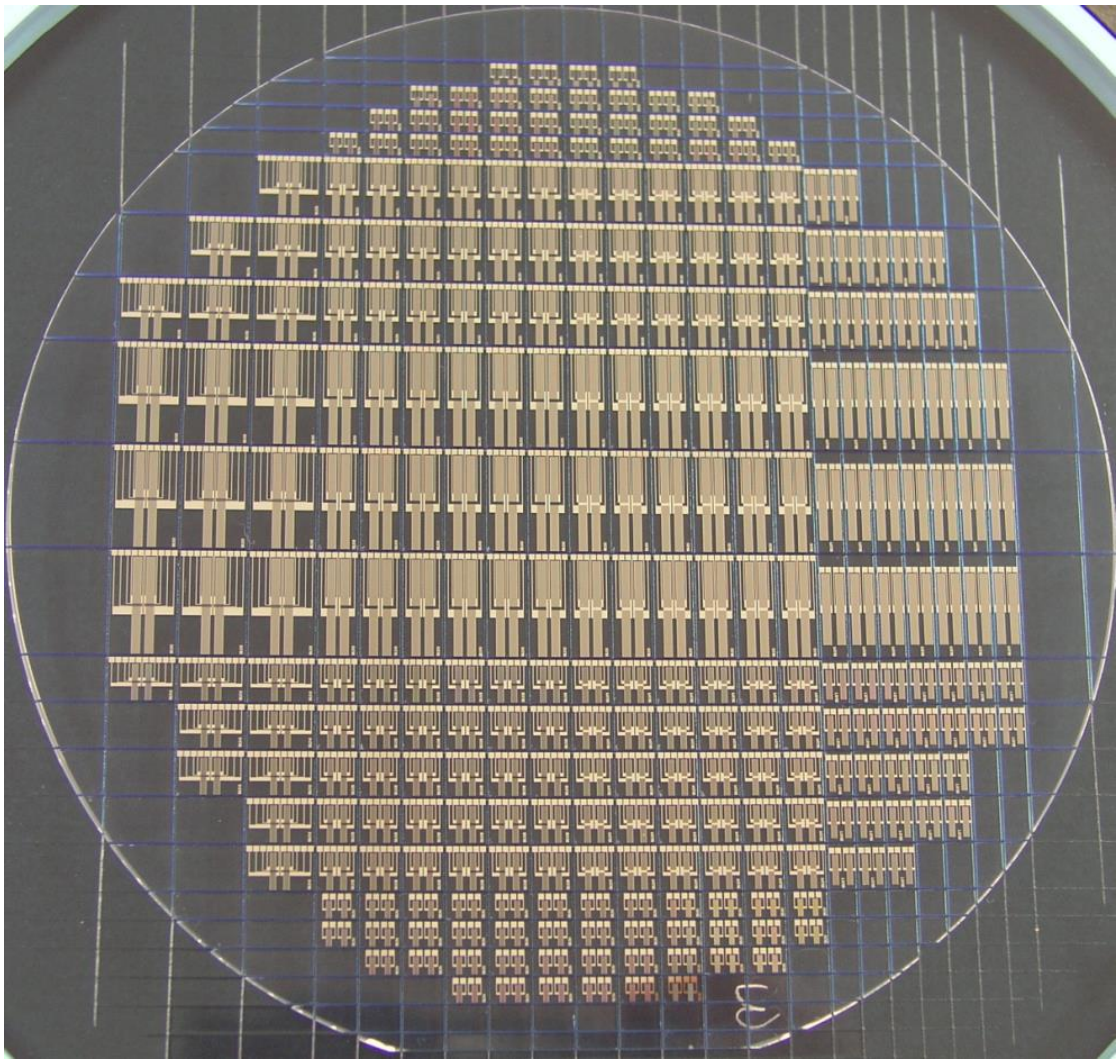

Figure AF2: Fabricated Rayleigh SAW microsensors on a 4" ST- Quartz wafer with Aluminum metallisation